UNCLASSIFIED

ORNL-1875(Del.)

UNITED STATES ATOMIC ENERGY COMMISSION

METALLURGY DIVISION SEMIANNUAL PROGRESS REPORT [FOR] PERIOD ENDING OCTOBER 10, 1954

By
W. H. Bridges

August 31, 1955

Oak Ridge National Laboratory
Oak Ridge, Tennessee

Technical Information Service Extension, Oak Ridge, Tenn.

UNCLASSIFIED

717 - 1

[redacted]

ORNL-1875 (Del.)

[redacted]

Contract No. W-7405-eng-26

METALLURGY DIVISION

SEMIANNUAL PROGRESS REPORT

for Period Ending October 10, 1954

J. H. Frye, Jr., Director

EDITED BY

W. H. Bridges

[redacted]

DATE ISSUED

AUG 31 1955

[redacted]

report
mission
amages
method,

[redacted]

[redacted]

OAK RIDGE NATIONAL LABORATORY
Operated by
CARBIDE AND CARBON CHEMICALS COMPANY
A Division of Union Carbide and Carbon Corporation
Post Office Box P
Oak Ridge, Tennessee

[redacted]

717 501

[redacted]

[redacted]

[redacted]

[redacted]

Reports previously issued in this series are as follows:

ORNL-28	Period Ending March 1, 1948
ORNL-69	Period Ending May 31, 1948
ORNL-407	Period Ending July 31, 1949
ORNL-511	Period Ending October 31, 1949
ORNL-583	Period Ending January 31, 1950
ORNL-754	Period Ending April 30, 1950
ORNL-827	Period Ending July 31, 1950
ORNL-910	Period Ending October 31, 1950
ORNL-987	Period Ending January 31, 1951
ORNL-1033	Period Ending April 30, 1951
ORNL-1108	Period Ending July 31, 1951
ORNL-1161	Period Ending October 31, 1951
ORNL-1267	Period Ending January 31, 1952
ORNL-1302	Period Ending April 30, 1952
ORNL-1366	Period Ending July 31, 1952
ORNL-1437	Period Ending October 31, 1952
ORNL-1503	Period Ending January 31, 1953
ORNL-1551	Period Ending April 10, 1953
ORNL-1625	Period Ending October 10, 1953
ORNL-1727	Period Ending April 10, 1954

[redacted]

[redacted]

CONTENTS

[redacted]

717-4

PUBLICATIONS

C. E. Curtis, L. M. Doney, and J. R. Johnson, "Some Properties of Hafnium Oxide, Hafnium Silicate, Calcium Hafnate, and Hafnium Carbide," *J. Am. Ceram. Soc.* **37,** 458–465 (Oct. 1954).

J. R. Johnson, "High Temperature X-Ray Camera," *J. Am. Ceram. Soc.* **37,** 360–362 (Aug. 1954).

[redacted]

METALLURGY DIVISION
SEMIANNUAL PROGRESS REPORT

SUMMARY

FUNDAMENTAL PHYSICAL METALLURGY

With the use of methods whereby the distribution of the fiber axis with respect to the crystallographic axes is obtained, a study was made of the fiber-texture type of preferred orientation in some extruded aluminum rod. The axis-distribution charts show the textures to be duplex, the <111> and <001> being the preferred directions of the fiber axis. For rods extruded at both slow and fast rates, the ratio <111>/<001> decreases from the front to the back end of the rod and, for corresponding locations is greater in the rod extruded at the faster speed.

The fiber-texture analysis was applied to the sheet-texture type of preferred orientation by simulating "fiber" axes about the rolling, normal, and transverse directions. From the axis-distribution charts, the ideal texture of some cold-rolled 65-35 brass was found to have the following components: $\{011\}\langle\bar{1}00\rangle$, $\{011\}\langle\bar{2}11\rangle$, and $\{111\}\langle\bar{1}2\bar{1}\rangle$. The ideal texture of cold-rolled 2S aluminum was found to be $\{123\}\langle\bar{4}33\rangle$.

Experiments to purify zirconium by the "zone-melting" technique have been started. The technique should prove useful with this reactive material because of the high purification factor and because of the absence of contaminating crucibles.

PHYSICAL METALLURGY OF REACTOR MATERIALS

Three transformation products of the decomposition of the beta eutectoid of the Ag-Zr system have been identified. They are (1) a pearlitic-type transformation product very similar to pearlite in steels, (2) a bainitic-type transformation product very similar to bainite in steels, and (3) a martensitic-type transformation product formed on quenching by a diffusionless transformation. The rate of transformation of the eutectoid at 750 and 800°C has been studied.

The tempering of the martensitic structure of a hypoeutectoid Ag-Zr alloy has been studied at 800°C. The as-quenched hardness decreases from 300 to 235 DPH at 15 sec and at 10 min at 800°C and to 190 DPH at 15 min and at 24 hr at 800°C. The changes in the microstructure are, progressively, a precipitation of the intermetallic compound, $AgZr_2$, in the matrix, the spheroidization and growth of the precipitate, nucleation of new unstrained alpha grains in the matrix, and the consumption of the deformed matrix by the new grains of alpha.

An anodizing procedure has been developed for the identification in bright-field illumination by color of the microconstituents of the Ag-Zr alloys.

Metallurgical treatments for the recovery of uranium from spent stainless steel fuel elements are being investigated. One method involves the melting of the fuel element under a nonmetallic material such as alkaline-earth fluorides, with which the uranium forms a slag. Another method depends on the increased reactivity of the stainless steel with the dissolver solutions when the steel has been heavily carburized.

Thorium slugs sealed in aluminum cans by the Al-Si bonding technique were found to be difficult to dissolve in an acid solution normally suitable for dissolving aluminum and thorium. The presence of an intermetallic compound which developed between the thorium and the Al-Si alloy in the canning operation was the dissolution barrier.

CERAMICS RESEARCH

On the premise that a selected ceramic fuel element is useful in a practical high-temperature gas-cooled reactor power system, a development and testing program has been undertaken.

An SiC-Si body, chosen for its low absorption cross section, suitable physical properties, and raw-material availability, has been developed. Homogeneous nonporous shapes can be produced consistently. A second phase of research is under way to develop, with the use of this SiC-Si body, a uniform fuel-bearing sandwich plate.

717 006.

[redacted]

A testing program has been designed in order to obtain sufficient information for reactor-power-system studies.

Some physical properties have been measured, and stability under neutron bombardment has been investigated. A gas "loop" has been made that simulates mechanical and thermal service conditions for a fuel element. Fission-product retention tests show that only gaseous isotopes escape from SiC-Si at 1000°C, and the number of these isotopes is reduced by a factor of at least 10^{-4} over unclad UO_2.

Two reactor power systems have been designed by ORSORT students. The first is a "package reactor" and the second, a "power-breeder." Both indicated considerable promise for this ceramic-fuel element and for associated concepts.

HRP METALLURGY

Metallurgical support to the HRP has continued. Impact tests on commercial iodide and Bureau of Mines titanium have revealed that there is little, if any, environmental effect on the impact properties, except under conditions allowing hydrogen embrittlement. Several different methods of welding stainless steels were evaluated, and a program was initiated to qualify the consumable-insert method and set up an operator-qualification standard. The study of the corrosion behavior of stainless steel welds has continued, and it has been found that ferrite content per se is not so significant a factor as was previously thought. Corrosion testing of titanium, Zircaloy-2, and stressed austenitic stainless steels has continued.

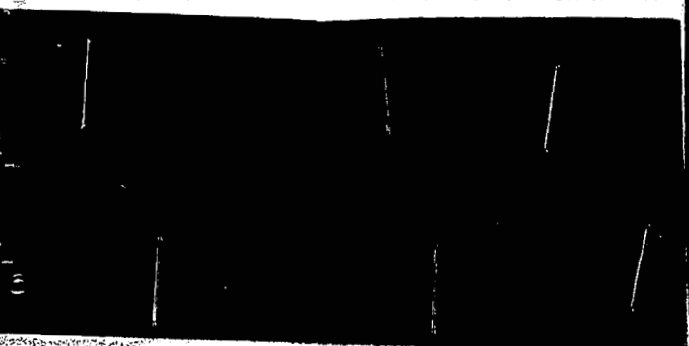

Results of recent brazing tests on full-sized components containing normal uranium are encouraging and tend to support the selection of this method of construction. Several problems encountered in the fabrication of a suitable composite fuel plate for brazing are described. The compound boron carbide, for instance, was found not to be a suitable burnout poison for use in the preparation of uranium dioxide–stainless steel fuel plates. Apparently, B_4C dissociates in the presence of stainless steel under the time-temperature conditions employed in the fabrication schedule and forms a low-melting eutectic phase. Two possible replacement compounds, ZrB_2 and BN, are presently undergoing rigorous time-temperature compatibility studies to determine their stability in contact with stainless steel.

Eighteen different brazed joints have been tested for 1000 hr in 565°F distilled water, at 1200 psi, in the autoclave to aid in the selection of a corrosion-resistant brazing alloy. Weight-change and posttest metallographic data obtained are given. An evaluation study was made on the six most promising brazing alloys on the basis of corrosion resistance, neutron economy, flow temperature, availability, and cost.

Arrangements have been completed to construct and irradiate an experimental stainless steel fuel element in the active lattice of the MTR core. The purpose of the experiment is to obtain performance data on certain engineering material combinations and design features to facilitate the construction of a highly reliable fuel component for long-time service in the package reactor.

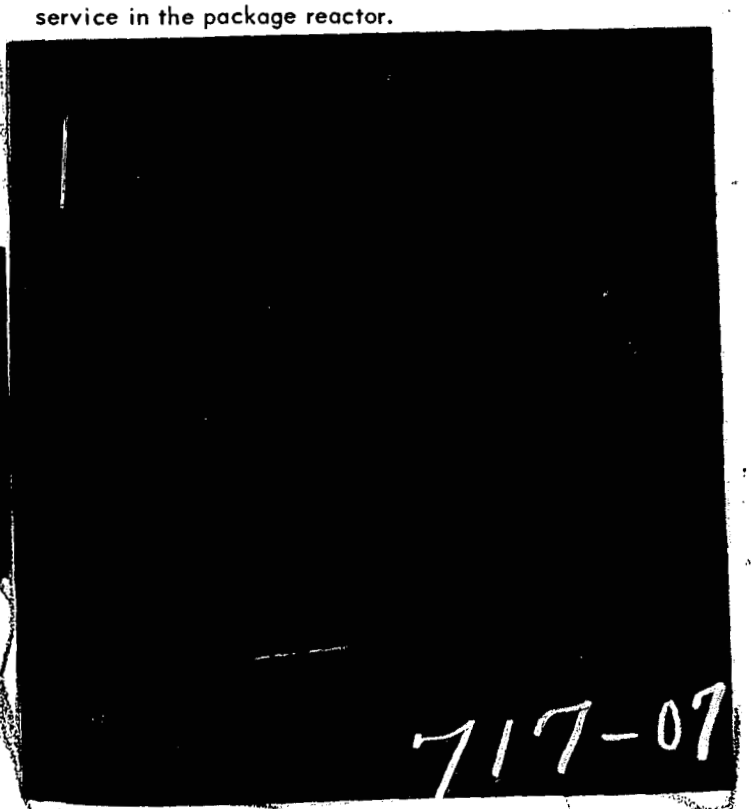

[redacted]

FUNDAMENTAL PHYSICAL METALLURGY

L. K. Jetter

PREFERRED ORIENTATION IN EXTRUDED ALUMINUM ROD

C. J. McHargue L. K. Jetter

With the use of methods previously described,[1,2] whereby data on the distribution of the fiber axis with respect to the crystallographic axes are obtained, a study was made of the fiber-texture type of preferred orientation in some extruded aluminum rod.

Two 0.89-in.-dia aluminum rods were extruded from a 3.125-in.-dia ingot (extrusion ratio 12.3) at a temperature of 450°F. One rod was extruded at a speed of 615 fpm and the other at 0.1 fpm. The rods were water-quenched at the die to retain, insofar as possible, the as-extruded structure.

On 0.19-in. spherical x-ray diffraction specimens taken from near the front end, the middle of the length, and near the back end of each extrusion, pole distribution data were obtained by the spectrometric method described previously.[3,4]

The pole distribution charts (R vs ϕ) for the {111}-{222} and the {002}-{004} planes for the specimens taken from the rod extruded at the faster speed are given in Fig. 1; those from the rod extruded at the slower speed are given in Fig. 2. The charts were obtained by normalizing the diffraction data (I vs ϕ). It was pointed out previously that $R = I(\phi)/I_{ran.}$ and that $I_{ran.}$ can be calculated by graphical integration of the function $I \sin \phi$ from $\phi = 0$ to 90 deg for the various $\{hkl\}$'s.

The axis distribution charts (T vs ϕ,β) deduced from these pole distributions are given in Figs. 3 and 4. On these charts the contours indicate angular locations of equal normalized axis density (T). The pole distributions calculated from these assumed axis distributions are compared with the experimental curves in Figs. 1 and 2. The calculated curves were obtained by averaging the axis density over a path through the unit triangle ϕ degrees from the pole of the plane under consideration [$R(\phi) = \overline{T}(\phi)$].

The axis distribution charts show the textures to be duplex, the <111> and the <001> being the preferred directions of the fiber axis. The axis density at first falls off symmetrically from the peaks at these locations but then asymmetrically to form a "saddle" along the <$\bar{1}$10> zone.

The volume fraction of material associated with each of the <111> and <001> components was computed from the pole distribution charts of Figs. 1 and 2. The results are summarized in Table 1. For both extrusions the ratio <111>/<001> decreases from the front to the back end of the rod and for corresponding locations is greater in the rod extruded at the faster speed.

Associated with this increase in the volume fraction of the <100> component is an increase in the number and size of strain-free grains or subgrains, as shown in the photomicrographs in Figs. 5 and 6. This change in structure is also evident in the increased spottiness of the Debye rings on the x-ray transmission photograms reproduced in Figs. 7 and 8.

It appears that this decrease in the <111>/<001> in extruded aluminum rod is a result of an annealing effect. The effect might be expected to be

TABLE 1. VOLUME FRACTIONS OF MATERIAL ASSOCIATED WITH THE <111> AND <001> COMPONENTS

Extrusion Speed (fpm)	Location in Extrusion	Volume Fraction <111>	Volume Fraction <001>	<111>/<001>
615	Front	0.885	0.115	7.5
	Middle	0.840	0.160	5.2
	Back	0.490	0.510	0.95
0.1	Front	0.675	0.325	2.1
	Middle	0.475	0.525	0.9
	Back	0.310	0.690	0.45

[1] L. K. Jetter, *Met. Semiann. Prog. Rep. Apr. 10, 1953*, ORNL-1551, p 6.

[2] L. K. Jetter and C. J. McHargue, *Met. Semiann. Prog. Rep. Apr. 10, 1954*, ORNL-1727, p 97.

[3] L. K. Jetter, *Met. Quar. Prog. Rep. Jan. 31, 1952*, ORNL-1267, p 21.

[4] L. K. Jetter and B. S. Borie, Jr., *Proceedings of the Spring Metallurgy Conference, March 24–26, 1952*, vol. 2, TID-5084 (June 1952), p 529.

[redacted]

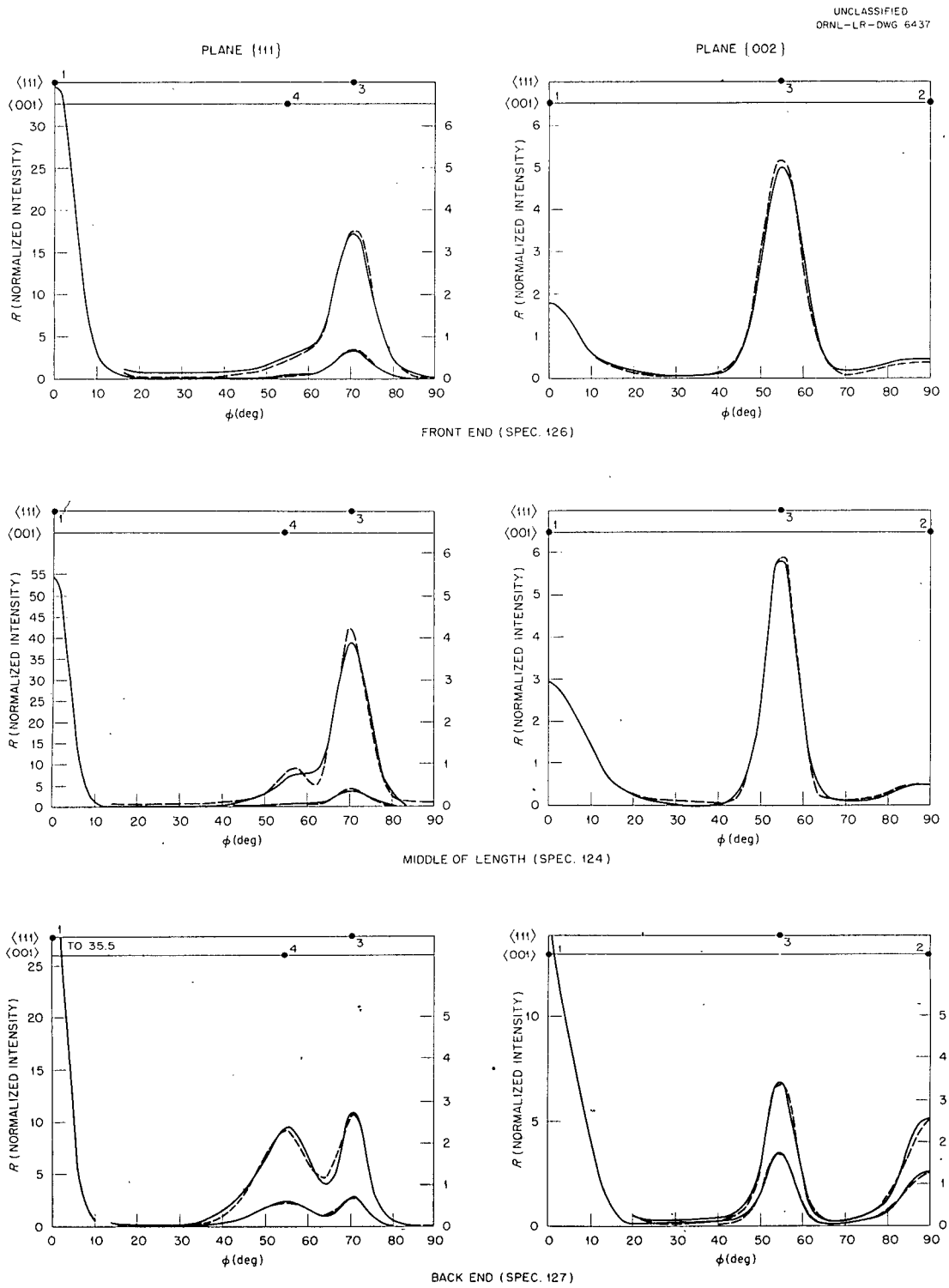

Fig. 1. Pole Distribution Charts for 0.89-in.-dia As-Extruded Aluminum Rod. Extrusion temperature, 450°F; extrusion speed, 615 fpm.

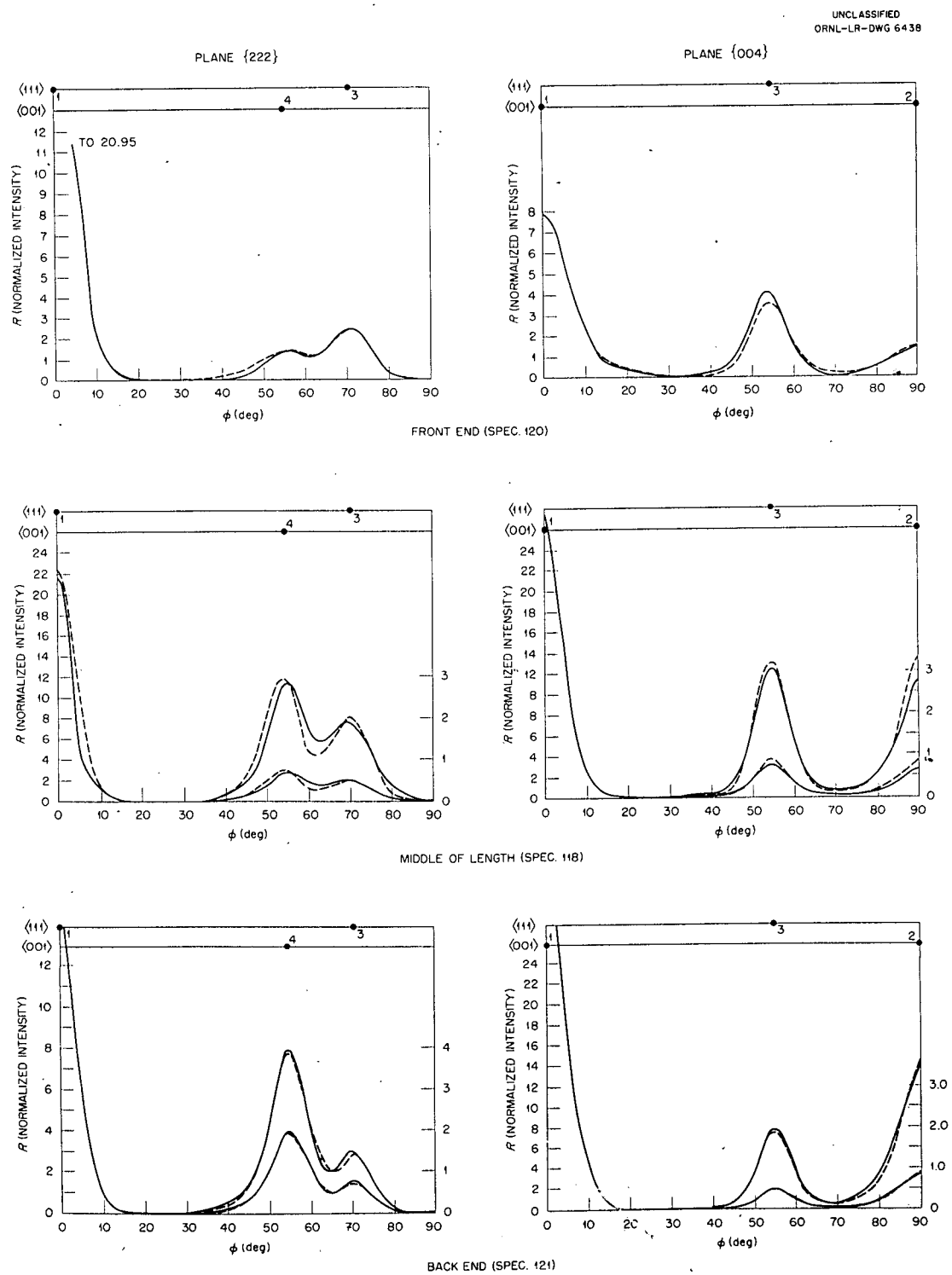

Fig. 2. Pole Distribution Charts for 0.89-in.-dia As-Extruded Aluminum Rod. Extrusion temperature, 450°F; extrusion speed, 0.1 fpm.

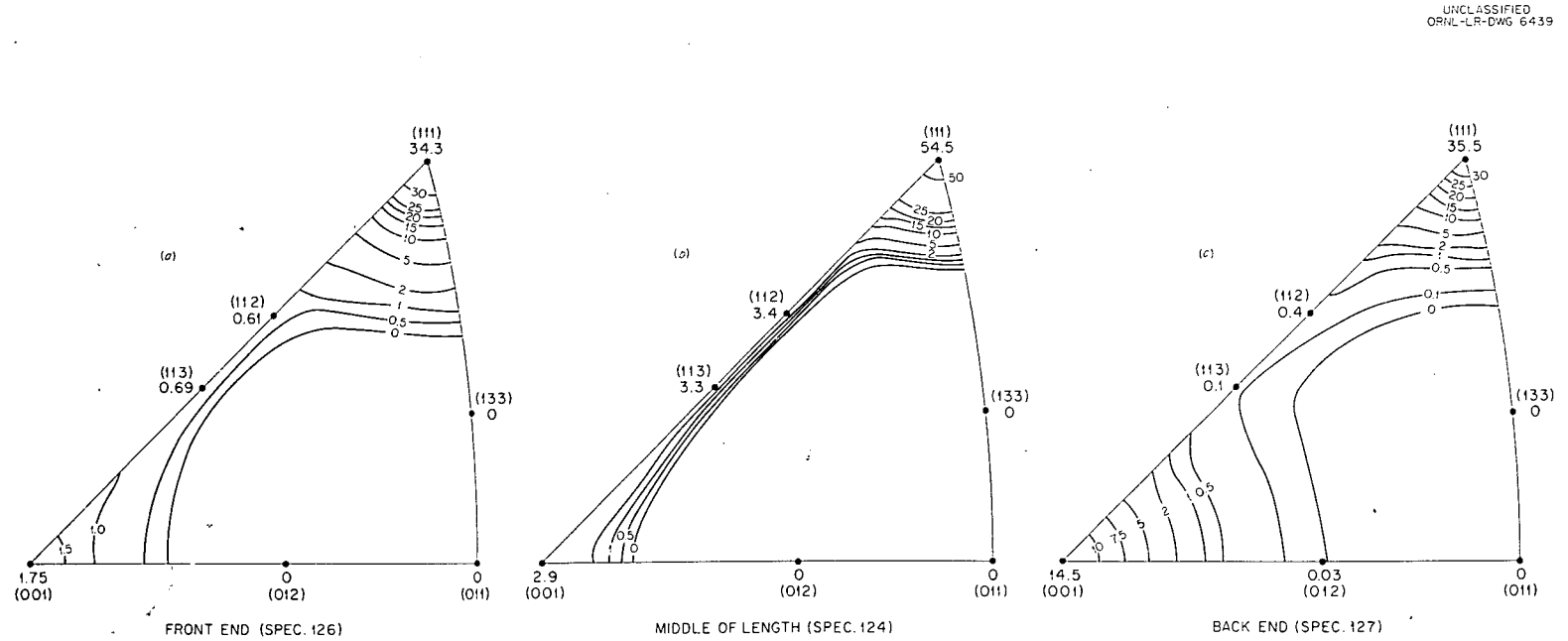

Fig. 3. Fiber Axis Distribution Charts for 0.89-in.-dia As-Extruded Aluminum Rod. Extrusion temperature, 450°F; extrusion speed, 615 fpm.

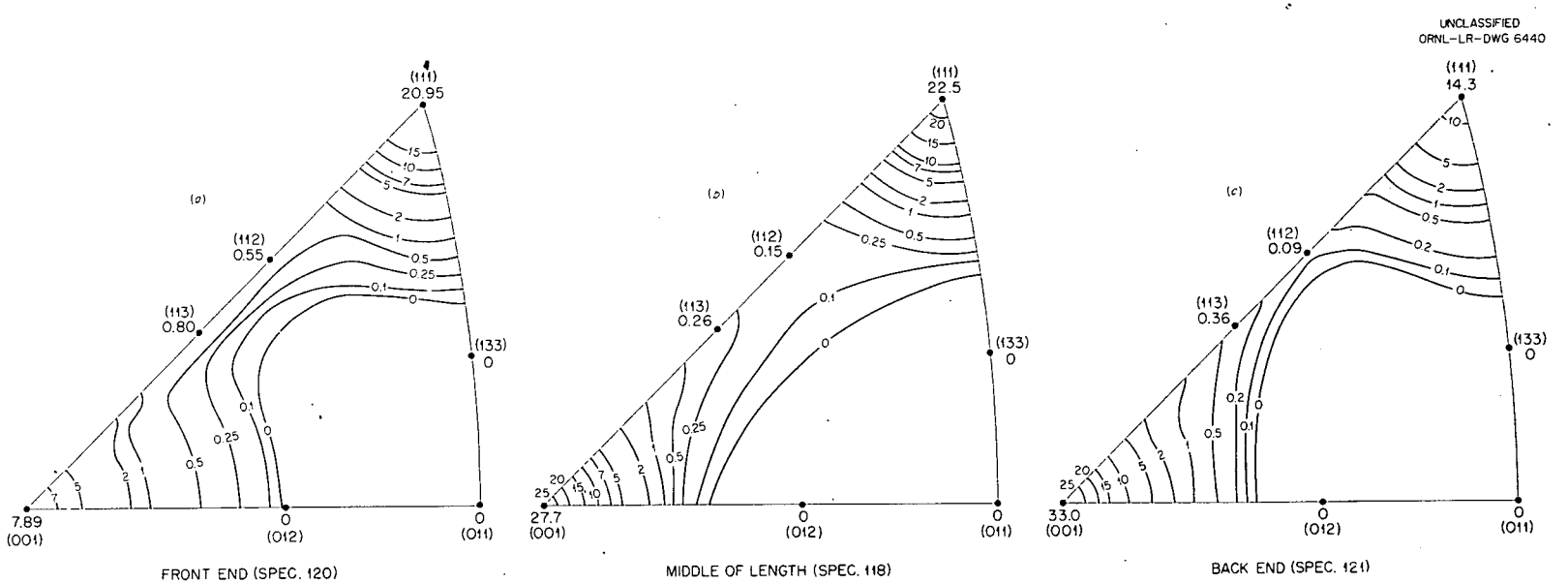

Fig. 4. Fiber Axis Distribution Charts for 0.89-in.-dia As-Extruded Aluminum Rod. Extrusion temperature, 450°F; extrusion speed, 0.1 fpm.

LONGITUDINAL

TRANSVERSE

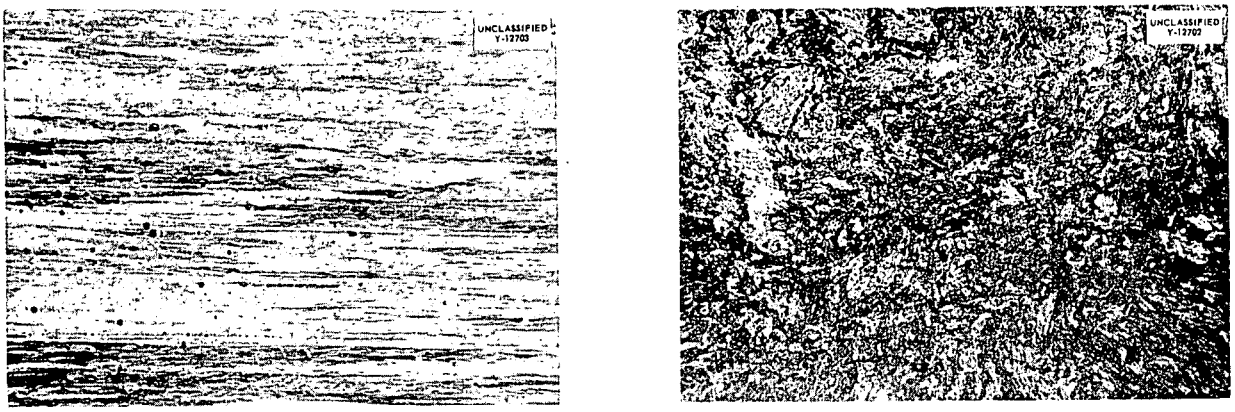

FRONT END (SPEC. 126)

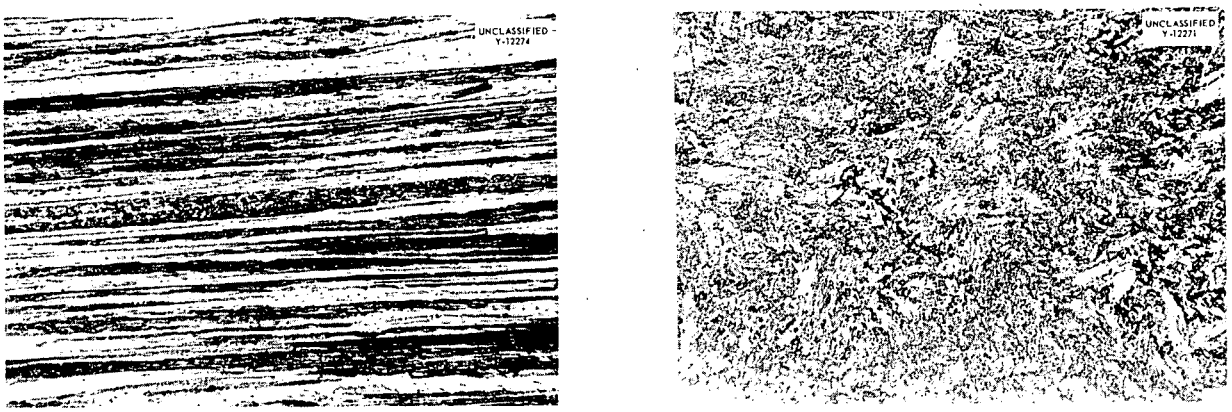

MIDDLE OF LENGTH (SPEC. 124)

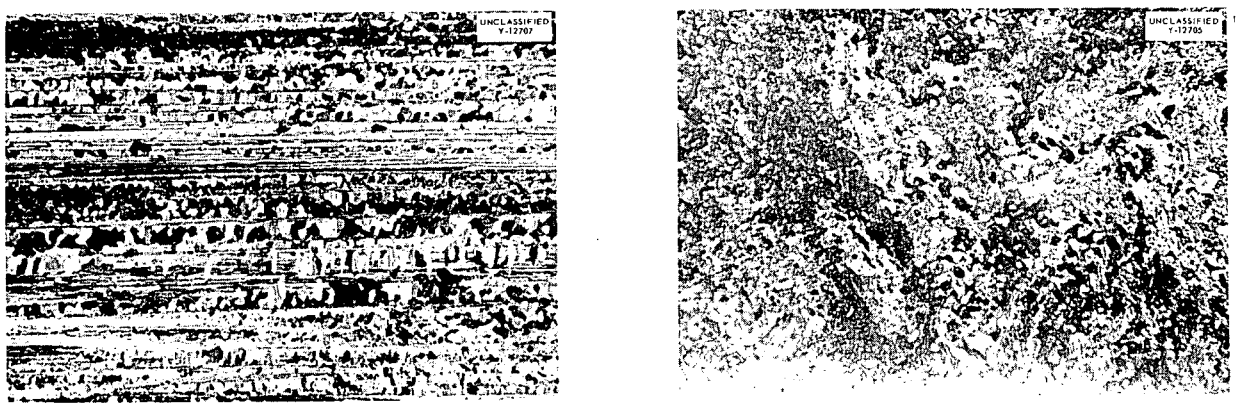

BACK END (SPEC. 127)

Fig. 5. Microstructure of 0.89-in.-dia As-Extruded Aluminum Rod. Extrusion temperature, 450°F; extrusion speed, 615 fpm.

LONGITUDINAL

TRANSVERSE

FRONT END (SPEC. 120)

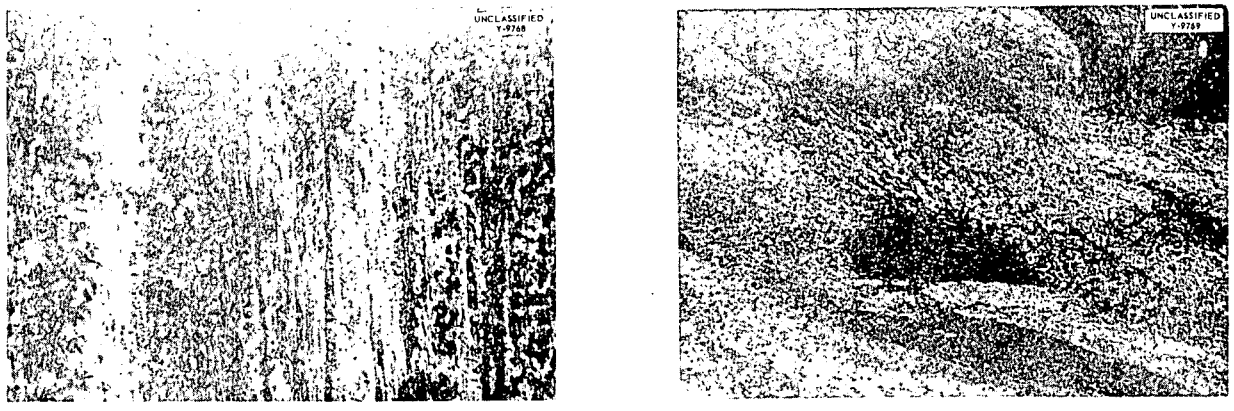

MIDDLE OF LENGTH (SPEC. 118)

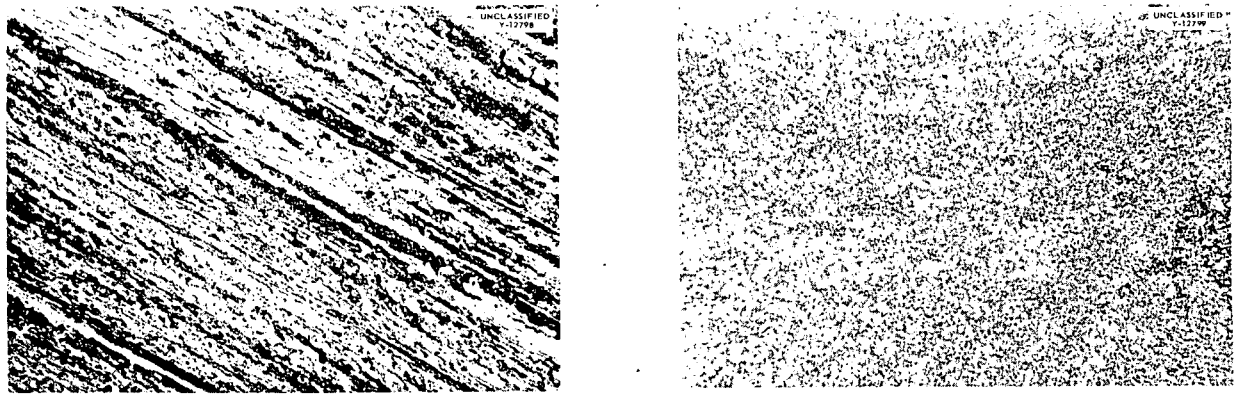

BACK END (SPEC. 121)

Fig. 6. Microstructure of 0.89-in.-dia As-Extruded Aluminum Rod. Extrusion temperature, 450°F; extrusion speed, 0.1 fpm.

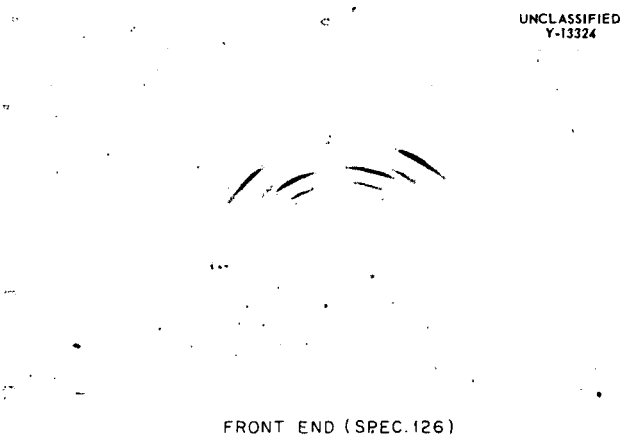

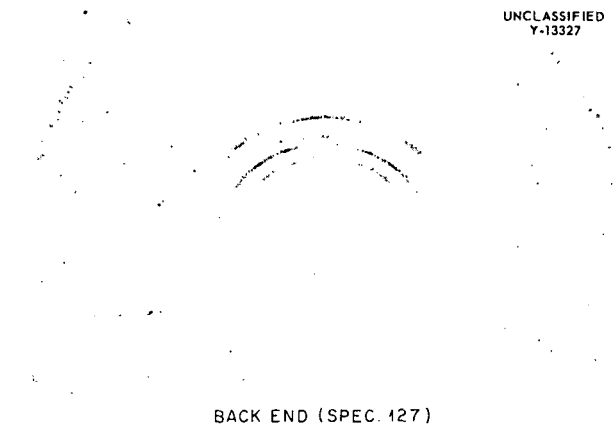

Fig. 7. X-Ray Transmission Photograms of 0.89-in.-dia As-Extruded Aluminum Rod. Extrusion temperature, 450°F; extrusion speed, 615 fpm.

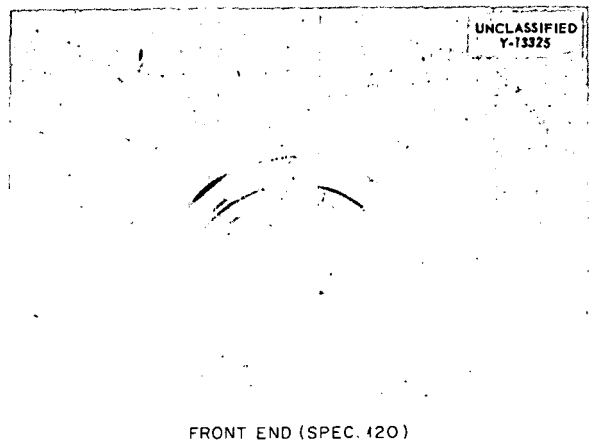

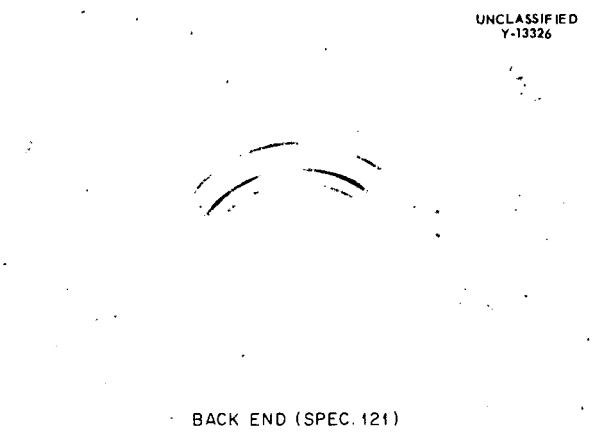

Fig. 8. X-Ray Transmission Photograms of 0.89-in.-dia As-Extruded Aluminum Rod. Extrusion temperature, 450°F; extrusion speed, 0.1 fpm.

greater from the front to the back end of the extruded rod, as a result of increase in temperature, and with decrease in extrusion speed, as a result of the increase in time before the extrusion enters the water spray, as is observed.

REPRESENTATION OF THE SHEET-TEXTURE TYPE OF PREFERRED ORIENTATION

C. J. McHargue L. K. Jetter

In a previous report[1] a thorough appraisal was made of methods of representing the fiber-texture type of preferred orientation. Analysis of preferred-orientation data by the conventional pole-figure method is difficult, if not uncertain, especially when the texture is complicated or not well developed. It was shown that, when the orientation distribution of the poles of the diffracting planes with respect to the fiber axis, as given by the pole figures or pole charts, is converted into orientation distribution of the fiber axis with respect to the crystallographic axes, the type and degree of preferred orientation is represented much more precisely. This new method of representation gives directly the most preferred crystallographic direction of the fiber axis for each component of the texture, the symmetry of distribution about these preferred directions, and the relative volumes of material associated with the various components.

The usual method of analysis of sheet-texture data gives the same ambiguities. It has been found to be instructive, however, to apply the fiber-texture analysis to the sheet-texture type of preferred orientation. Some reference axis in the sheet is treated as a "fiber" axis, and a "fiber" texture is induced by rapidly rotating the x-ray diffraction specimen about this reference axis while the specimen is scanned through ϕ, the angle between the reference axis and the diffracting plane pole. The axis distribution chart deduced from the pole distribution charts obtained in this way, for each of the three reference axes of a sheet – the rolling, normal, and transverse directions – gives the desired data.

With the use of this method, some samples of cold-rolled 65-35 brass sheet and of cold-rolled aluminum sheet were examined. Pieces of each sample were bonded with adhesive to produce laminates sufficiently thick for 0.45-in.-dia spherical diffraction specimens to be prepared. Pole distribution data were obtained by the spectrometric method described previously.[3,4]

The pole distribution charts (R vs ϕ) for the {111} and {002} planes for the brass sheet are given in Fig. 9. The axis distribution charts (T vs ϕ,β) deduced from these pole distributions are given in Fig. 10. The pole distributions calculated from these assumed axis distributions are compared with the experimental curves in Fig. 9.

The more preferred crystallographic directions of the rolling direction are the <112> and the <001>. The axis density falls off symmetrically and rapidly from the peak at <112> but asymmetrically along the <$\bar{1}$10> zone from the peak at <001>. The more preferred directions of the normal direction are the <011> and the <111>. The most preferred direction of the transverse direction is the <111>, although the axis density at <011> is also high. These charts are consistent with the assumption of the following ideal textures: {011}<$\bar{1}$00>, {011}<$\bar{2}\bar{1}$1>, and {111}<1$\bar{2}$1>. These are illustrated on the stereographic projection in Fig. 11. The best previous determination of the texture of cold-rolled brass sheet revealed only the {011}<$\bar{2}\bar{1}$1> component.

The pole distribution charts for the {111} and {002} planes for the aluminum sheet are given in Fig. 12 and the axis distribution charts in Fig. 13.

The most preferred direction of the rolling direction is near <334>. The axis density falls off symmetrically and rapidly from this peak. The most preferred direction of the normal direction is not located at any low index direction – it is about 2.5 deg from <123>. The axis density falls off asymmetrically from this peak. The most preferred direction of the transverse direction is <133>. The ideal texture is thus {123}<$\bar{4}\bar{3}$3> and is illustrated on the stereographic projection in Fig. 14. The preferred crystallographic directions lie 90 deg from one another, as is required for the determination to be consistent. Also illustrated in Fig. 14 is the ideal texture determined by previous investigators using conventional pole-figure techniques.

It is quite evident that axis distribution charts provide a very satisfactory means of representing data not only of the fiber-texture type but also of the sheet-texture type of preferred orientation. They give the desired information directly and precisely, and many features and details not readily discernible from the pole distribution charts are plainly evident.

PURIFICATION OF ZIRCONIUM BY ZONE MELTING

G. D. Kneip J. O. Betterton

Isothermal heat treatment of zirconium and the establishment of the resulting phases present in equilibrium in the vicinity of the *bcp* → *bcc* transition temperature provide an extremely sensitive method of determining the over-all impurity content of the material. Studies of a number of batches of grade-1 zirconium crystal bar show a two-phase region approximately 40°C wide (834–875°C) in the least pure, and 20°C wide (855–875°C) in the most pure, materials.

For the study of the binary alloy systems of zirconium which exhibit very limited solubility of the alloying element in zirconium or which have eutectoid or peritectoid temperatures near the zirconium-transition temperature, a source of metal containing fewer impurities than grade-1 zirconium crystal bar is highly desirable.

Because of the reactive nature of zirconium, it appears that an investigation of the zone melting might be particularly fruitful because of its relatively high purification factor and because the material need not be in contact with a contaminating crucible.

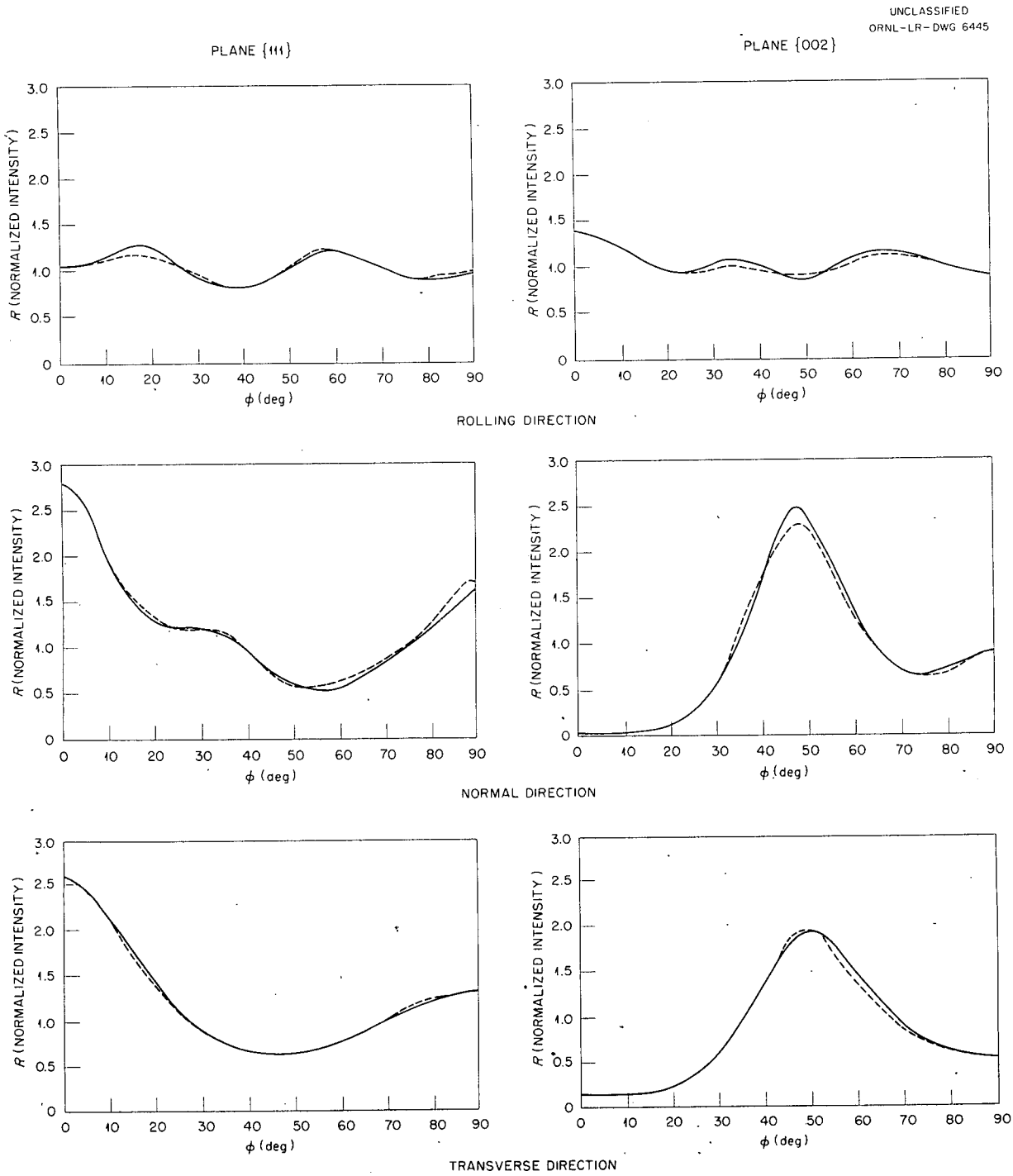

Fig. 9. Pole Distribution Charts for 0.057-in.-Thick Cold-Rolled 65-35 Brass Sheet (Specimen 110Z).

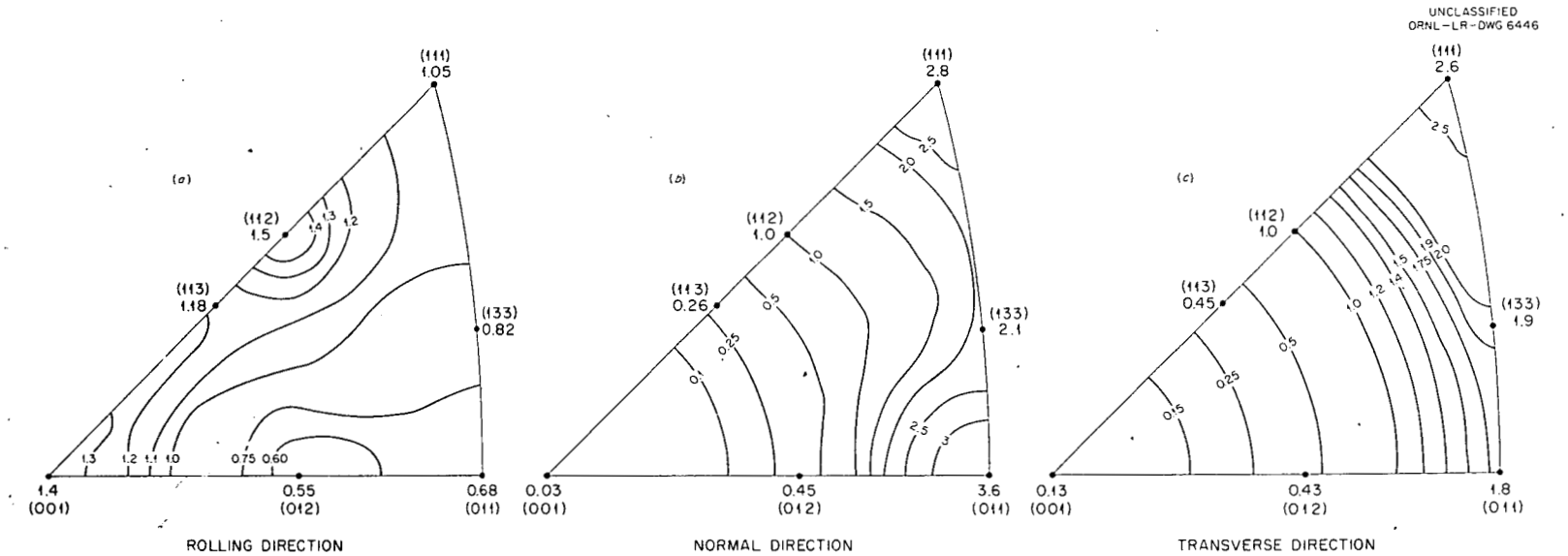

Fig. 10. Axis Distribution Charts for 0.057-in.-Thick Cold-Rolled 65-35 Brass Sheet (Specimen 110Z).

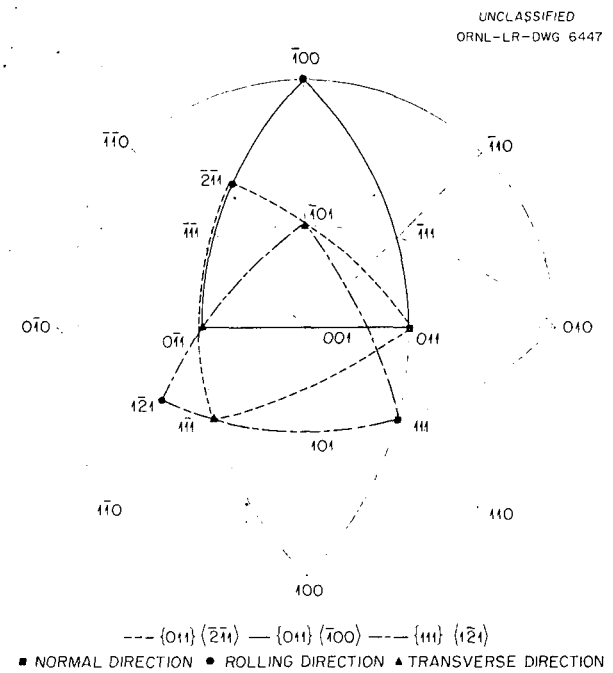

Fig. 11. Ideal Textures for Cold-Rolled 65-35 Brass Sheet.

According to Keck, Green, and Polk,[5] the maximum-radius rod which will support a stable floating zone is given by

$$x_{max} = 0.65 \left(\frac{2\alpha}{\rho g} \right)^{1/2} ,$$

where α is the surface tension and ρ the density of the material. Although the value of the surface tension of zirconium has not been reported in the literature, it can be estimated from the shape of ingots which have been arc melted and allowed to solidify on a relatively flat surface. Thus, considering a mass of liquid, the surface energy must equal the potential energy, and assuming that the mass takes the form of an oblate spheroid as a result of the forces of surface tension and gravity, then

$$\alpha A = mgx , \quad (1)$$

where

α = surface tension,
A = area,
m = mass of the liquid,
g = gravitational constant,
x = distance from the center of mass to the bottom of the spheroid.

The area of the spheroid can be expressed as a function of its major and minor axes, a and b, as

$$A = 2\pi a^2 + \pi \frac{b^2}{e} \ln \frac{1 + e}{1 - e} ,$$

where

$$e = \frac{\sqrt{a^2 - b^2}}{a} ,$$

and the mass can be expressed as a function of the density, ρ, and the volume of the spheroid as follows:

$$m = \rho V = \rho \frac{4}{3} \pi a^2 b .$$

Thus Eq. 1 can be rewritten as

$$\alpha = \left(a^2 + \frac{b^2}{e} \ln \frac{1 + e}{1 - e} \right) = \frac{4}{3} \rho g a^2 b ,$$

or the surface tension α is

$$\alpha = \frac{\frac{4}{3}\rho g a^2 b}{a^2 + (b^2/e) \ln [(1 + e)/(1 - e)]}$$

$$= \frac{8360 a^2 b^2}{2a^2 + (b/e) \ln [(1 + e)/(1 - e)]} ,$$

where a and b are the major and minor axes, respectively, of the spheroid in centimeters and the density of zirconium has been taken to be 6.4 g/cm^3.

With the use of this equation the value of the surface tension has been computed for a number of arc-cast buttons of zirconium. The values observed show some dependence on the size of the ingot, as shown in Fig. 15, probably because the melts were not actually spheroids and because the melts were made in a depression of hemispherical shape in the hearth. The value of the surface tension of zirconium, extrapolated to zero volume to eliminate these effects, is found to be 220 dynes/cm at the melting point.

The maximum radius, then, for rods at equal radii, which supports a stable floating zone of

[5] P. H. Keck, M. Green, and M. L. Polk, *J. Appl. Phys.* 24, 1479 (1953).

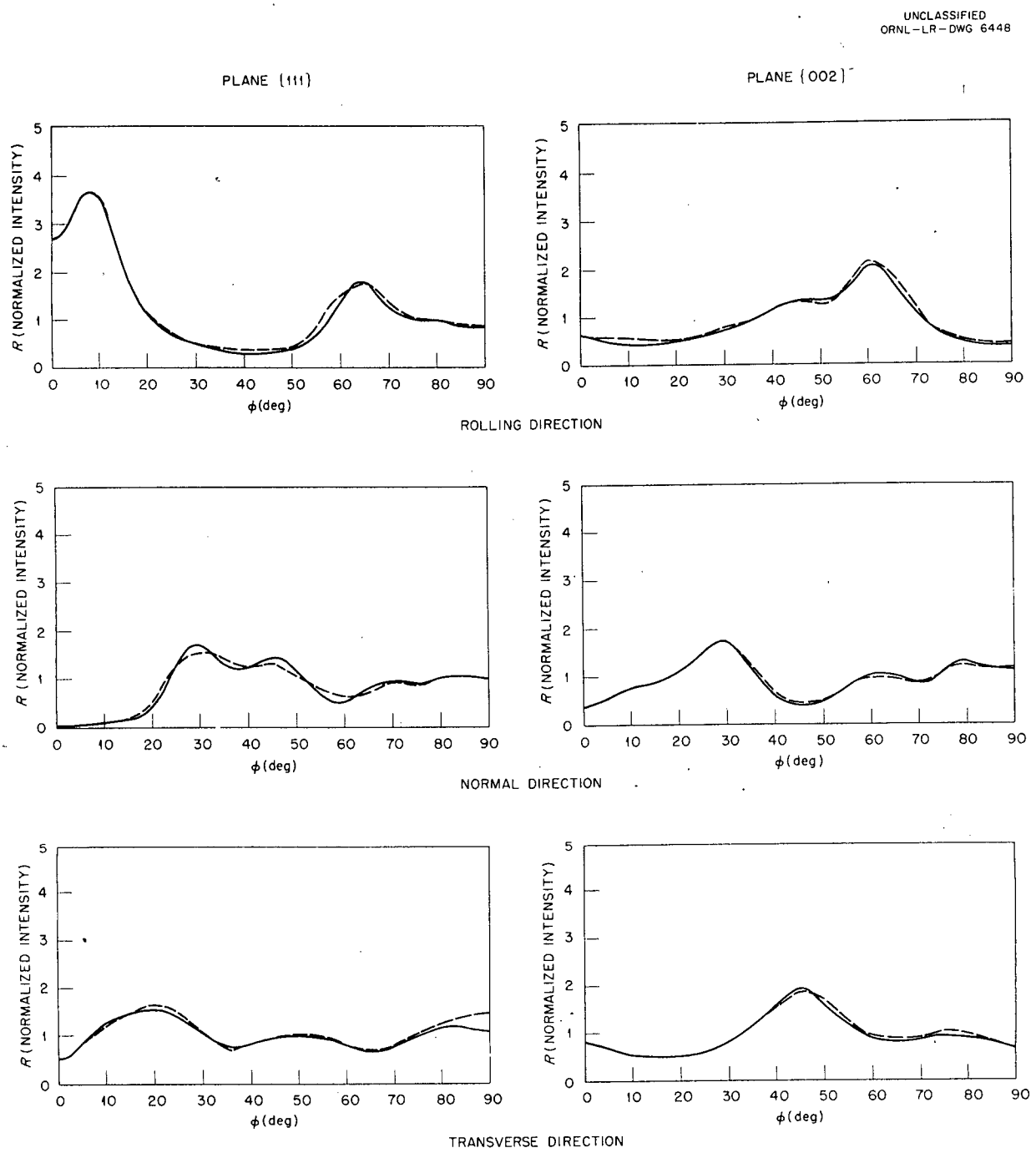

Fig. 12. Pole Distribution Charts for 0.046-in.-Thick Cold-Rolled Aluminum Sheet (Specimen 111Y).

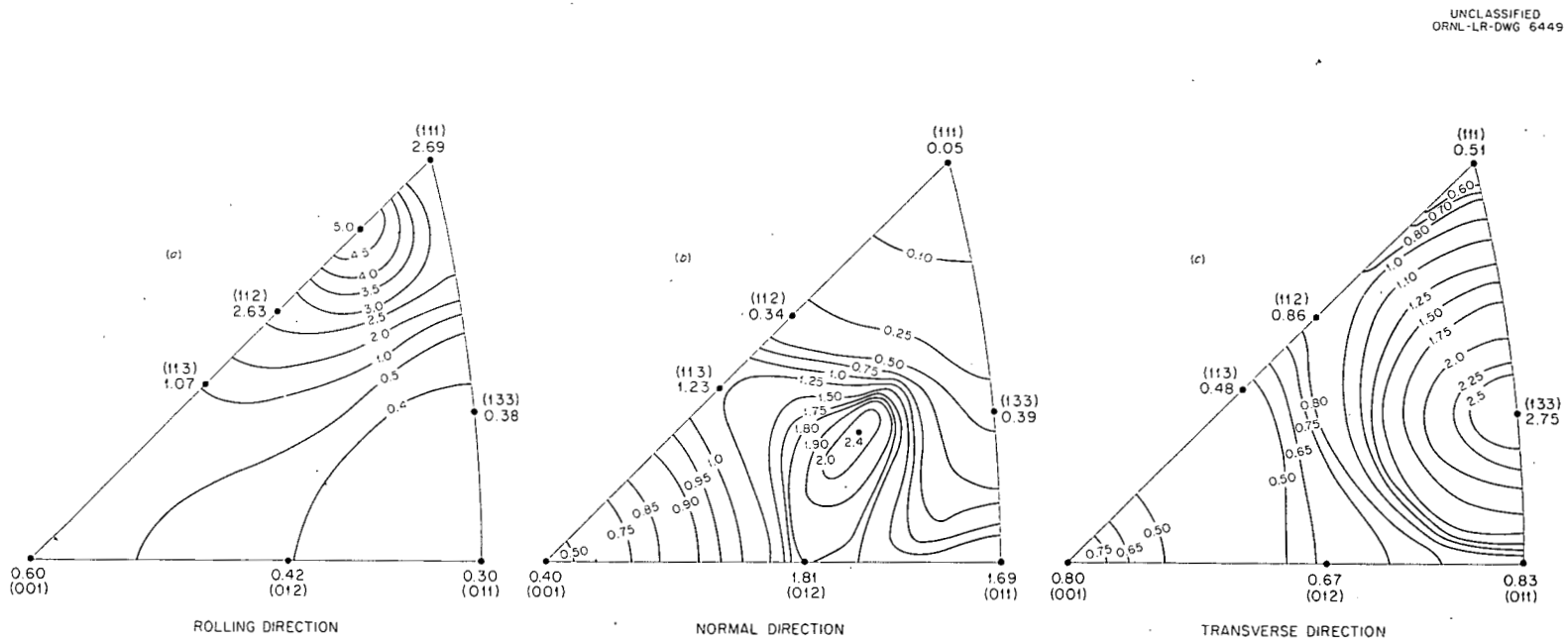

Fig. 13. Axis Distribution Charts for 0.046-in.-Thick Cold-Rolled Aluminum Sheet (Specimen 111Y).

zirconium occurs for

$$r = 0.65\left(\frac{2\alpha}{\rho g}\right)^{1/2} = 1.7 \text{ mm}.$$

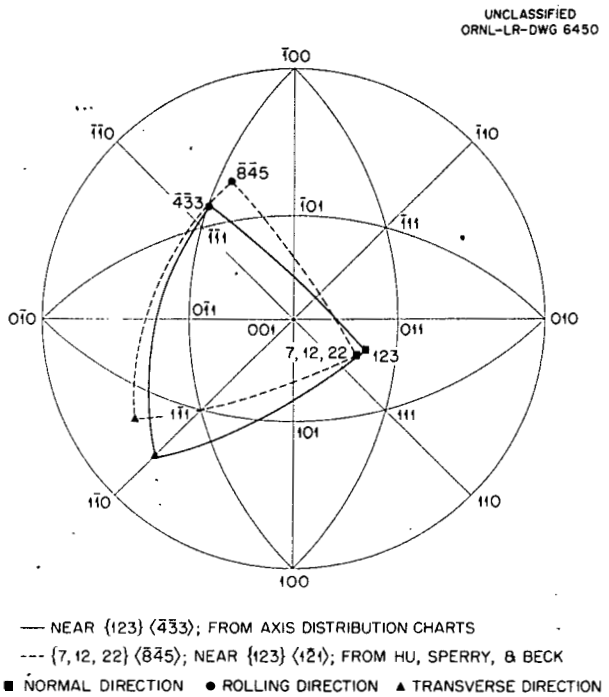

Fig. 14. Ideal Textures for Cold-Rolled Aluminum Sheet.

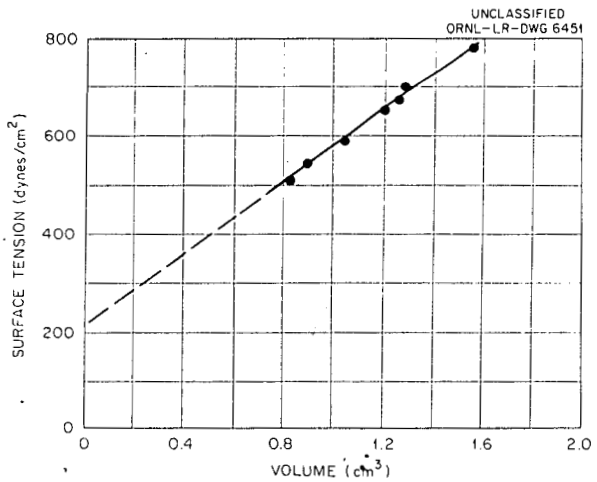

Fig. 15. Surface Tension of Zirconium as Calculated from Major and Minor Axes of Arc-Melted Getter Buttons vs Button Volume.

Thus for zirconium the production of stable floating molten zones is possible for rods approximately 3.5 mm (⅛ in.) in diameter and smaller.

If iron is assumed to be the sole impurity affecting the zirconium $\alpha \rightarrow \beta$ transition, then from the zirconium-iron diagram,[6] Fig. 16, it can be seen that an iron concentration of only 50 ppm will produce a two-phase region nearly 20°C wide and that the iron content must be reduced to about

[6] *The Reactor Handbook*, vol. 3, p 567, Technical Information Service, AEC, 1953.

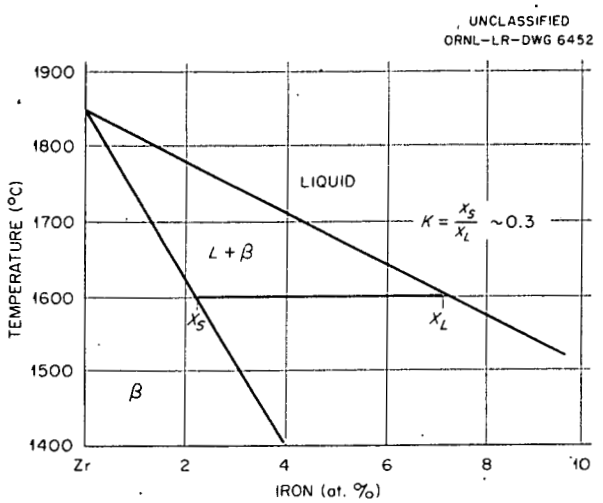

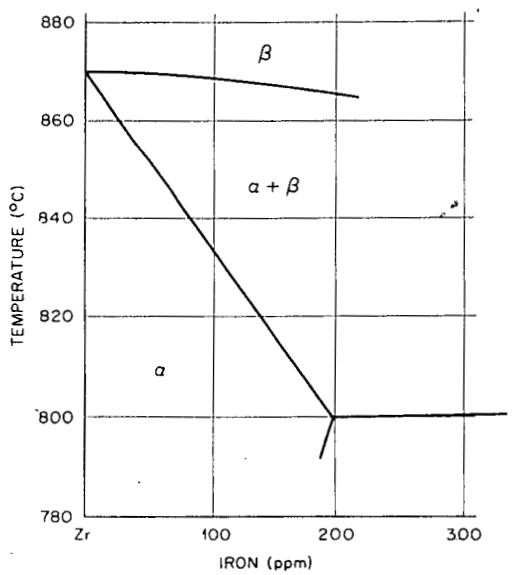

Fig. 16. Portions of Zirconium-Iron Phase Diagram.

15 ppm to reduce the extent of the two-phase region to 5°C. For the case of iron in zirconium the distribution coefficient, k, the ratio of the solute concentration in the solid to that in the liquid, is about 0.3.

According to Lord,[7] the impurity concentration after one pass, $c_1(a)$, as a function of the number of zone lengths melted, a, is given by

$$c_1(a) = C_0[1 - (1 - k)\, e^{-ka}] ,$$

and after successive passes

$$c_2(a) = c_1(a) - (1 - k)C_0\, e^{-ka}\,[1 - e^{-k}\,(1 - ka)] ,$$

$$c_3(a) = c_2(a) - (1 - k)C_0\, e^{-ka}\left\{1 - e^{-k}\,(1 - ka) - k\, e^{-2k}\left[(1 - ka) + \frac{a}{2}\,(2 - ka)\right]\right\} .$$

Figure 17 shows the impurity content vs distance along the bar for one pass through three passes, as calculated from these equations. A very few passes of the molten zone over the zirconium bar should reduce the iron content, or the content of a similar impurity, at the point at which the molten zone is started to such an amount as to be undetectable as a two-phase region after isothermal annealing.

Movement in the opposite direction occurs for impurities such as oxygen and carbon, which raise the melting point. Thus, in order to obtain relatively pure material, it may be necessary to make quite a number of passes and then crop both ends of the ingot.

A preliminary experiment conducted with an available 5-mm-dia zirconium rod showed the floating zone to be on the verge of stability, as had been predicted. On one specimen three passes were made successfully. During the fourth pass, however, the rod parted at about the mid-position, owing to the irregularities in diameter caused by the first three passes. Figure 18 shows a rod after two passes of the molten zone.

The experimental apparatus is illustrated in Figs. 19 and 20. Three-millimeter-diameter zirconium rod, which should support a stable zone, is being fabricated for further experiments.

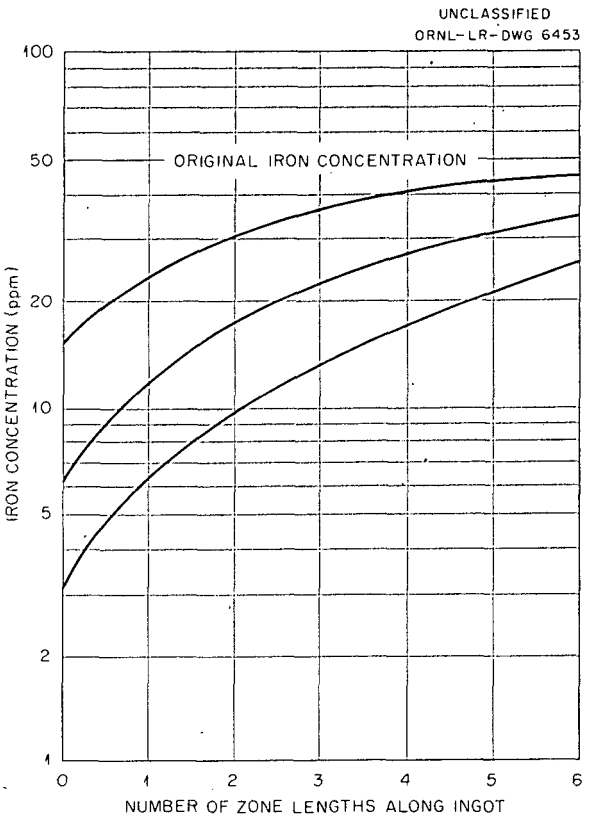

Fig. 17. Impurity Concentrations After Zone Melting (k = 0.3).

[7] N. W. Lord, *J. Metals* 5, 1531 (1953).

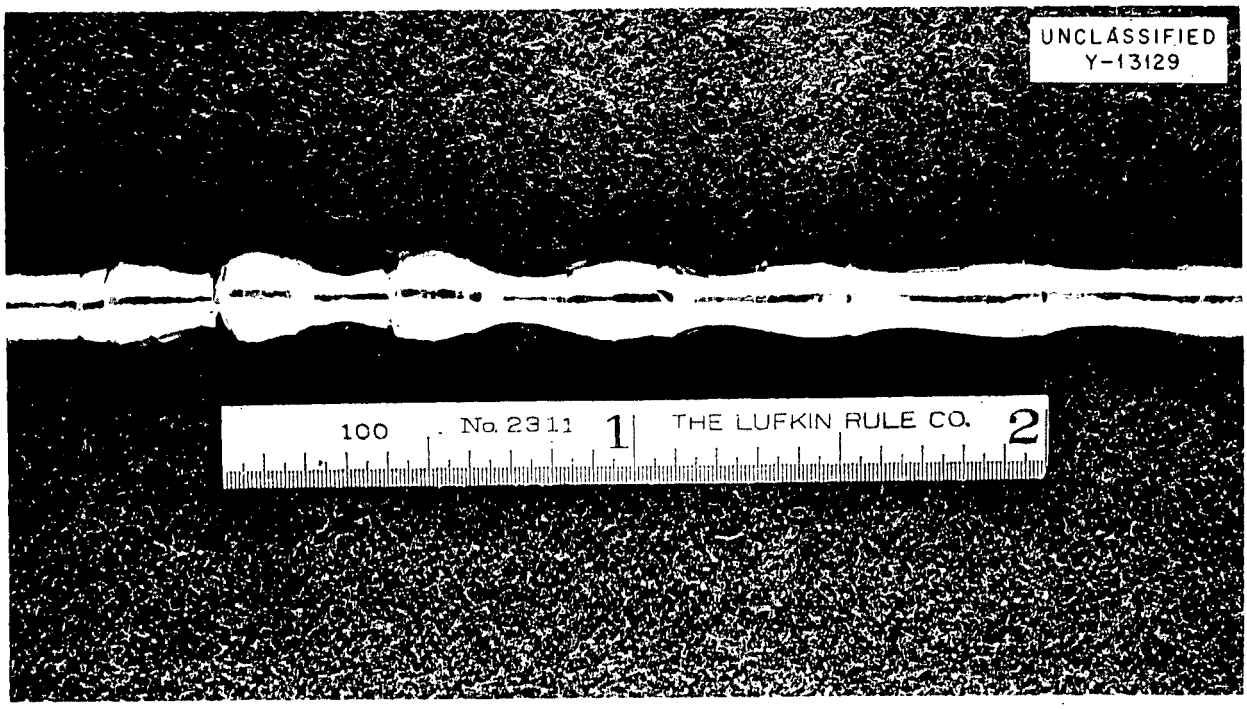

Fig. 18. Arc-Melted Zirconium Rod.

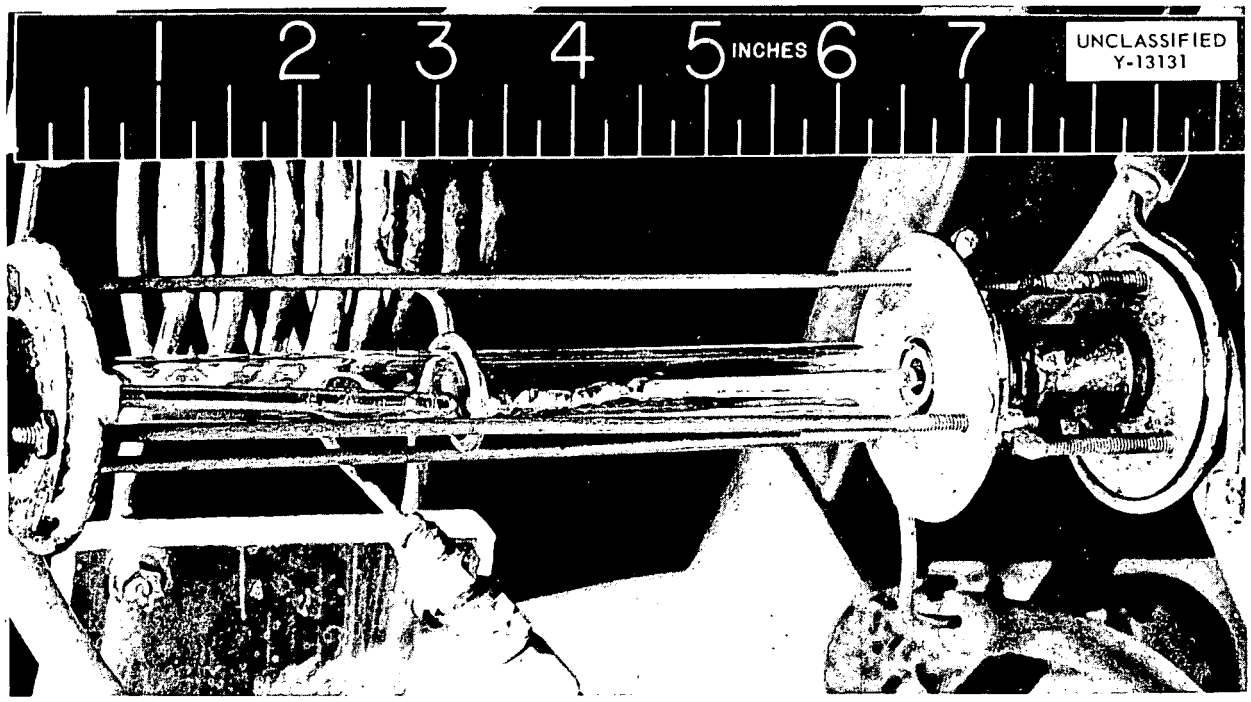

Fig. 19. Zone-Melting Furnace.

717 028
24

UNCLASSIFIED

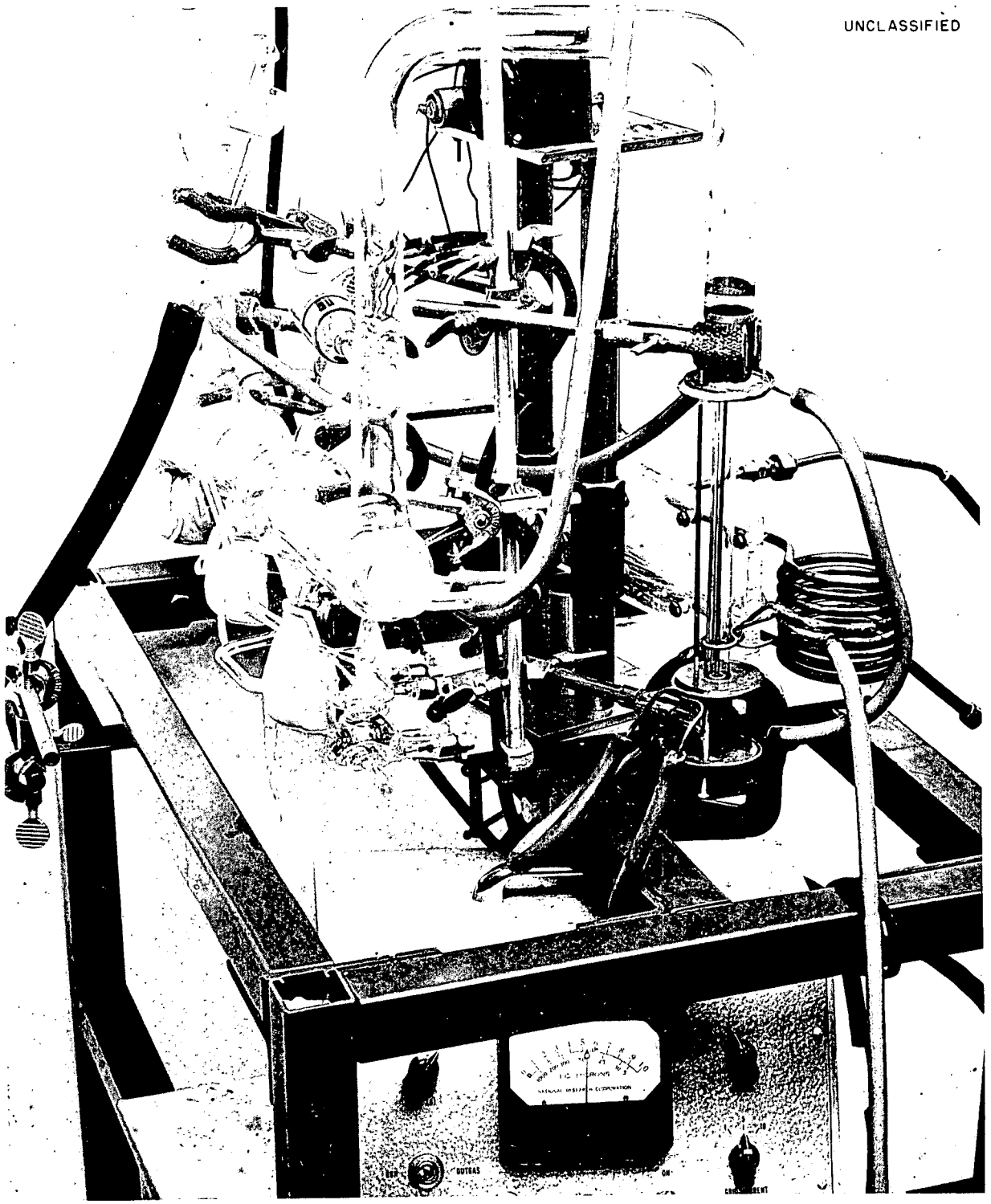

Fig. 20. Zone-Melting Equipment, Showing Traveling Work Coil.

PHYSICAL METALLURGY OF REACTOR MATERIALS

E. J. Boyle

TRANSFORMATION KINETICS OF ZIRCONIUM-BASE ALLOYS

M. L. Picklesimer E. E. Stansbury

Phase-diagram studies have shown the presence of a eutectoidal transformation in the Ag-Zr system. Transformation-kinetics studies of these alloys have been initiated in an effort to determine whether improved mechanical properties may be derived from isothermal transformation of zirconium-base alloys.

Several eutectoid Ag-Zr ingots of nominal 3.5 at. % Ag have been arc-cast in a consumable-electrode arc furnace for use in studying the transformation kinetics of the Ag-Zr eutectoid.[1] Single-melt ingots were not sufficiently homogeneous to provide enough material for the transformation studies. One double-melted ingot appeared to be homogeneous, but it cracked when it was rolled. Transformed specimens indicated that the ingot was contaminated, although the contaminant has not been revealed by chemical analysis.

It has been necessary to use single-melt ingots to determine some of the characteristics of the transformation kinetics. Three types of transformation products have been identified. These are (1) a pearlitic-type transformation product quite similar to pearlite in steels and having a lamellar structure, which is nucleated in the grain boundaries and which grows into the grain at an approximately constant temperature; (2) a bainitic-type transformation product nucleated in the grain boundaries, consisting of individual alpha needles surrounded generally by a precipitate presumed to be $AgZr_2$, and growing only in certain directions governed by the original beta grain; and (3) a martensitic-type transformation product very similar to martensite in steels, consisting of fine needles, and formed on the quench to room temperature by an apparently diffusionless transformation. The progress of the transformation to bainite, pearlite, and alpha has been studied at 750 and 800°C. The partial TTT diagram is quite similar to that for a hypoeutectoid steel, with the exception that the bainitic-type transformation occurs at all temperatures at which the pearlitic type occurs. The progress of the transformation at 800°C may be described as follows: Alpha first forms in some of the grain boundaries, then bainite forms, and then pearlite. All may be forming at the same time in the early stages of transformation. In the alloys studied so far, the alpha formation was complete at 800°C in 3 min and occupied 2% of the volume of the specimen, the bainite formation was complete in 5 min and occupied 15% of the volume, and the pearlite formation was complete in less than 60 min and occupied the remainder of the volume. The formation of alpha and bainite reached completion before 25% of the specimen was transformed. The progress of the transformation at 750°C was the same, except that it was faster. Unfortunately, enough homogeneous alloy was not available for the study to be continued at that time.

The tempering of the martensitic structure at 800°C has been studied in another hypoeutectoid ingot of nominal 3 at. % Ag. Specimens were held for 30 min at 900°C and quenched in mercury in the transformation equipment.[1] These specimens were reinserted individually into the center lead pot of the transformation equipment at 800°C for times varying from 15 sec to 24 hr and were again quenched in mercury. The hardness of the specimens decreased from the original as-quenched hardness of 300 DPH (100-g load) to 235 DPH at 15 sec, 1 min, and 5 min and to 190 DPH at 15 min, 2 hr, and 24 hr. The changes in the microstructure were (1) precipitation of the intermetallic compound in the martensite matrix, (2) growth and spheroidization of the precipitate, (3) nucleation of new alpha grains in the depleted matrix, and (4) growth of the new alpha grains into the depleted martensite matrix until the microstructure consisted of recrystallized large-grained alpha containing dispersed large particles of the intermetallic compound $AgZr_2$. Complete recrystallization of the depleted matrix at 800°C required at least four days. Lack of sufficient material of the same composition has prevented further study at other temperatures.

Considerable time and effort have been expended in developing metallographic techniques for use

[1] E. E. Stansbury and M. L. Picklesimer, *Met. Semiann. Prog. Rep. April 10, 1954*, ORNL-1727, p 1.

on these alloys. Scratch-free polishes have not been obtained without considerable polish relief, whereas polishing with fine diamond paste leaves undesirable scratches that must be etched out. Most polishing is stopped after 4-0 paper has been used, and the surface is prepared for etching by chemical polishing with a solution consisting of 50 ml of H_2O, 20 ml of HNO_3, 5 ml of HCl, and 3 ml of HF. Two etching solutions have been developed that are satisfactory, one working better than the other for specimens in different conditions. One consists of the chemical polishing solution with HF replaced by 0.3 g of $NH_4F \cdot HF$, and the other is the I_2 and KI etch reported previously.[1]

An anodizing procedure, based on the procedure and solution reported by Ence and Margolin,[2] has been developed for the identification (in bright-field illumination), by color, of the microconstituents of the zirconium-base alloys. The solution consists of 20 ml of glycerine, 35 ml of H_2O, 60 ml of alcohol, 5 ml of H_3PO_4, 10 ml of lactic acid, and 2 g of citric acid, the composition not being very critical. If the etched specimens are immersed in the solution for 1 to 4 sec (depending on the surface area) at 110 v, the colors developed in bright-field illumination are as follows: martensite, yellow; pearlite, red; bainite, dark red; alpha, blue to pink, depending on time; aged martensite, brown to purple; and $AgZr_2$, tan to light brown. At 20 v for 2 to 10 sec, the colors developed are, primarily, different shades of the same color. However, fine details of the microstructure obscured by the 110-v anodizing and not revealed by straight etching are revealed by the 20-v treatment. Contrast in the microstructure under polarized light is markedly increased by the 20-v treatment. The precipitate formed around the bainite needles is revealed by the 20-v treatment and is obscured by the 110-v treatment.

Mounted specimens have been successfully polished electrolytically in concentrated HCl at 4 to 10 v by the following procedure. Each specimen is completely immersed in the solution, and the surface to be polished is situated uppermost, a stainless steel wire-screen cathode being placed above the specimen. The polishing is difficult to control in that a gross unevenness of the surface may develop; such unevenness is not too serious for cursory examination at high magnification but is unsatisfactory for low magnification. The technique has been successfully used to put zirconium-base alloys into solution for chemical analysis without contaminating the solution with the fluoride ion.

The automatic feed mechanism for the consumable-electrode-arc furnace[1] has been completed and installed in the arc furnace. Test melts have not, as yet, been made.

SLAGGING EXPERIMENTS ON STAINLESS STEEL FUEL ELEMENTS

J. A. Milko

Work has been continued on the problem of concentrating the uranium from stainless steel fuel elements by melting the elements under a nonmetallic phase. Several different types of nonmetallic phases were used, as is indicated below. In the work described, compacts of UO_2 in a matrix of stainless steel were used to simulate fuel elements.

An attempt was made to melt a compact in a graphite crucible under a cover consisting of sodium carbonate and sodium tetraborate, but the cover boiled away before the compact melted.

When a compact was melted under a slag consisting of 114 g of CaO, 60 g of Al_2O_3, and 126 g of SiO_2, the uranium contents of the slag and metal were 11.38 and 0.001%, respectively, indicating that the UO_2 had been extracted by the slag almost quantitatively. The cooled slag was hard and brittle, and to extract the uranium from it would probably be difficult.

Compacts were melted under slags consisting of CaO, SiO_2, and CaF_2, in which the molecular ratio of CaO to SiO_2 was approximately 2 to 1, in an attempt to find a material that would quantitatively extract uranium from the metal phase and that would disintegrate when it was cooled. None of the resulting slags disintegrated when they were cooled, and the uranium was not extracted completely, as is shown by the data in Table 2.

A compact melted in a graphite crucible in air under a mixture consisting of 72% CaF_2 and 28% FeF_2 resulted in the extraction of substantially all the uranium into the fluoride phase, the metal analyzing 0.001% uranium and the slag 8.57% uranium. A test with similar materials melted in a partial vacuum was unsuccessful because too much of the fluoride volatilized. In disagreement

[2] E. Ence and H. Margolin, *J. Metals* 6, 346 (1954).

subsequent chemical recovery processes. Uranium recovery from carburized stainless steels is being studied by J. E. Savolainen, of the Chemical Technology Division, who has established the feasibility of a possible recovery process.[3]

A technical report covering both metallurgical and chemical studies on this process is being written. Only a brief summary of the work will be reported here.

Basic steps of a possible recovery process are listed below:

1. Carburization, to add carbon to the stainless steel.
2. Homogenization, to diffuse the carbon throughout the steel so that passivity is completely destroyed.
3. Dissolution treatment with $CuSO_4$ solution, which reacts with the active iron-nickel matrix. Iron and nickel are taken into solution and copper is plated out. Uranium dioxide and chromium carbides are not affected.
4. Reaction with nitric acid to dissolve the uranium dioxide and copper. The chromium carbides (and some iron carbides) remain as solids, which may be stored if they are sufficiently low in uranium.
5. Treatment of the nitric acid solution by solvent extraction for recovery of uranium.

The following test is described to illustrate techniques and as an example of the uranium recovery that has been obtained from a laboratory test.

A specimen of fuel plate (clad with 0.005 in. of type 304 stainless steel, with a stainless steel core 0.020 in. thick containing 34 wt % uranium dioxide) was carburized for 1 hr at 975°C. The specimen, then containing about 1.4% carbon, was homogenized for 1½ hr at 1150°C. For dissolution, the specimen was treated with boiling $CuSO_4$ solution for 17½ hr. The solution was analyzed for uranium. The fuel element, then coated with copper, was treated in boiling 70% nitric acid for 2 hr, and the solution was analyzed for uranium. The insoluble residue was dissolved in aqua regia and analyzed for uranium.

The distribution of the uranium recovered in the three solutions is shown in Table 4.

TABLE 4. DISTRIBUTION OF URANIUM RECOVERED IN THREE SOLUTIONS

Solution	Total Uranium Recovered (%)
$CuSO_4$ solution	0.03
HNO_3 solution	99.25
Residues in aqua regia	0.72

These results and the techniques used are not typical of optimum procedures, but they do indicate that very high uranium recoveries may be attained.

Further work is being done to optimize chemical dissolution techniques and to define the degree of carburization required. Thus far, activity tests indicate that maximum dissolution rates are obtained with about 2% carbon; other factors, however, must also be considered.

Sufficient carburizing experiments have been made to show that small test specimens of type 304 stainless steel can easily be carburized to contain up to 4% carbon. These experiments were made in a 2-in.-dia ceramic tube furnace by passing an atmosphere of about 18% methane in dry hydrogen through the furnace at about 1½ fpm. Under these conditions, the relation between carburizing time, temperature, and amount of carbon absorbed by type 304 stainless steel 0.031 in. thick is shown in Fig. 21.

Carbon can be uniformly distributed throughout the thickness of fuel elements by homogenizing in an inert atmosphere for 2 hr at 1100°C. This treatment is required in order to allow uniform and complete reaction between the stainless steel and the dissolving solutions. The sensitizing treatment previously used to cause precipitation of the chromium carbide is not necessary, since the carbides are formed directly from the austenite.

From these results it seems apparent that carbon absorption and diffusion in stainless steel fuel elements will not be major problems in development of this method for recovery of uranium.

OXIDIZING OF ZIRCONIUM FUEL ELEMENTS

R. E. Adams

Metallurgical treatments are being studied in an effort to assist in the recovery of uranium from zirconium-type fuel elements.

TABLE 2. RESULTS OF MELTING STAINLESS STEEL–UO_2 COMPACTS UNDER SILICATE SLAGS

No.	Slag Composition (%)			Uranium Content (%)	
	CaO	SiO_2	CaF_2	Metal	Slag
1	65	35	10	0.14	7.61
2	45	24	31	0.91	20.73
3	45	24	31	0.61	10.46

with the results of former experiments in which compacts were melted under a mixture of CaF_2 and FeF_2, a recent melt made under a mixture of 61% CaF_2 and 39% FeF_2 yielded a metallic button containing 0.93% uranium and a slag containing 17.7% uranium. Further experiments are being made in an attempt to explain this discrepancy.

A compact melted under a mixture of 71% NaF and 29% FeF_2 resulted in a metallic button containing only 0.001% uranium and in a slag containing 11.47% uranium.

A test in which a compact was melted under pure CaF_2 resulted in only partial extraction of the uranium; the metal contained 0.57% uranium and the slag 8.5% uranium. About the same fraction of uranium was extracted when a compact was melted under a mixture of 84% CaF_2 and 16% Fe_2O_3, as is indicated by the resulting uranium content of the metal being 0.68% and that of the slag 11.14%.

REDUCTION OF UF_4 WITH ALUMINUM

J. A. Milko

A number of years ago it was found that uranium-aluminum alloys rich in aluminum could be produced from metallic aluminum and UF_4 by simply permitting the molten aluminum to reduce UF_4 dissolved in molten cryolite ($3NaF \cdot AlF_3$). When properly carried out, the reduction of uranium is substantially complete. Because of the possible economy of this method for making alloys for fuel elements with enriched uranium, as compared with bomb reduction of UF_4 and then alloying with aluminum, a study is being made of the reduction of UF_4 from molten fluorides to produce uranium-aluminum alloys. A large fraction of the uranium in the salt phase can be reduced and can enter the metal phase because the activity of the uranium in the metal is much smaller than unity for the alloys of interest. Work has been done on the production of alloys containing 20% uranium, approximately 2.8 at. %.

Four reductions of uranium from a fluoride phase were made; the quantities of materials used are indicated in Table 3. In carrying out each reduction, the fluorides were mixed; added to a graphite crucible, together with aluminum; and then heated to a temperature of 1150°C for 10 min. The quantities of aluminum and UF_4 were such that an alloy containing 20% uranium would result if all the uranium was reduced. The exact amount of recovery was somewhat uncertain, however, because of the sampling technique used. Additional reductions have been made in which an improved sampling practice was used, but analyses are not yet available.

TABLE 3. REDUCTION OF UF_4 INTO ALUMINUM

No.	Weight (g)			Uranium Content (%)	
	UF_4	Al	NaF	Metal	Fluorides
1	133	416	149	17.48	1.62
2	133	416	101	18.41	5.9
3	133	416	63	18.99	1.51
4	133	416	44	19.13	1.47

CARBURIZING OF STAINLESS STEEL FUEL ELEMENTS

R. E. Adams

Carburization of the stainless steel fuel elements proposed for the Package Power Reactor is being examined as a method for facilitating uranium recovery from the spent fuel elements. Carburization of these elements causes essentially all the chromium to combine chemically with carbon. This effectively removes chromium from the austenitic matrix, so that the metal is not passive. In this condition, stainless steel may then react with relatively weak dissolving solutions, and the uranium can be extracted by simple chemical methods.

The utility of the carburizing treatment for recovery of uranium is thus intimately related to

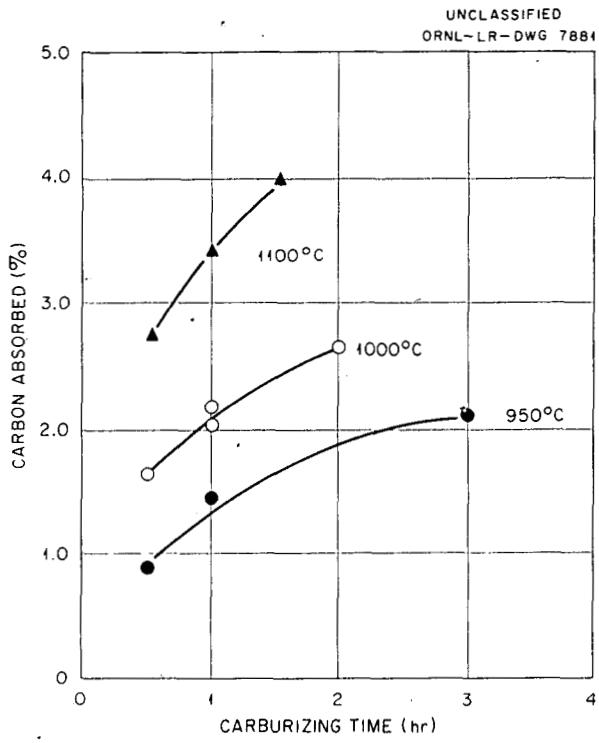

Fig. 21. Effect of Time and Temperature on Amount of Carbon Absorbed in 0.031-in.-Thick Type 304 Stainless Steel.

Preliminary work has indicated that it may be possible to oxidize zirconium-type fuel elements completely and to treat the resulting oxide powder with nitric acid so that the uranium dioxide is dissolved, thus leaving the zirconium dioxide as a waste solid.

Oxidizing tests have indicated that specimens of dummy STR fuel plates can be reduced to an oxide powder by heating them in air for about 6 hr, at 950°C. Extraction with nitric acid has shown that some of the uranium is soluble. The completeness of uranium recovery is not known, however, since uranium analysis of the zirconium dioxide residue has not yet been obtained.

METALLOGRAPHIC EXAMINATION OF ALUMINUM-SILICON-BONDED THORIUM SLUGS

R. J. Gray

A thorium slug canned in aluminum by the Al-Si bonding technique was examined metallographically for R. P. Wischow of the Chemical Technology Division of ORNL.

Considerable difficulty had been encountered in dissolving the canned slug in 13 *N* HNO_3, 0.038 *M* NaF and 0.0025 *M* $Hg(NO_3)_2$. Metallographic examination of the as-canned slug revealed two intermetallic compounds between the Al-Si alloy and the thorium, as shown in Figs. 22*a* and *b*. These compounds were identified by R. M. Steele by x-ray analyses as β-$ThSi_2$ and $ThSi_2$. Apparently, silicon diffused into the thorium and formed the two compounds. It can be concluded that the diffusion was in this direction by the presence of the dark globular-shaped ThO_2 within both the thorium and the compound layers. A continuous fracture was also present in the intermetallic compound, as shown in the photomicrographs (Fig. 22) and also by the easily parted, smooth, bright interfaces of a semicylindrical slug section and aluminum can shown in Fig. 23. This fracture would have considerable effect on the heat-transfer properties from the thorium to the aluminum can, if thorium slugs canned by this procedure were used in a reactor.

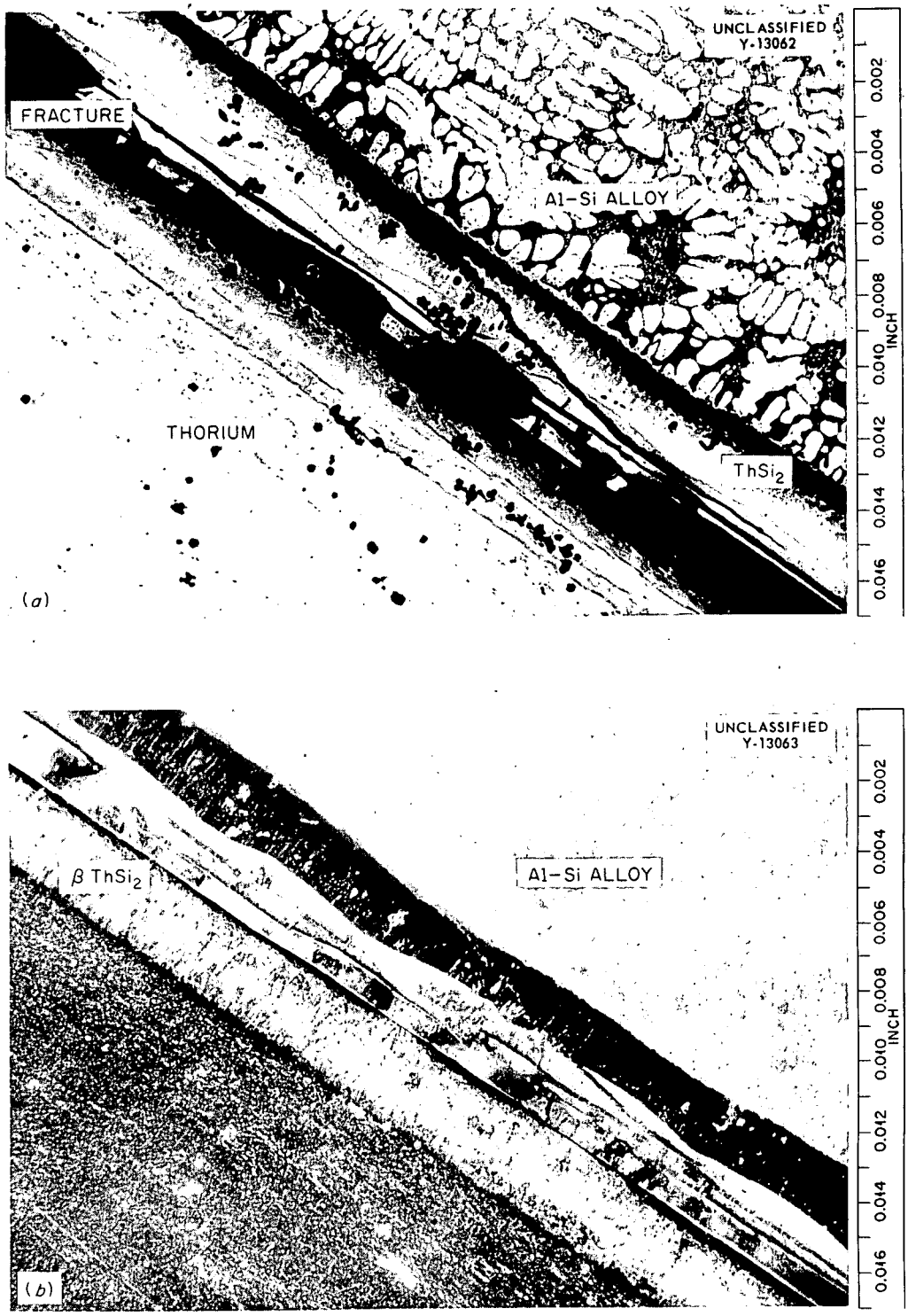

Fig. 22. Photomicrograph of Bond Between Thorium and Al-Si Alloy. (*a*) Bright field; note continuous fracture in intermetallic compounds. (*b*) Polarized light; note two compound layers.

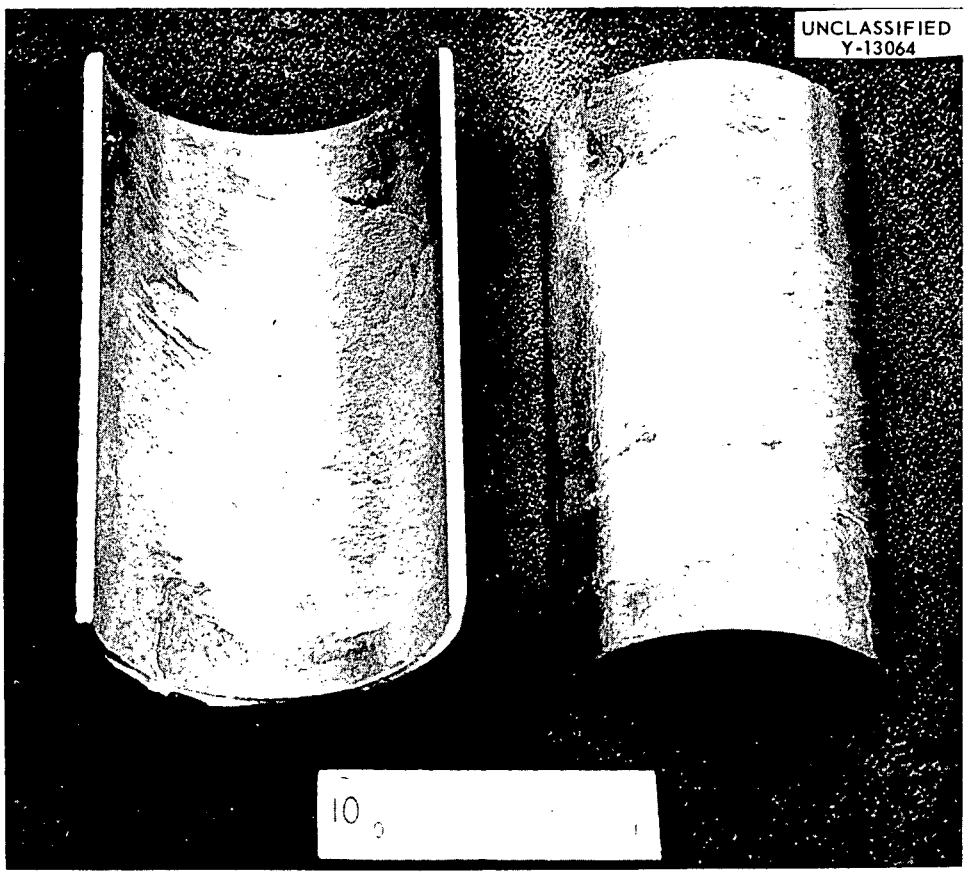

Fig. 23. Semicylindrical Section of Al-Si Bonded Thorium Slug. Note smooth bright surface of aluminum can on left and thorium on right, denoting poor bonding.

CERAMICS RESEARCH

J. M. Warde
J. R. Johnson
C. E. Curtis
L. M. Doney
S. D. Fulkerson
R. L. Hamner
A. J. Taylor
G. D. White

DEVELOPMENT OF A CERAMIC FUEL ELEMENT AND ASSOCIATED REACTOR CONCEPTS

Introduction

The advantage of high temperatures in reactor power systems can be realized by use of refractory ceramic materials. Satisfactory power plants using gas coolants at high temperatures are an engineering reality. Because of the brittle nature of ceramics and the fact that their corrosion resistance to high-temperature liquids is not any better than that of metals in general, liquid cooling of ceramics involving plumbing systems is not practical at present. It was early established, therefore, that the most compatible and practical high-temperature system would be a gas-cooled reactor power plant with ceramic core materials.

In the selection of materials for fuel elements and moderator, three general criteria were applied:

1. low thermal-neutron capture cross section,
2. optimum physical properties (high thermal conductivity, no porosity, high-temperature strength, low expansion, high service temperature, corrosion resistance to gas coolant),
3. economy (fabricability by standard methods, availability of pure raw materials).

A study of known materials indicated that the oxides were generally unsatisfactory because of their poor thermal conductivities and that most carbides, nitrides, and silicides could not be made nonporous. A silicon-bonded silicon carbide was chosen for a fuel-element material because it more nearly met the above requirements than any other material considered. A body of this kind has been made for a number of years by The Carborundum Company under the trade-mark name Durhy. This product, however, was unsatisfactory for reactor use because of its porosity and relative inhomogeneity. A program was undertaken to produce a satisfactory body containing the necessary fuel and to conduct the required tests.

For economy and safety, graphite was chosen over beryllium oxide as the moderator material. This choice then made necessary the use of a closed-cycle inert-gas system. Nitrogen, carbon dioxide, and helium have been considered as coolants.

Two reactor designs in which these principles and materials are used have been made by ORSORT summer study groups. The first, a package reactor, indicated that a very compact and relatively simple power system could be built with the use of existing equipment. The second, a power-breeder reactor, showed that the ceramic fuel element and associated concepts had a good potential in this field also. The plant design results in 60 Mw of electric power at 40% over-all efficiency, and a conversion ratio of 1.0 was obtained, with the use of the U^{233} cycle. Only equipment which is now available or considered practical was utilized in the design.

Summary of Development and Testing

Producing a suitable SiC-Si body for reactor use is a major development problem. In attempting to obtain a nonporous homogeneous body, many materials and techniques have been used. The basic method for producing SiC-Si, invented by The Carborundum Company, consists in impregnating a porous carbon body with molten silicon. An exothermic reaction occurs simultaneously, generating cubic SiC. Previously known materials and techniques yielded unsatisfactory bodies; so a special program of development was instigated.

The porous carbon or graphite body may be obtained in several ways, but the method most easily controlled is that of mixing powdered graphite with a material which is partially volatile so that, in a subsequent baking step, the graphite body formed from such a mix will be porous. The additive must also serve as a binder for the formed graphite bodies so that they can be readily handled. After baking, it must leave a residue which tends to knit the structure together, giving the baked product suitable strength. This product must be strong so that it can be handled, and it must hold together in the impregnation process. Of a number of materials tried, glucose

has been found to be the most satisfactory so far. Such binders as naphthalene, Carbowax, etc., which volatilize completely, are unsatisfactory. Starches, sugars, etc., on the other hand, are generally satisfactory in this respect.

Another feature of the initial mix which requires careful control is the grain size. Nonporous homogeneous SiC-Si with a minimum of unreacted carbon can be produced only by using very fine grained (~1 to 10 μ) graphite particles and then by making certain that the graphite-additive mix is also very fine grained before forming the body to the desired shape.

Associated with the nature of the binder and grain size is the forming pressure. The most satisfactory forming method conceived for producing fuel-bearing elements of SiC-Si is dry-pressing of the powdered mix in a steel die. The porosity and thus the impregnability of the body are sensitive to the forming pressure. Many of the binders which are otherwise satisfactory are too sensitive to the forming pressure to be practical.

The baking process is the simplest and most easily controlled step in the entire operation; difficulties arise, however, from reactions of the fuel materials with water vapor and possibly other gases which are given off as the binder volatilizes. Thus uranium carbide readily oxidizes, and there are indications of some oxidation of the uranium silicides. Also, UO_2 may go to U_3O_8. These reactions involve volume changes, some of which damage the body. The most successful baking process when the fuel materials are either the silicides or the oxides of uranium is a 1000°C treatment in an argon atmosphere.

Impregnation is best carried out by using induction heating of a graphite crucible containing the silicon. The reaction, forming SiC from the porous carbon body, is quite rapid if the silicon is near its boiling temperature (1800–2000°C). A slower, more controlled, impregnation reaction occurs at about 1700°C. Less warpage and less tendency to absorb excess silicon are also noted at lower temperatures.

Testing of the SiC-Si fuel-element material should be carried out in the reactor under simulated service conditions. Nevertheless, a number of useful tests can be made prior to such an experiment. In addition to physical-property measurements, an engineering evaluation of both the fuel element and the moderator materials is under way. A device has been constructed in which nitrogen is blown over an electrically self-heated specimen at high velocity. This test will primarily serve to measure erosion-corrosion of the graphite. With the use of the same electric power source, the fuel-element specimens are heated in air to destruction by thermal stress to determine the maximum allowable heat flux.

One of the requirements for fuel elements in a closed-cycle reactor power system is that they retain fission products so as not to contaminate the power machinery. An indication of fission-product retention can be obtained in a simple comparative test. A small button containing uranium in its core, simulating a fuel element, is exposed to neutrons in order to generate fission products. It is then heated in a sealed silica glass tube so that volatile fission products which escape from the button are contained. One end of the tube is immersed in liquid nitrogen after cooling, and the fission products are condensed and frozen. This end of the tube is sealed off, and its activity is measured. This test indicates that less than 0.01% of the xenon generated will escape at operating temperatures. The activity of other products such as iodine and tellurium is too low to identify. There has been some evidence of migration of neptunium to the surface of the test samples.

Designs have been made for in-pile gas loops for testing fuel plates containing enriched uranium. The experience and data from the tests outlined above will be used to modify these designs.

Over-all Program

Table 5 is a proposed outline of the steps that must be taken before an actual reactor power system can be built. Many of these steps (those marked with an asterisk in the table) have been under way for some time.

Reactor Power-Plant Design Summary

The fuel element and associated concepts are ideal for a closed-cycle power system. Two such systems have been designed by S. T. Robinson of Sanderson & Porter and are described below in the reactor power-plant studies. These studies were made by two independent groups of ORSORT students. The group was headed by J. Gallagher, and the Breeder Reactor group was headed by J. Smith.

TABLE 5. CERAMIC REACTOR PROGRAM

Body Development	Testing	Supporting Calculations	Reactor Calculations
*1. Selection of base composition	*1. Physical-property measurements	1. Fission-product diffusion *a. Buildup of volatile elements *b. Coolant activity c. Adsorption	*1. Effect of uranium percentage in element on size
*2. Fuel studies	*2. Diffusion of fission products	2. Fuel-element thermal calculations *a. Thermal stresses b. Power density	2. Effect of heat flux on size
*3. Improvement of body	*3. Engineering evaluation	3. Surface effects *a. Erosion-corrosion b. Temperature effects	3. Effect of coolant activity
	*4. Neutron damage to SiC-Si		*4. Criticality
	5. LITR-enriched-plate test		*5. Heat removal
	6. In-pile engineering test		6. Control
	7. Initial reactor experiment		7. Initial reactor experiment design

*Work has been in progress for some time.

Although the designs here presented are not complete or final, they contain sufficient detail to indicate the usefulness of the ceramic fuel elements in two very different kinds of reactor power systems.

[redacted]

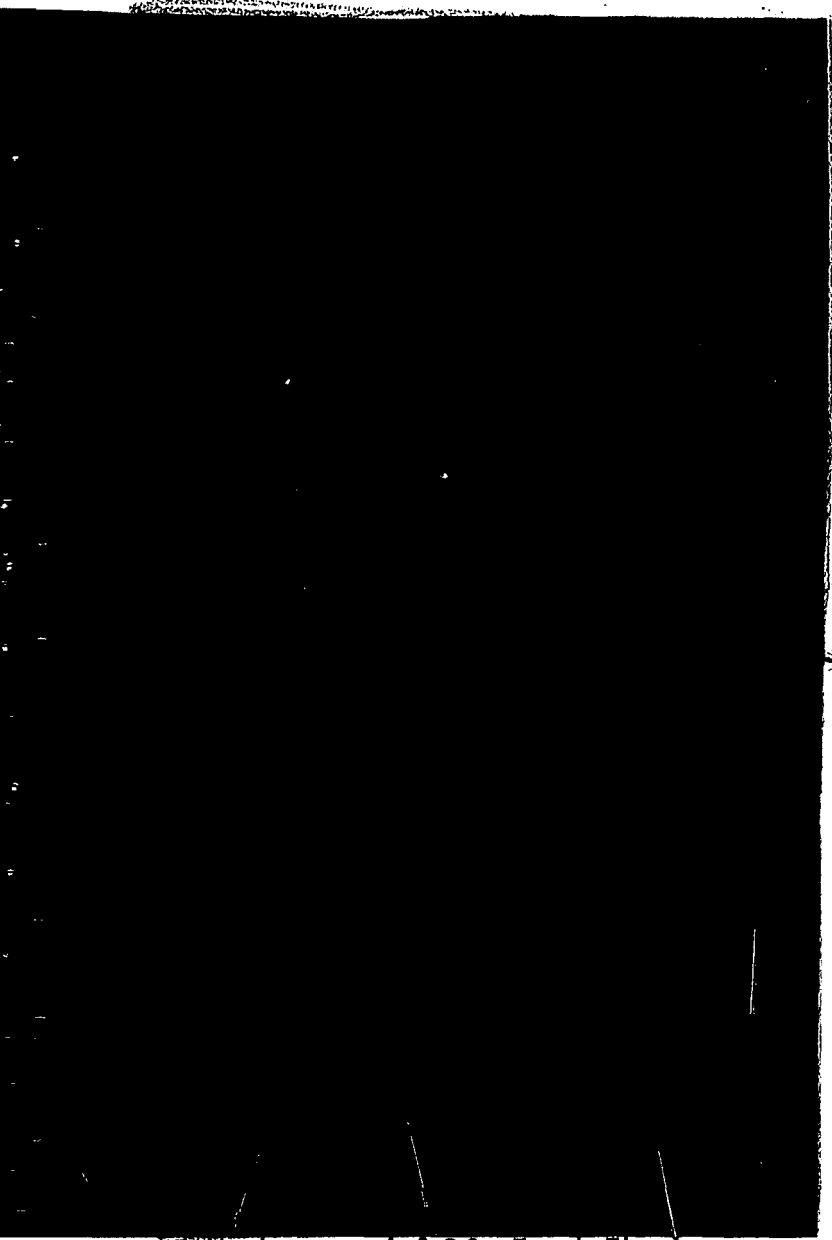

Application of SiC-Si Fused Elements in a Power Breeder Reactor. – The use of SiC-Si in fuel elements for a power breeder reactor was studied. The system was designed to furnish 60 Mw of electricity and have as high a conversion ratio as possible consistent with an economically feasible system. It was decided that the reactor would be cooled with helium and that the helium would be used as the working fluid in a closed-cycle gas turbine. Helium was chosen as the working fluid because of its superior heat-transfer characteristics and its very low thermal-neutron capture cross section.

A flow sheet of the system chosen is shown in Fig. 30. The helium, at 100 psi pressure, is heated to 1400°F in the reactor. The heated gas is then expanded through two gas turbines, the high-pressure turbine driving the compressor set and the low-pressure turbine driving the generator. The over-all station efficiency is approximately 40%.

A drawing of the reactor and pressure vessel is shown in Fig. 31. The reactor uses as fuel material U^{233} from thorium in an SiC-Si matrix, clad with SiC-Si. The moderator is high-density graphite and the blanket is ThO_2. As can be seen in Fig. 32, the fuel is arranged in flat plates, five fuel plates making a fuel assembly. There are 137 fuel assemblies inserted into the high-density graphite moderator to form the core. The blanket is ThO_2 perforated with circular coolant holes.

The turbine-compressor set and the turbine-generator set are located above ground in the open air. The remainder of the equipment is located below ground level for shielding purposes. The activity of the coolant stream is kept to such a level that the turbines and compressors need not be shielded. This is accomplished by bleeding off about 1% of the working fluid from the outlet of the compressor, sending it through a regenerator, thence through an expansion turbine, and back through the regenerator to the inlet of the compressor set. The outlet temperature of the expansion turbine is well below –200°C – a temperature low enough to condense any volatile fission products that may escape from the fuel element. This purification system causes a very small loss ($\sim \frac{1}{4}\%$) in station efficiency.

The reactor as designed has an initial conversion ratio of approximately 1.0. It is believed that, by more careful design, this ratio can be increased to the point that the reactor would be a true breeder reactor, with the possibility of a small over-all breeding gain.

A possible serious limitation of this reactor is common to all heterogeneous breeder reactors – the necessity for shutting down the system periodically to replace spent fuel elements. The cycle time of the reactor, as designed, was 73 days, but this could be increased with very little difficulty to about six months.

A cost study revealed that electricity at the bus bars would cost approximately 7.9 mills/kwh. This estimate was based on conservative estimates of chemical-processing and equipment costs.

Development and Fabrication of Fuel Plates

General. – The efforts of the Ceramics Laboratory have been directed, first, toward developing a

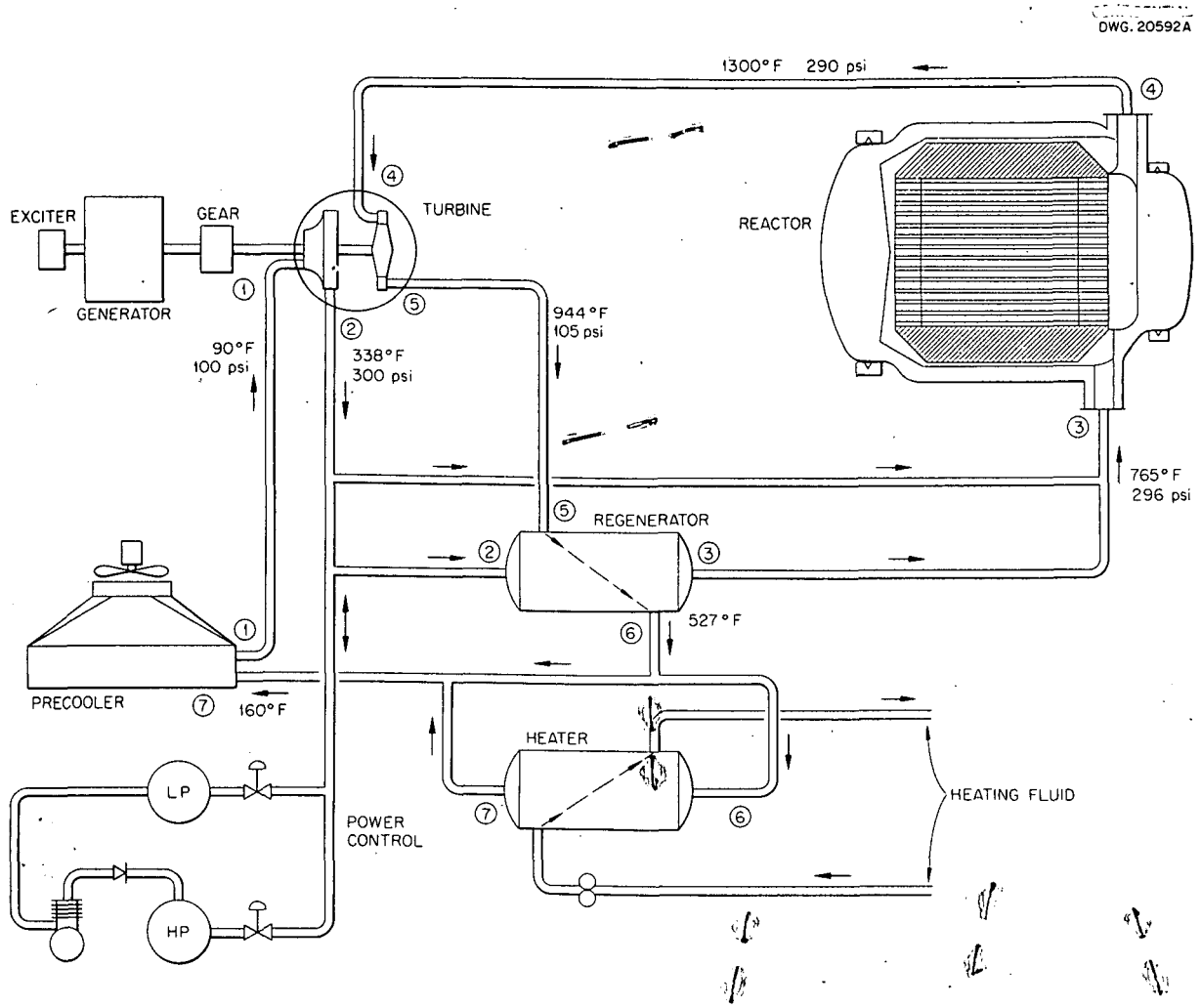

Fig. 25. Power Plant Flowsheet (Temperatures and Pressures at Maximum Monthly Output).

tight and strong Si-SiC body and, second, toward fabricating fuel elements, with the Si-SiC body being used as a base material.

Body Development. – In the search for an optimum base composition, it was necessary that different grades of carbon and graphite be studied with respect to forming characteristics, reactivity, and structure of the finished Si-SiC product.

Since there was no known technique for cold-forming a porous carbon or graphite structure with sufficient strength for processing, studies were made of various organic binders which could be either completely volatilized after the base structure was formed or partially volatilized, leaving a carbon residue.

Binder Materials. – Volatile binders – naphthalene, Carbowax, and cetyl alcohol – were added in amounts up to 20 wt %. The base structures in which these binders were used were very strong in the "green" state; they became fragile, however, after the binders were volatilized, and they disintegrated during the siliconizing process.

The semivolatile binders included terphenyls, nitrocellulose, Bakelite, organic flours, and sugars. The nitrocellulose-bonded structures failed during the volatilization operation. The structures exfoliated during the siliconizing process when they were bonded with terphenyls or Bakelite. Wood flours proved to be poor binders in the green state. Wheat flour was satisfactory as a binder when it was added in sufficient quantity (50%); however, inconsistent results

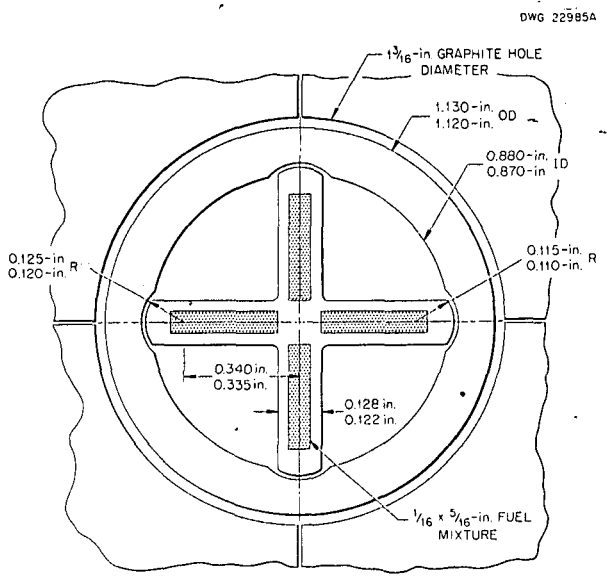

Fig. 26. Section of Fuel Element for Closed-Cycle Gas Turbine Plant.

were obtained when the structures were siliconized.

The sugars have proved to be highly satisfactory binder materials. Added in the form of dextrin, glucose, or the commercial product Karo, such additives make for a strong piece in the green state, the strength increasing as the volatile materials are driven off. In addition, the structure of the finished Si-SiC and the reproducibility of results obtained with the sugar-type binders were far superior to those obtained with the other binder materials.

Carbon and Graphite. – Composition studies were made in which carbon and graphite available in the laboratory were used.

Norblack, an insulating grade of carbon, was satisfactorily reactive, but, due to its grainy nature, was harder to form and made a rather weak green body. In addition, carbon particles visible to the naked eye were distributed throughout the siliconized body.

The graphites were much more satisfactory with respect to formability, green strength, and structure of the finished piece.

Selection of Base Composition. – In order to determine an optimum composition for the base material, an extensive experiment was conducted to select the type of graphite and the type and quantity of sugar which, combined, would make the best and most reproducible structure.

Bodies of the Acheson and Dixon grades of graphite were prepared with the use of glucose and Karo syrup as binders in quantities varying from 18 to 48 wt % sugar content. The following observations were made:

1. The green strength decreased with decreasing sugar content.
2. Residual carbon in the finished piece decreased with decreasing sugar content. This is illustrated by *a* and *b*, Fig. 33.
3. For a specific grade of graphite, glucose produced a finer grained structure than did dextrin or Karo.
4. With the use of glucose as a binder, the finer grained Dixon graphite produced a finer grained structure with residual carbon than did the Acheson grade; this is noted in comparing *a* and *c*, Fig. 33.
5. For a given composition, the use of a finer mix resulted in a finer grain structure and less residual carbon in the finished piece. This is evidenced by *d* and *e*, Fig. 33.

As a result of this experiment the composition T-91-A, which contains 38% sugar and 62% Dixon graphite, was selected for a basic material (*a*, Fig. 33).

Development of Fuel Body. – In order that the core of "meat" of the sandwich-type fuel plate be compatible with the shell or "bread," the core was composed of shell composition plus U, UC_2, UO_2, U_3O_8, and USi_3.

The metal and the carbide were oxidized as the volatile materials from the binder were driven off, and the subsequent volume change disrupted the piece.

With UO_2, U_3O_8, and USi_3, the fuel plates usually split or exploded during the siliconizing process. This is understandable with the oxides, because of the evolution of oxygen or carbon dioxide at impregnation temperatures, which amounts to approximately 800 cc of gas per fuel plate (calculated).

The silicide has produced similar results; the reason for this has not been determined although it is possible that impurities such as sulfur introduced during the process of materials preparation may be at fault.

The present approach to this problem is either to introduce the uranium as a more pure silicide or to introduce the uranium as the oxide and carburize

DWG 22980A

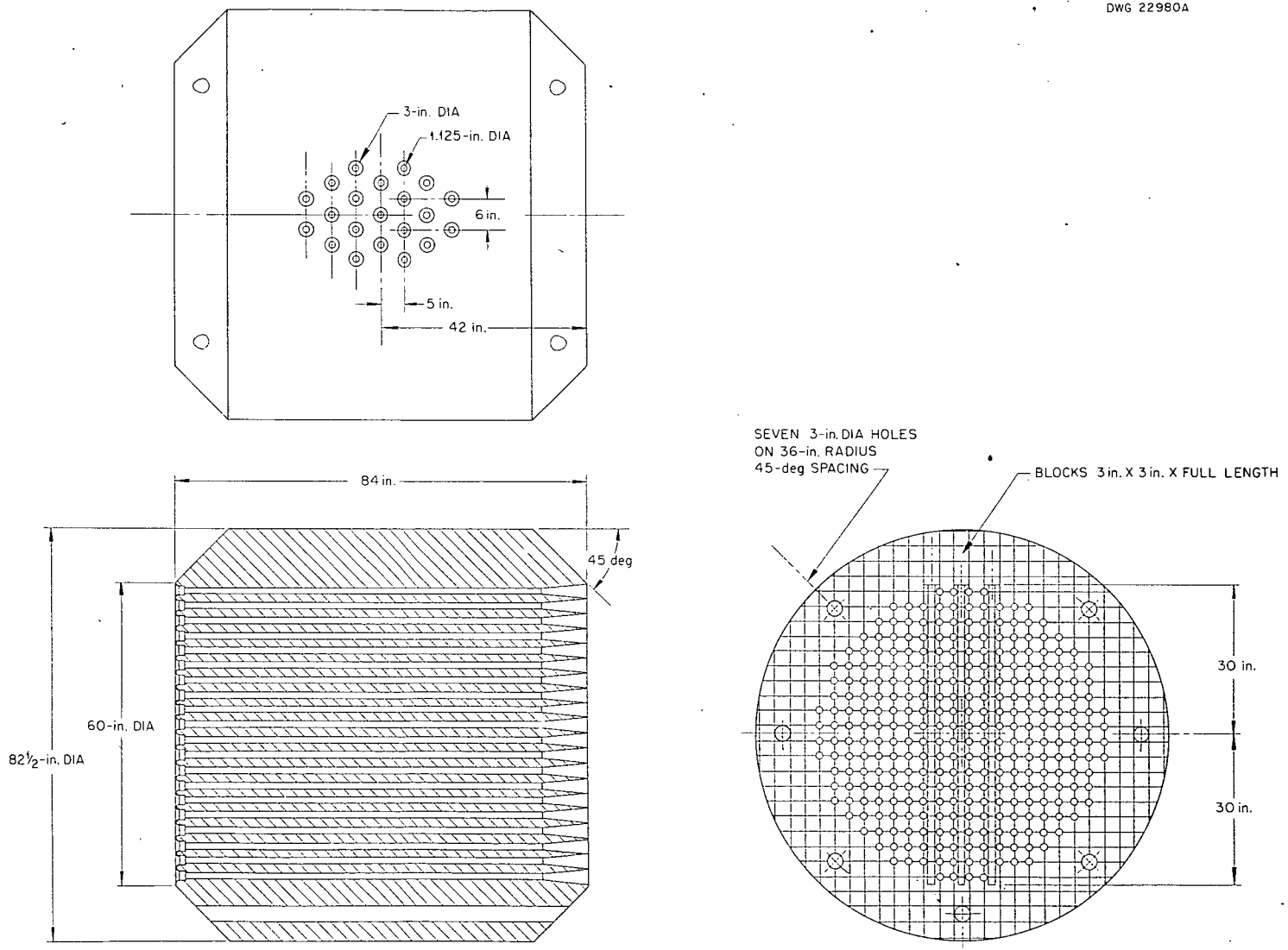

Fig. 27. Graphite Core for Closed-Cycle Gas Turbine Plant.

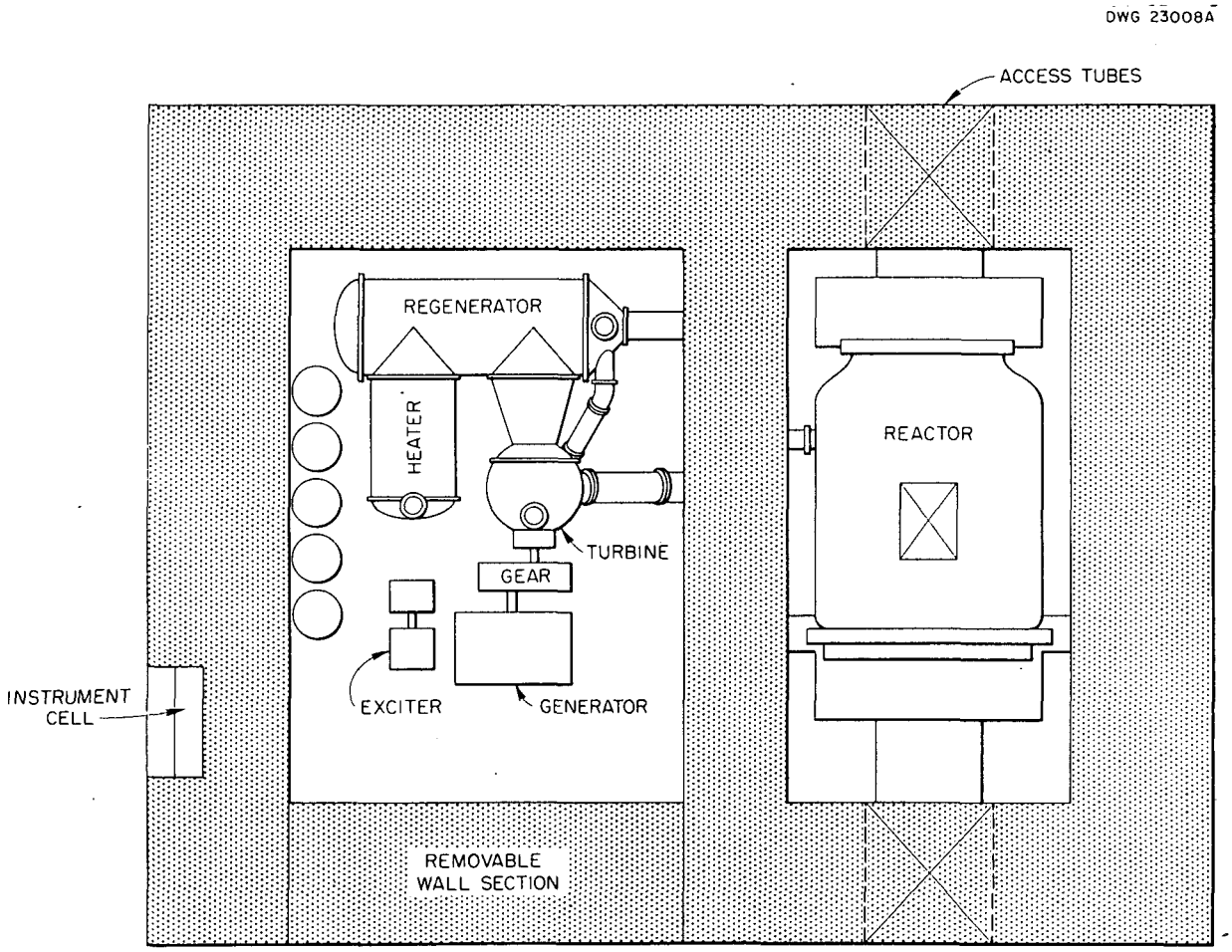

Fig. 28. Top Elevation of Reactor and Machinery Cell.

it in place before impregnation. In addition, efforts are being made to ensure against disruption due to differential shrinkages between the core and the shell, which could break the bonds between the two or prevent their bonding as the volatile materials are driven off.

Fabrication. – *Preparation of Raw Materials.* – The preparation of raw materials was accomplished as follows:

1. The raw materials, graphite plus glucose, are wet-mixed to form a stiff dough.
2. The dough is dried in an oven at 140°C, leaving a hard mass of graphite and sugar.
3. The hard dough is ground in a hammer mill and screened through a 325 mesh sieve. Most of the particles fall in the range of 5 to 10 μ.

The fuel material is prepared in the same manner, the fuel being wet-mixed with the base composition.

Forming of Plates. – The forming of the initial structure is illustrated in Fig. 34.

Processing of Green Plates. – After the body is formed, the volatile materials are driven off by baking the specimen in an argon atmosphere at 1000°C. This leaves a strong wood-like structure of graphite particles bonded by the coke from the sugar; this structure can be readily handled without being damaged.

Siliconizing. – The plate is placed on a graphite ladle and lowered into a graphite crucible containing molten silicon at approximately 1800°C. An exothermic reaction is evidenced by an increase in specimen temperature to approximately 2300°C.

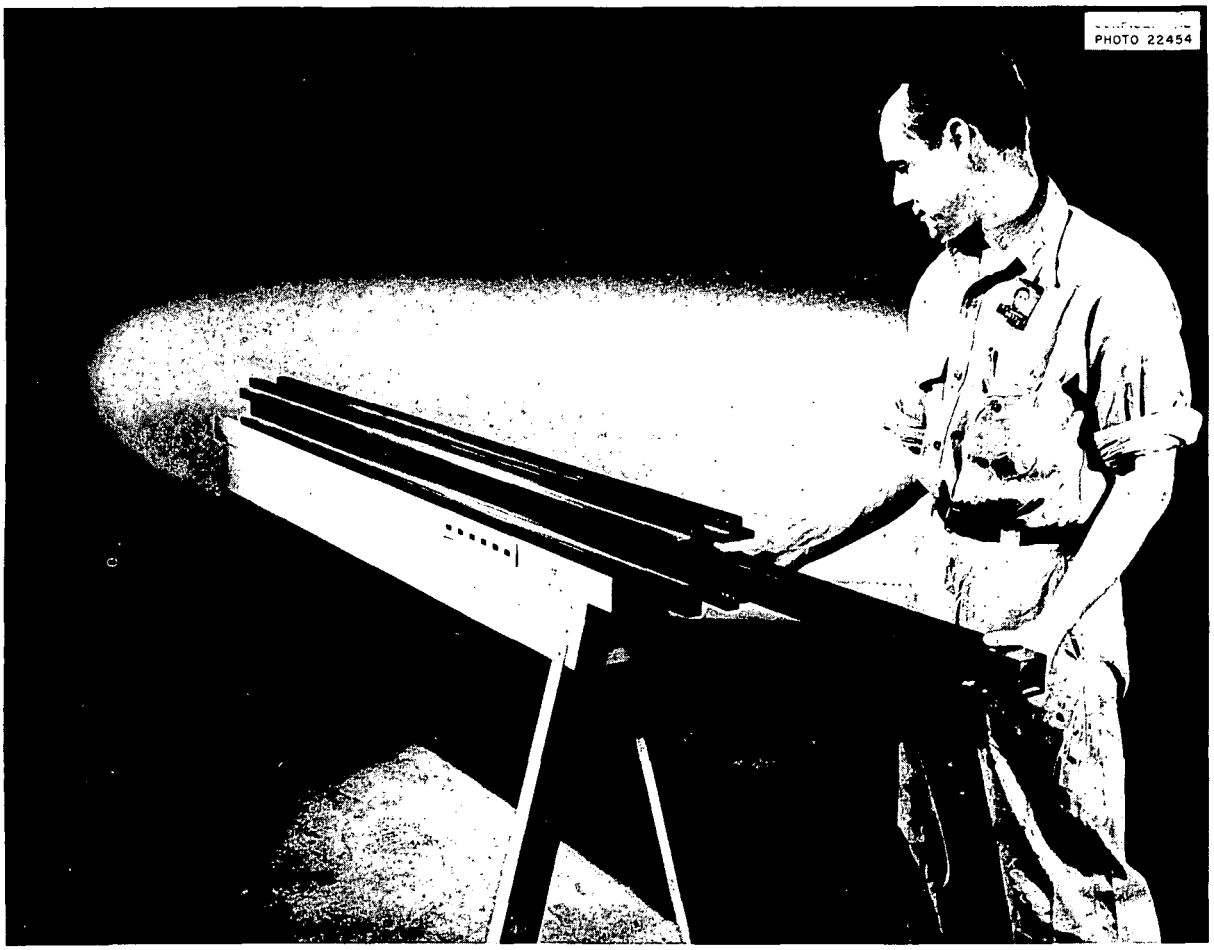

Fig. 29. Full-Size Model of Four Moderator Blocks and One Fuel-Unit Assembly Made of High-Density Graphite.

When it is evident that the reaction has subsided, the specimen is withdrawn from the crucible and cooled in air.

Finishing. – Since the piece is coated with some excess silicon and silica as it emerges from the crucible into the air, the rough surface must be ground so that the finished plate will be within the prescribed tolerances.

Inspection. – The plate is x-rayed standing on edge and resting on the flat side. The radiograph indicates unreacted portions, placement of the uranium, cracks, or any leakages of the uranium phase that might have occurred during the siliconizing operation.

Principal Problems Encountered in Fabrication. – (1) Effect of pressure. – The pressure used in the cold-forming operation has been observed to be one of the major variables throughout the process. Both the initial and finished pieces are markedly affected by pressures in the relatively short range from 50 to 300 psi. At the lower pressures the green strength is decreased; shrinkage during the bakeout is decreased; the reaction rate with the silicon increases; the number and size of silicon pockets are increased. As the pressure is increased in the cold-forming operation, the reaction rate is slowed; the amount of residual carbon increases until a point is reached at which only a skin reaction takes place, leaving a porous carbon core. The effect of increasing the pressure is illustrated by *b* and *d*, Fig. 33.

Since the compressibility of any body composition

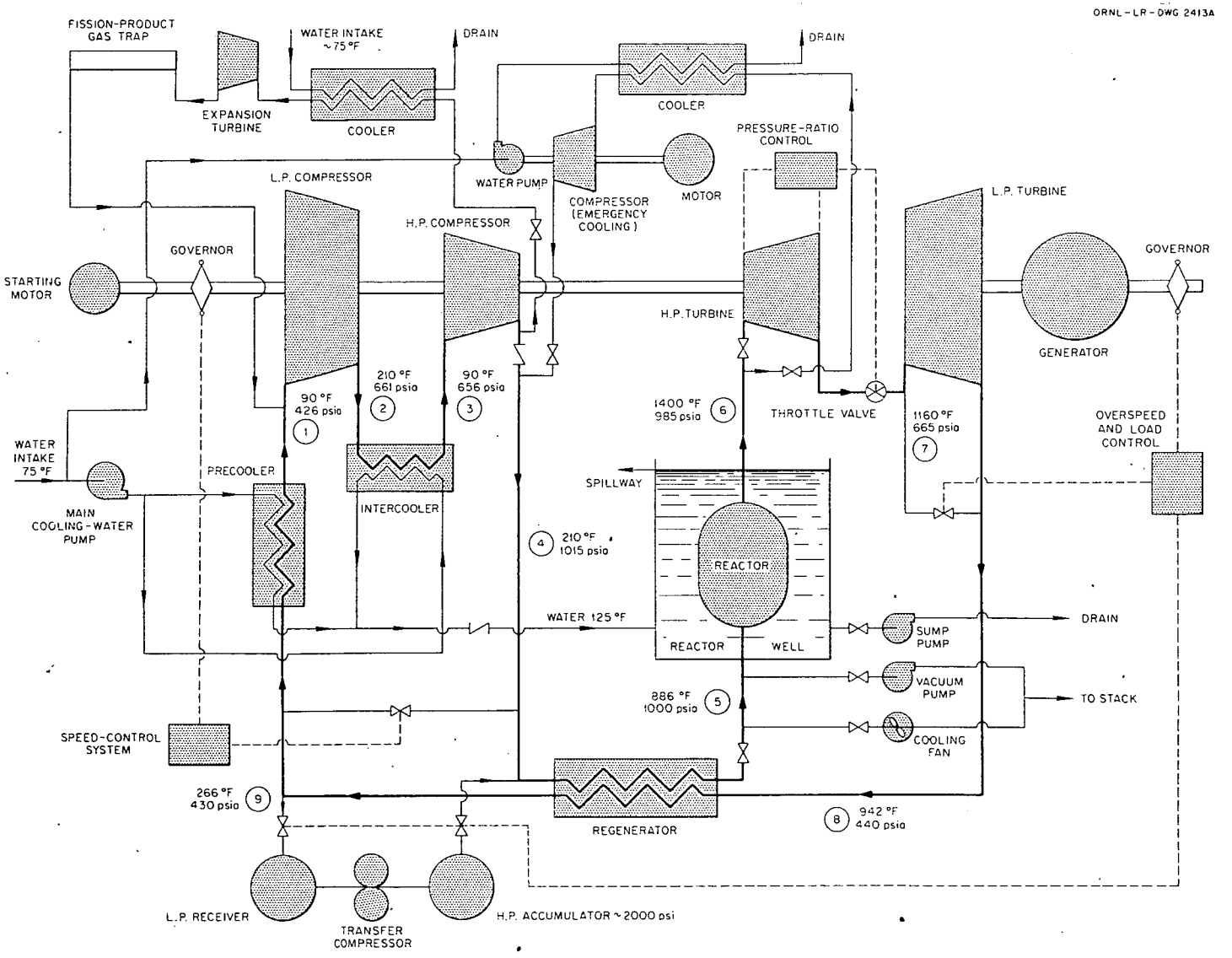

Fig. 30. Flowsheet of Power Breeder Reactor System.

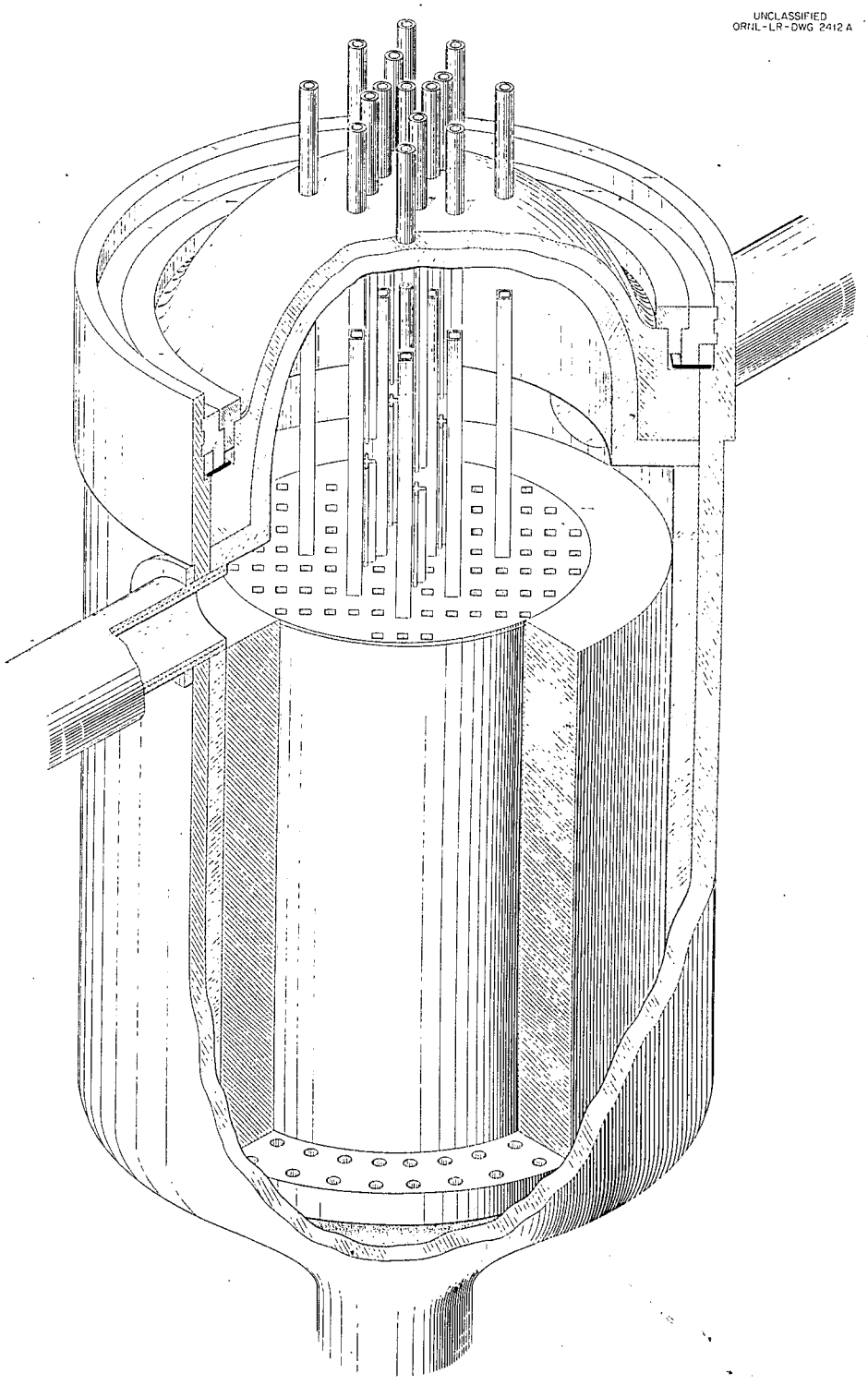

Fig. 31. Power Breeder Reactor and Pressure Vessel.

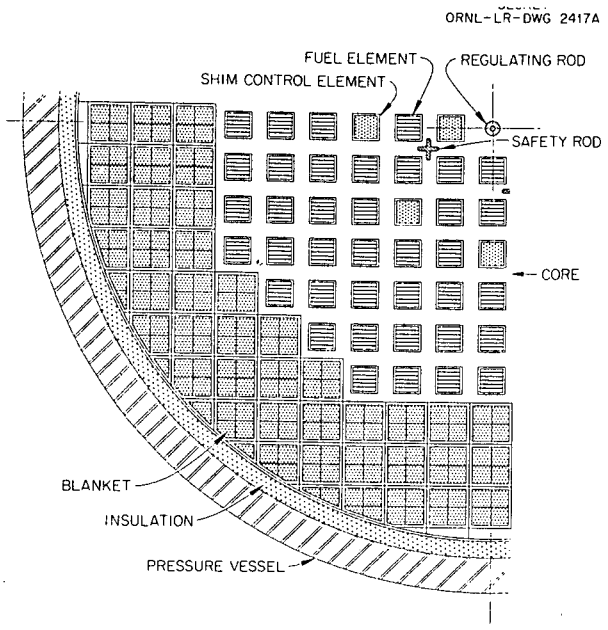

Fig. 32. Cross Section of Power Breeder Reactor.

is different from that of any other, it was necessary to determine an optimum pressure for every body composition investigated. The upper limit for most compositions was approximately 100 psi.

The bodies in which sugar was used as a binder have proved to be less sensitive to pressure than any other compositions. These bodies were impregnated at forming pressures up to 300 psi, and reproducible results were obtained; the upper limit for pressure has not yet been determined.

(2) Effect of temperature. – Although the silicon becomes molten at approximately 1420°C, reaction with the carbon structure has not been observed to take place below 1700°C. At this temperature the surface tension of the silicon appears to remain very high, and the reaction is slow to start. As the temperature is increased, the rate of reaction increases, but the specimen is more prone to warp during impregnation. The degree of warpage, however, is not attributed entirely to increasing temperatures. Because of the relatively small size of the present setup for impregnation, plates can only be immersed endwise, which enhances the chance for warpage. A larger setup is being designed which will allow a plate to be immersed in any position. For the composition selected, temperatures in the range 1700 to 1800°C have been the most satisfactory.

(3) Sweating. – Excess silicon is taken into the structure during the impregnation operation and sweats out as the specimen cools. Attempts are being made to improve the impregnation technique so that only the amount of silicon required for complete reaction enters the structure, thus preventing or minimizing the sweating problem.

Status of Fuel-Element Fabrication. – The first phase of the fuel-element program is considered to be satisfactorily complete; that is, a strong, tight, fine-grained Si-SiC body has been developed which should serve as a very good base material for the proposed fuel element.

There still remains considerable work to be done in completing the second phase, that of reproducibly fabricating fuel plates. This is believed to be partly a matter of improving technique, but it is expected that a major effort will be involved in developing a satisfactory fuel mix.

The Testing Program

Physical Properties. – Some physical-property measurements have been made on the Si-SiC bodies and are given below in cgs units except as noted. (Thermal conductivity was calculated from a comparative thermal diffusivity test with aluminum; a direct measurement, 100 to 1000°C, is under way. The T-91-A body was described in the preceding section, "Selection of Base Composition.")

Density	3.0	T-91-A body
Specific heat (see Fig. 35)	0.293 (400–1000°C)	T-91-A body
Thermal conductivity	0.4 (100°C)	T-91-A body
Tensile strength, psi	~10,000	Wheat-flour body
Expansion per °C	4.2×10^{-6} (0–1000°C)	T-91-A body

In addition, oxidation resistance was noted to be excellent. A microscopic film of silicon dioxide forms on the surface and acts as a barrier to further oxidation. This test was conducted at 1000°C for two weeks. The weight gain of a 15-g sample with a 4-in.^{2} surface was 0.08%.

Bench Loop Test. – A circulating-gas loop with provision for electric self-heating of the fuel elements or graphite plates has been made. Figure 36 shows this test apparatus. A plate-type test specimen is on the table in the foreground.

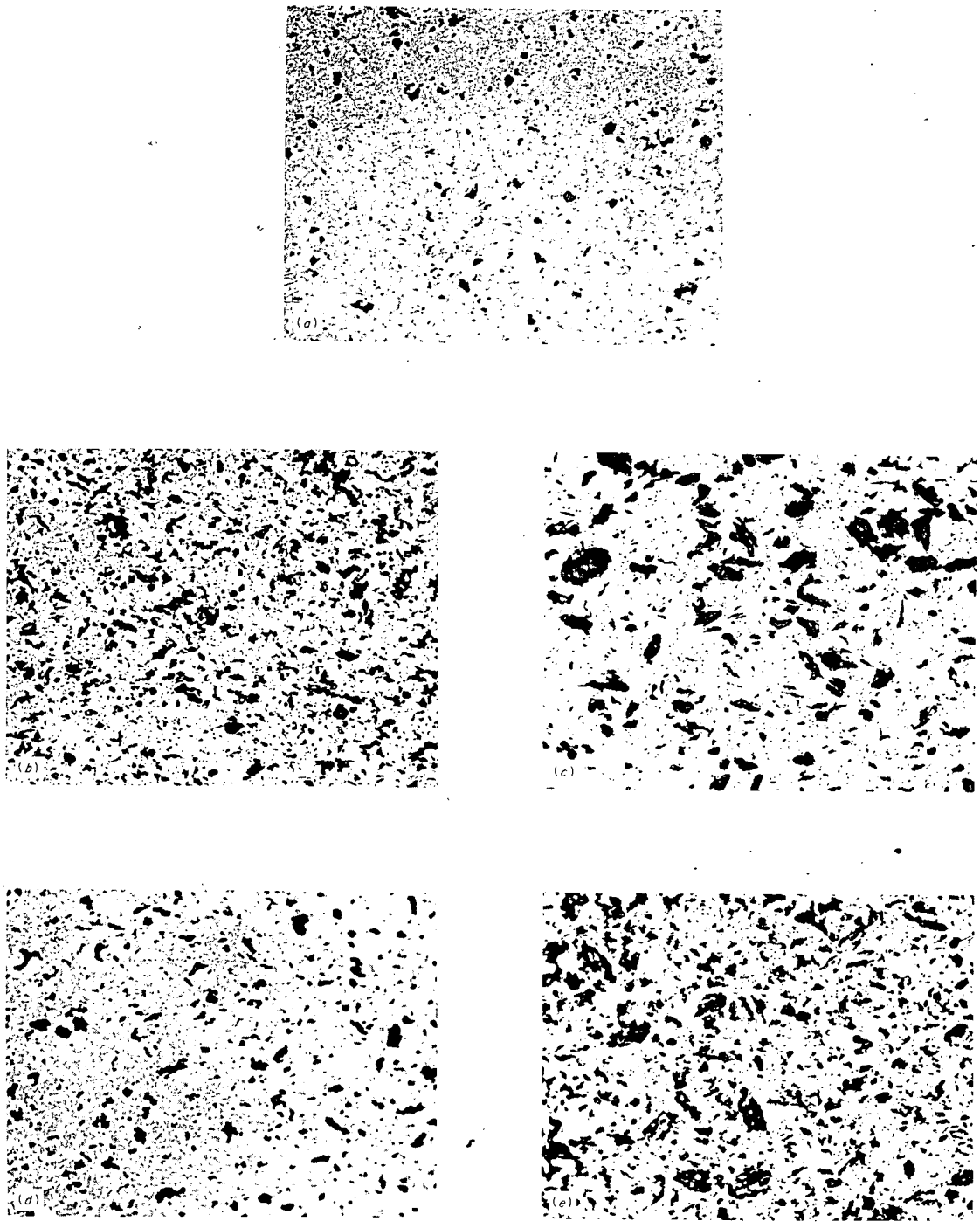

Fig. 33. Si-SiC Bodies; Black Phase, Graphite; Gray Phase, Cubic SiC; White Phase, Silicon. (*a*) 62% Dixon graphite–38% sugar; 300 psi; (*b*) 52% Dixon graphite–48% sugar; 300 psi; (*c*) 62% Acheson graphite–38% sugar; 300 psi; (*d*) 52% Dixon graphite–48% sugar; 70 psi; fineness of grind, over 50% less than 20 μ; (*e*) 52% Dixon graphite–48% sugar; 70 psi; fineness of grind, over 50% between 20 and 44 μ. 250X. Reduced 31.5%.

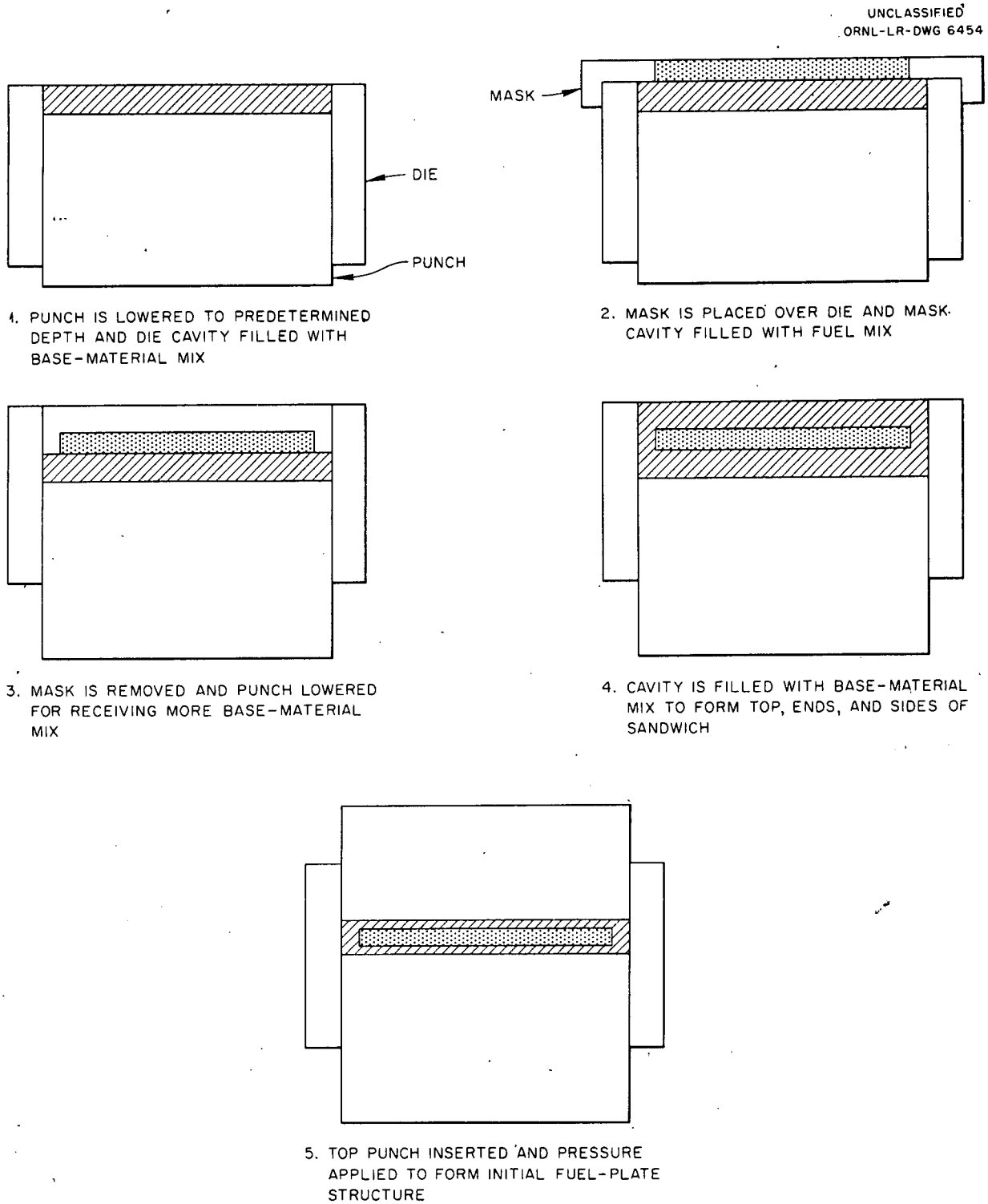

Fig. 34. Cross Section Illustrating the Cold-Forming of Initial Fuel-Plate Structure.

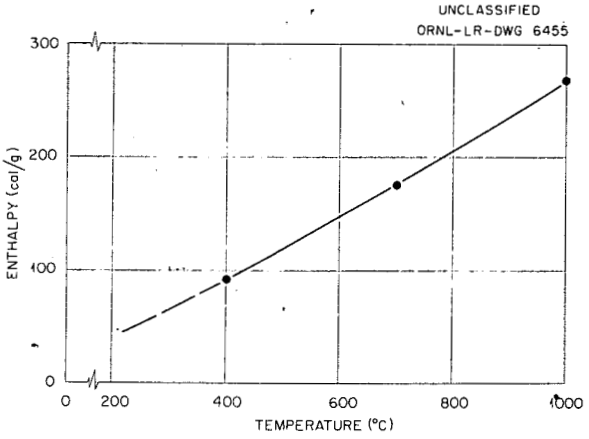

Fig. 35. Heat Content, SiC-Si; Specific Heat, 0.293 (400 to 1000°C).

Only preliminary studies have been made. Gas velocities of 200 fps can be attained. A 12-kw low-voltage power source is available to the equipment. Two SiC-Si plates, $3 \times 1 \times \frac{1}{8}$ in., have been heated in static air, with 700 and 1200 w/in.^{2} being driven from them at failure. The 700-w plate had an obvious defect. The 1200-w plate was representative of the better specimens. Failure occurred only after repeated heating and cooling at this load.

A 1000-hr erosion-corrosion test with high-density graphite plates as samples is the next experiment.

Neutron-Damage Test. – A neutron-radiation experiment carried out by M. Wittels, of the Solid

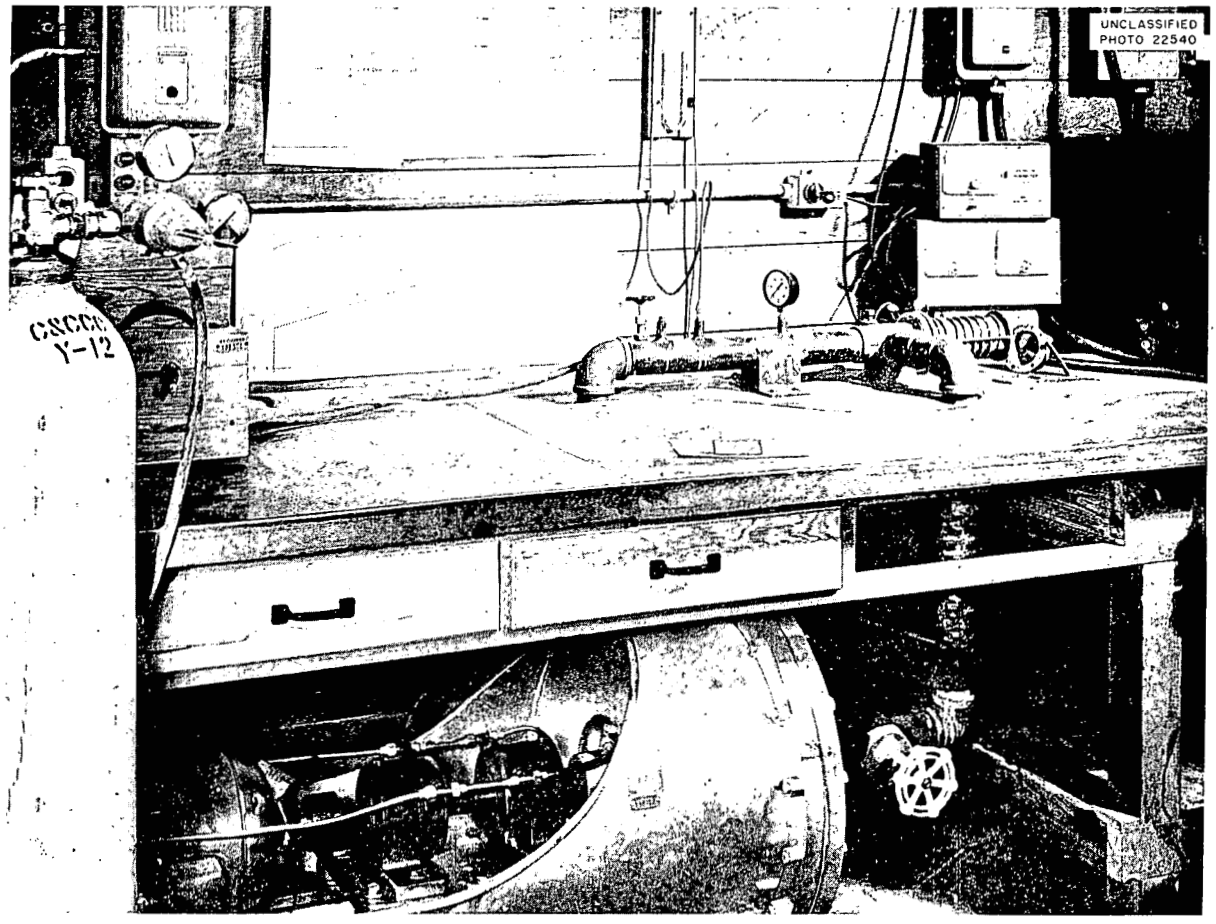

Fig. 36. Circulating-Gas Loop Test.

State Division, revealed the following:

Exposure, fast neutrons	1.09×10^{20}
X-ray lattice	Si, no change
Measurements	β-SiC-a_0 expanded 0.76 ±0.10%
Temperature of exposure, °C	~100

Wittels believes that the lattice expansion will approach a maximum at less than 1.25%. Since most ceramics self-heal or anneal out such damage when heated to temperatures in the range 600 to 1000°C, it is not expected that radiation damage will be a problem inasmuch as the operating temperatures for the SiC-Si fuel element will be in this range. The irradiated sample above has been recharged into the LITR for further bombardment; when it is removed, it will be examined to determine the annealing temperature range.

Fission-Product Diffusion Test. – The relative ability of materials to retain fission products is being measured with the use of a simple heating-collecting system. It is recognized that these results are not necessarily indicative of retention ability in a fuel-bearing material which has undergone considerable burnup; however, they serve to screen materials and indicate their probable usefulness as fuel-element materials. In addition to the SiC-Si specimens, several other cermets have been examined. Stainless steel and some oxide compacts will be tested in the future.

A schematic view of the test is shown in Fig. 37. The specimen is irradiated for seven days in a flux of 5×10^{11} neutrons/cm^2/sec. It is then sealed in a silica glass container (Fig. 38) and heated for 24 hr at a selected temperature. On removal from the furnace, the stem end of the container is immersed in liquid nitrogen for 5 hr, after which the stem is sealed off from the container and removed for radiochemical analysis. The equipment for this process is shown in Fig. 39. Activities are measured and isotopes are identified with the use of an ionization chamber, a scintillation counter, and a gamma spectrometer.

The activities of the specimens are compared with the activities of standard samples which contain the same amount of UO_2 enclosed only in an aluminum silicate "glass" wool so that gaseous or volatile fission products can escape with little or no hinderance during furnace heating. It is evident from Table 6 that the volatile fission

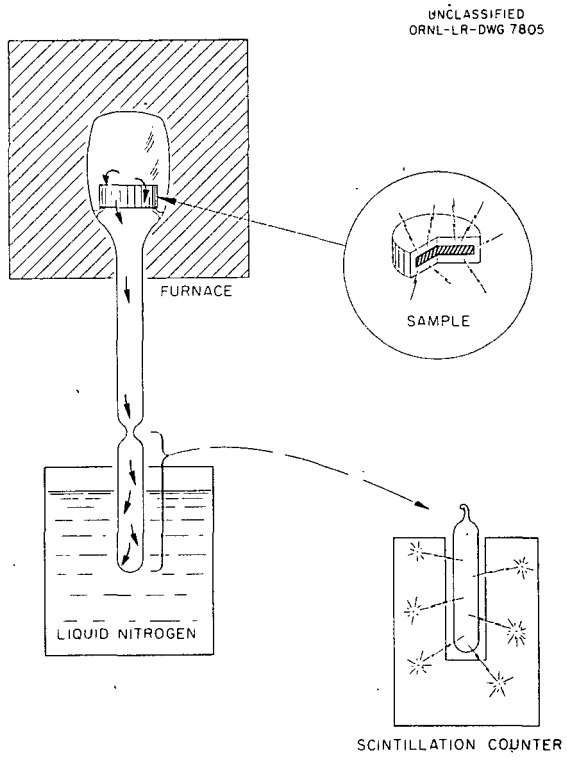

Fig. 37. Fission-Product Diffusion Test.

products are retained in the UO_2 grains at irradiation temperatures. The standard for the SiC-Si specimens (G-224-1) contains 22.4 mg of UO_2, and the standard for the other cermets contains 3.3 mg of UO_2.

The isotopes which are pure beta emitters and those having very short half lives would not be detected in this experiment; Xe^{133}, $I^{133,132,131}$, Te^{132}, and Mo^{99} were found. Small amounts of other activities were found when the container tube of a standard sample was washed. It was also discovered that neptunium apparently migrated to the surface of the specimens. Some was also found in the "glass" wool surrounding the specimens. The neptunium was found to be on the surface of the specimens immediately after irradiation, before heating. It must be pointed out that the specimens were probably self-heated (100–300°C) during reactor exposure. Neptunium was not found in the sealed-off tubes. Tables 6, 7, and 8 show the results of a number of tests.

The data presented in Tables 6, 7, and 8 indicate that, in all probability, only gaseous or volatile fission products will be of concern. The

TABLE 6. TABULATED RESULTS FOR STANDARD COMPACTS

Compact Specimen No.	Isotope	Measured Activity (photons/min)	Activity Corrected (d/min)	Number of Atoms Diffused Through at Time of Removal from Furnace ($N_1 \times 10^{10}$)	Theoretical Total Number of Atoms at Time of Removal from Furnace[a] ($N_0 \times 10^{10}$)	Efficiency of Collecting System (%)	Estimated Accuracy (±%)
G33-3[b]	Xe^{133}	3×10^6	9×10^6	11.00	17.72	62	30
	I^{133}	2×10^6	2.2×10^6	1.15	1.72	68	30
	Te^{132}	3×10^6	3×10^6	2.68	8.85[c]	30	30
	I^{132}	7×10^6	7×10^6	2.62	2.20	118	30
	I^{131}	3×10^6	3.75×10^6	7.02	15.2	46	30
	Mo^{99}	3×10^6	3.3×10^6	2.68			
			Activity Ratio to G33-3[d]	UO_2 Ratio	Efficiency Ratio Change		
G224-1[e]	Xe^{133}	3×10^7	10	6.8	1.47	91	50
	I^{133}[f]	2.5×10^7	11.5	6.8	1.69	115	50
	Te^{132}[g]	1.7×10^7	5.7	6.8	0.838	25	50
	I^{132}	3×10^7	4.3	6.8	0.633	75	50
	I^{131}	2×10^7	6.7	6.8	0.985	45	50
	Mo^{99}	1.5×10^7	5.0	6.8	0.736		

[a] Calculated by use of data from LRL-153, *Theoretical Study of Fission Product Gaseous Activity from a Homogeneous Reactor*, by J. R. Donaldson (June 1954).

[b] Detailed radiochemical analysis of 87% of the activity dissolved from tube in dilute nitric acid given in Table 7.

[c] Calculated from data and not from LRL-153.

[d] $\frac{\text{Activity ratio to G33-3}}{UO_2 \text{ ratio}} \times \%$ efficiency of G33-3 = efficiency of G224-1

[e] Rough calibration, absolute error probably less than 50%.

[f] Some Ru^{103} may contribute.

[g] Some $Xe^{133m,135}$ may contribute gammas.

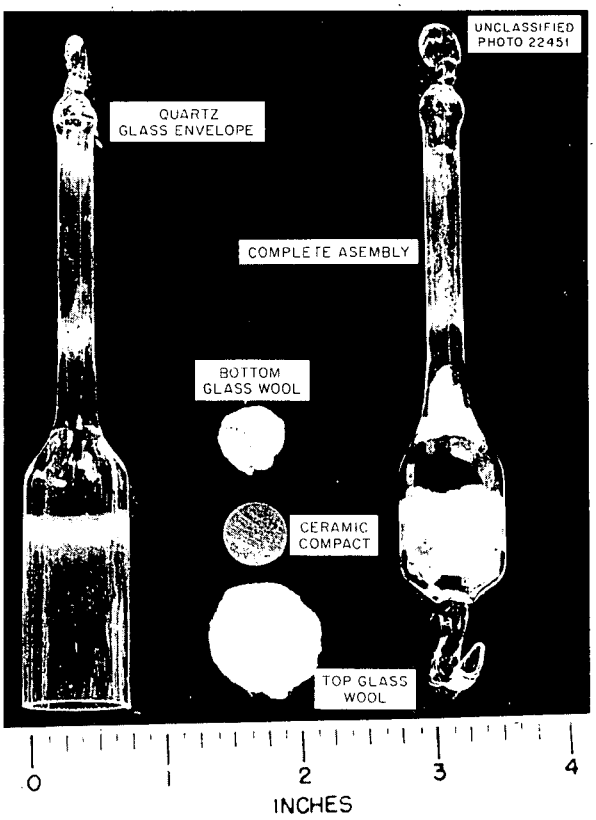

Fig. 38. Glass-Envelope Assembly.

TABLE 7. RADIOCHEMICAL ANALYSIS OF G33-3 NITRIC ACID WASH FROM TUBE*

Component	Counts/min/ml	Percentage of Gross
Gross gamma	7.7×10^4	
Tellurium gamma	2.9×10^4	38
Iodine gamma	2.0×10^4	26
Molybdenum gamma	6.3×10^3	8
Rare-earth gamma	810	1
Barium gamma	186	0.2
Zirconium gamma	100	0.1
Gross beta	7130	
Rare-earth beta	113	1.6
Strontium beta	45	0.6

*Determination made after approximately one week of decay from time of removal from furnace or ten days from time of removal from irradiation.

observed reduction of these fission products is sufficient to make some of the cermets interesting for fuel-element applications. In a reactor, further reduction can probably be obtained by continuously bleeding-off a portion of the coolant gas and passing it through an expansion turbine, where it is cooled to about −115°C. The cooled gas, going next through a coil immersed in liquid nitrogen, will lose its volatile fission products by condensation and freezing.

More detailed studies are in progress. A continuation of the neptunium study is intended.

PROCESS FOR OBTAINING LARGE-GRAINED UO_2

For a number of applications, particularly for fabrication of stainless steel fuel elements, UO_2 in grain sizes from 50 to 120 μ is required. Fusion and sintering are not acceptable methods for producing large-grained UO_2; fusion is wasteful of material, and sintering tends to produce agglomerates which are not so strong as desired.

A process has been developed which yields large-grained UO_2 and has no complicated or wasteful features. Large-grained anhydrous UO_3 was heated in a hydrogen atmosphere to about 1500°C. Large crystals of UO_2, the stable high-temperature oxide, developed from the UO_3. The UO_3 can be made in large crystals by autoclaving at 250°C fine-grained material which contains a trace of nitrate. In all probability 1200°C heating will be adequate. A detailed investigation is under way.

THORIUM OXIDE

Two thorium oxide rods clad with aluminum were irradiated in the LITR ($\sim 2 \times 10^{20}$ nvt) for 120 days. One of the rods was ½ in. in diameter by 4.5 in. long and consisted of pure ThO_2 (86% of theoretical density); the other was 1.1 in. in diameter by 4.5 in. long and consisted of ThO_2 plus ½ wt % CaO (96% of theoretical density). After the exposure the ends of the aluminum cladding were removed, and it was seen that the color of the ThO_2 had changed to a dark chocolate brown. No cracks were observed in the rods, and they appear to be mechanically sound. The aluminum cladding showed no significant dimensional changes, which indicates that the ThO_2 is dimensionally stable under the above exposure conditions.

TABLE 8. TABULATED RESULTS FOR CERMET COMPACTS

Compact Specimen No.	Temperature of 24-hr Heating (°C)	Type of Activity Detected as Products of Diffusion	Ratio of Diffused Activity to Activity of G33-3 Standard, Fission-Product Retention Factor	Compact Composition	Uranium Compound in Compact	Remarks
A33-5	1000	W^{187} in all A samples (forming impurity) and constituted majority of activity; Xe and I present	2.4×10^{-1}	28% Al_2O_3–72% Cr	UO_2, 3.3 mg	W^{187} contamination in all A specimens due to grinding-media contamination in specimen preparation
-7	1000		1.5×10^{-3}	28% Al_2O_3–72% Cr	UO_2, 3.3 mg	
-3	900		2×10^{-4}	28% Al_2O_3–72% Cr	UO_2, 3.3 mg	
-4	900		4×10^{-4}	28% Al_2O_3–72% Cr	UO_2, 3.3 mg	
-1	800	Not identified	4×10^{-5}	28% Al_2O_3–72% Cr	UO_2, 3.3 mg	
-2	800	Not identified	8×10^{-5}	28% Al_2O_3–72% Cr	UO_2, 3.3 mg	
B33-2	1000	Xe, Te, I	3.3×10^{-2}	80% ZrC–20% Fe	UO_2, 3.3 mg	UO_2 distributed throughout specimens
-5	1000	Xe, Te, I	1.5×10^{-2}	80% ZrC–20% Fe	UO_2, 3.3 mg	
C33-3	1000	Xe, Te, I	1×10^{-1}	80% TiC–20% Ni	UO_2, 3.3 mg	UO_2 distributed throughout specimens
-6	1000	Xe, Te, I	6×10^{-2}	80% TiC–20% Ni	UO_2, 3.3 mg	
D33-7	1000	Xe, Te, I	2×10^{-3}	80% MgO–20% Ni	UO_2, 3.3 mg	
-9	1000	Xe, Te, I	3×10^{-3}	80% MgO–20% Ni	UO_2, 3.3 mg	
-1	900	Not identified	4×10^{-5}	80% MgO–20% Ni	UO_2, 3.3 mg	
-2	900	Not identified	9×10^{-5}	80% MgO–20% Ni	UO_2, 3.3 mg	
-3	800	Broken specimen		80% MgO–20% Ni	UO_2, 3.3 mg	
-4	800	Not identified	2×10^{-5}	80% MgO–20% Ni	UO_2, 3.3 mg	
E224-1	900	Xe, Te, I, trace Au^{198}	7×10^{-4}	SiC-Si	USi_3, 26.5 mg	Stringer of USi_3 to surface of specimens; therefore surface of specimens contaminated with uranium
-2	900	Xe, Te, I	9×10^{-4}	SiC-Si	USi_3, 26.5 mg	
-3	900	No elements could be identified	2×10^{-4}	SiC-Si	UO_2, 22.4 mg	

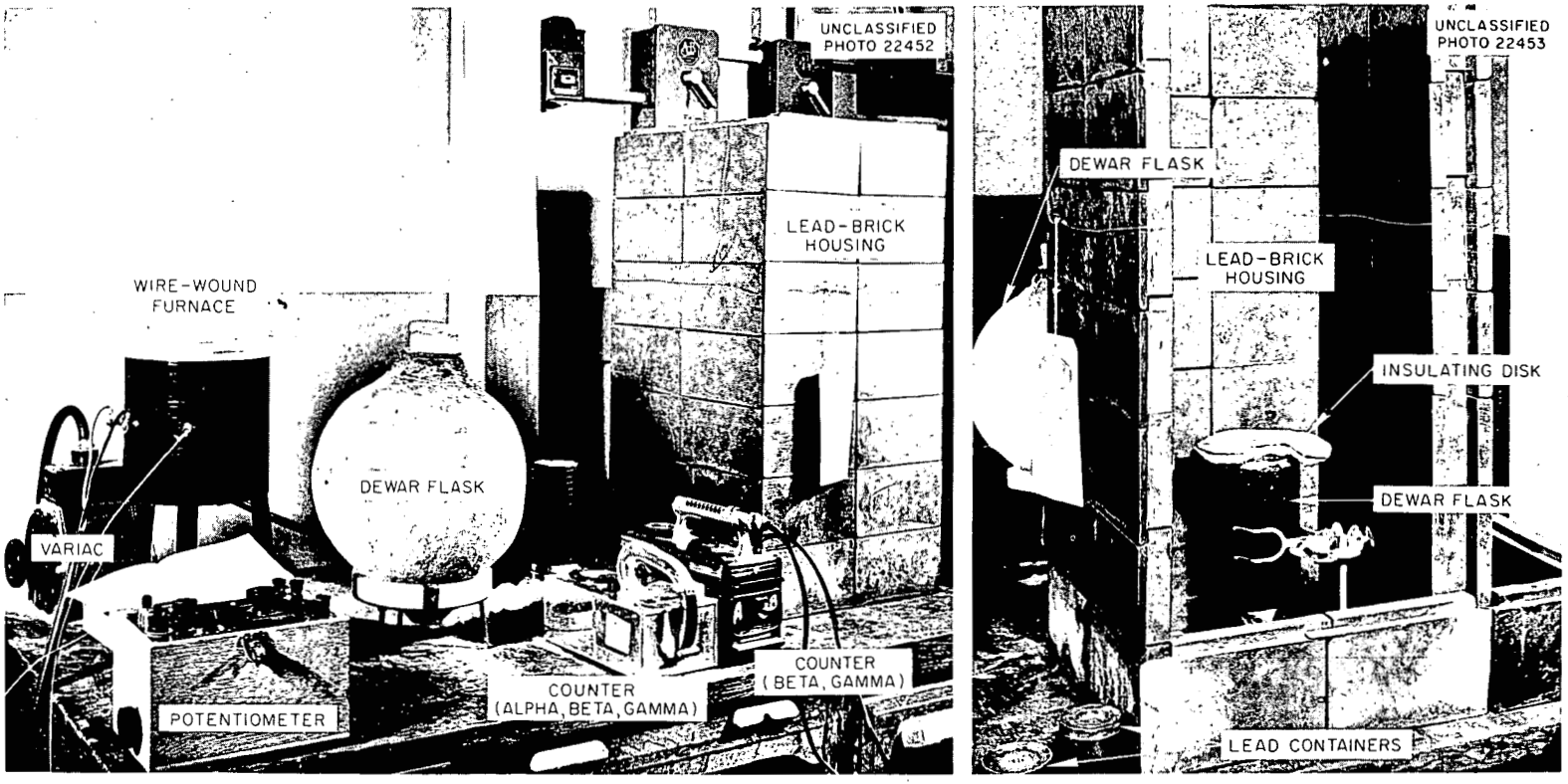

Fig. 39. Apparatus and Equipment for Fission-Product Diffusion Test.

PHOSPHATE COATING

Further work progressed on a fluoride-resistant phosphate coating for mild steel. Phosphate-coated mild steel will ultimately be substituted for nickel-coated steel vessels now in use in the gaseous diffusion process.

Preliminary tests of two coatings, P-6 and P-8 (Table 9), applied to mild steel have been performed in UF_6 at 250°C. Coating P-6 was resistant to the fluoride; however, P-8 was badly attacked. The thermal expansion of coating P-6 was too low for good adherence to the metal to be obtained. In order to increase the thermal expansion of the coating, modifications of P-6 were made. Composition P-19 is the best coating thus far produced. It has not yet been tested for fluoride resistance.

CERAMIC ASPECTS OF WASTE DISPOSAL

The safe disposal of high-level radioactive wastes is of basic importance to future reactor operations, and studies by the Ceramics Group include examination of the possibility of underground fixation of dangerous isotopes in ceramic masses, utilizing the heat present in the radioactive wastes to effect partial fusion, and the evaluation of natural impermeable barriers to the passage of waste solutions.

Effect of Various Solutions on the Permeability of Clays

A series of experiments was performed in order to obtain preliminary data concerning the effect of various solutions on the permeability of various clays and combinations of clays.

Ordinary 500-ml graduates were used (ten divisions on the graduate are equivalent to $1\frac{1}{8}$ in. in length or 50 ml in volume), and all measurements will be reported in divisions of the graduate.

Tap Water. – Clay was tamped into the bottom of the graduate and was then covered with three divisions of –200 mesh bentonite. At the end of six days, the clay underneath the bentonite was damp. This experiment was repeated with ten divisions of granular bentonite (No. 90, American Colloid Co.). The bentonite swelled and separated, but the bottom clay has remained dry over a period of several weeks. This is not unusual, since bentonite sandwiches have been used for sealing lagoons containing fresh water.

Simulated W-8 Solution. – Ten divisions of dry clay, followed by four divisions of bentonite, followed, in turn, by three divisions of dry clay were placed in the column. Simulated W-8 solution, which is strongly basic, rapidly permeated the bentonite layer and went into the clay underneath. This solution destroys, to a considerable extent, the coherence of the bentonite gel. With such solutions, bentonite would not be a satisfactory sealing material.

Hope Solution. – For the test with Hope solution the column was packed as follows: nine divisions of dry clay, six divisions of bentonite, and a layer of clay placed on top. The graduate was then filled with the solution. The bentonite swelled to about 15 divisions. It moved up the tube as a small amount of the solution went through the bentonite and reacted with the calcite, which is in the clay, forming CO_2.

Summary. – Bentonite sandwiches would not be suitable for sealing pits containing either W-8 or the acid Hope solution.

Permeability of Clays as Affected by W-8 Solution from the Lagoon

In these experiments 1000-ml graduates were used. They were fitted with a stopcock and a tube at the bottom, as shown in Fig. 40, and were packed with various clays and combinations of clays. They were filled with radioactive waste from the lagoon, the stopcock was opened, and the solution was allowed to flow into beakers. All measurements were made in terms of divisions on

TABLE 9. COATING COMPOSITIONS IN WEIGHT PERCENTAGES OF OXIDES

Coating	P_2O_5	Al_2O_3	BaO	BeO	SrO	ZnO	Sb_2O_3	Li_2O	Na_2O
P-6	70	15				10	5	2	
P-8	57.9	7.9	26.3			2.6	3.6		1.7
P-19	73	10		6	2	5	2	2	

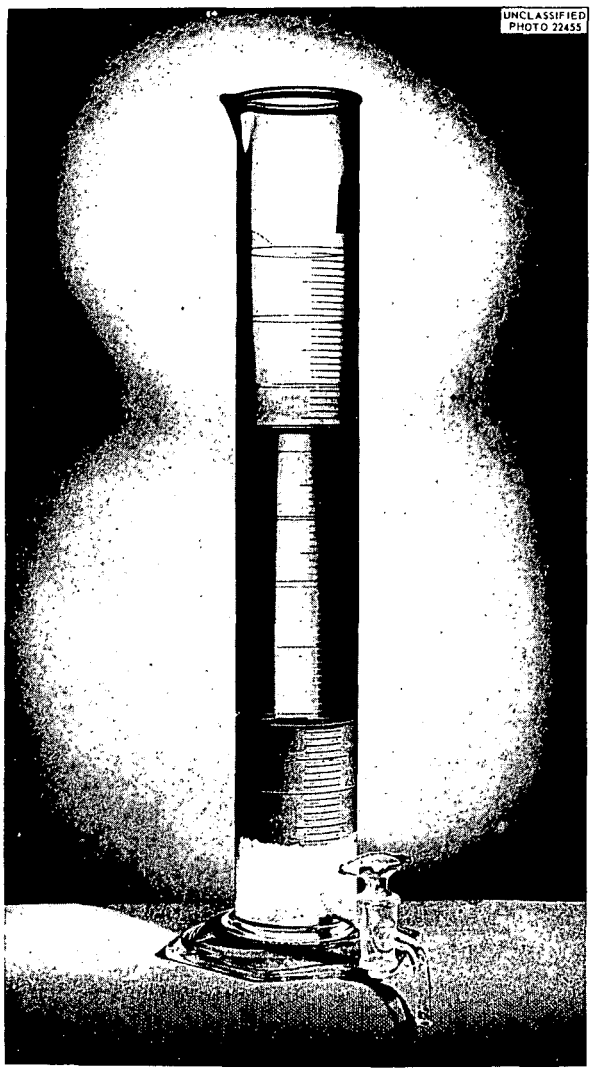

Fig. 40. Graduate (1000 ml) Used in Testing Permeability of Clays.

the graduates (ten divisions equal 1½ in. or 100 ml); –8 +50 mesh crushed insulating brick was used in the bottom of the graduates. The results of the tests are as follows:

1. Thirteen divisions of insulating brick and 16 divisions of finely ground Conasauga top soil packed damp were used. Tap water rapidly permeated the clay.

2. The column was packed the same as for test 1. W-8 solution (from the lagoon) rapidly permeated the clay.

3. Thirteen divisions of insulating brick, five divisions of Conasauga clay, six divisions of No. 90 coarse bentonite, and five divisions of Conasauga clay were used. The solution penetrated the bentonite within one day.

4. Thirteen divisions of insulating brick, six divisions of Conasauga clay, and ten divisions of mixed 75% Conasauga clay and 25% bentonite started to leak at the end of 48 hr. This mixture was better than the bentonite alone but was not satisfactory.

5. Thirteen divisions of insulating brick, six divisions of Conasauga clay, ten divisions of air-floated Gleason ball clay (H. C. Spinks Clay Co., Inc., Paris, Tennessee) did not leak even after ten days and evidently makes a good seal. This clay costs $17.50 per ton, f.o.b. Paris, Tennessee; consequently, this experiment will be repeated, and the shredded Gleason clay, which costs $7.50 per ton, will be used.

6. Thirteen divisions of insulating brick, six divisions of Cordova, Alabama, fire clay (16 mesh) was examined three days after the W-8 solution had been poured in, and the solution had permeated the clay.

7. Thirteen divisions of insulating brick, six divisions of Conasauga clay, ten divisions of mixed 50% Gleason clay and 50% Conasauga clay had leaked within three days but not so rapidly as had No. 6.

Conclusions. – To date, the only clay found to be impermeable to the waste solution is the air-floated Gleason ball clay.

Gels Made from Hope Solution and Natural Carbonate Minerals

At the start of this investigation, gels were formed by adding either finely ground Knox dolomite or Chickamauga limestone to Hope solution and by stirring the mixture frequently. The gel is evidently aluminum hydrate. Ordinary 500-ml graduates were used. The graduate was packed with ten divisions of dry Conasauga clay, seven divisions of bentonite, and four divisions of dry clay. The gel was formed by frequent stirring of 142 g of Knox dolomite and 500 ml of Hope solution. The gel was strongly acid but contained unreacted dolomite. The gel was poured into the graduate and did not wet the top clay. Two inches of the gel was removed from the top of the graduate, and the graduate was filled with water. The bentonite swelled and separated,

leaving a gap, and the clay underneath remained dry. A similar column was arranged by using finely ground Chickamauga limestone, and it behaved in the same manner as the graduate containing the Knox dolomite gel.

Conclusions. – The above tests indicate that the gel will be inactive when it is poured into a pit which has a dry clay bottom. Consequently, a more thorough study of the jelling characteristics of carbonates and Hope solution was indicated.

Gel Formation. – Agricultural limestone (dolomite) was obtained from Mascot, Tennessee. As received, practically all of it would pass –20 mesh. The following proportions were used:

No.	Mascot–20 Mesh Dolomite (g)	Hope Solution (ml)
1	65	250
2	70	250
3	75	250

These were mixed, with frequent stirring by hand, and none of them formed a gel readily. The sample was then passed through a hammer mill, which reduced it to about –50 mesh. The mixtures were stirred by hand, as before, and the following results were obtained: No. 1, gel formed in 6 hr; No. 2, soft gel was formed in 6 hr; No. 3, gel was not formed in 6 hr. These results showed that the speed of gel formation is increased by grinding the dolomite.

A further series of experiments was made in which a Hamilton Beach mixer was used for stirring. With 60 g of the –20 mesh Mascot dolomite and 250 ml of Hope solution, a gel was formed in 80 min. The same dolomite, after being passed through a hammer mill, which reduced it to about –50 mesh, formed a gel in 50 min. Another series of experiments gave the following results:

Mascot–20 Mesh Dolomite (g)	Hope Solution (ml)	Time of Gel Formation
50	250	No gel, 3 hr
55	250	Gel, 2 hr
60	250	Gel, 50 min
65	250	Gel, 50 min

It was then considered that 60 g of Mascot –20 mesh dolomite with 250 ml of Hope solution would make a satisfactory gel. This is equivalent to 2 lb of dolomite per gallon of Hope solution.

The test was repeated, and –20 mesh Chickamauga limestone screenings from the quarry near X-10 were used. Limestone screenings, too fine for use in construction, are available in large quantities, and it would be inexpensive to screen this material through –20 mesh.

The results of the test were as follows:

Chickamauga–20 Mesh Limestone (g)	Hope Solution (ml)	Time of Gel Formation
50	250	No gel, 60 min
55	250	Soft gel, 60 min
60	250	Soft gel, 50 min

Other results indicate that the limestone forms a gel more readily than the dolomite. However, with 250 ml of Hope solution and either 60 g of the –20 mesh Mascot dolomite or 60 g of the –20 mesh Chickamauga limestone, a satisfactory gel can be formed in about 1 hr, providing that there is rapid, thorough mixing. This proportion is equivalent to 2 lb of either of the carbonate minerals to 1 gal of Hope solution. Calculations show that, to form a satisfactory gel, it is not necessary to add enough of the carbonate to react with all the aluminum nitrate.

Fixation of Radioactive Isotopes in Gels

It was thought that it should be possible to form a ceramic body by (1) making a gel with limestone and Hope solution with the simultaneous addition of local clays or silica, (2) dehydrating the gel, and (3) sintering the resulting mixture. Chemical analyses were made of the Chickamauga limestone and the Conasauga surface clay, with the following results:

Chickamauga Limestone

Component	Per Cent
Acid (insoluble, largely SiO_2)	8.21
R_2O_3	1.23
CaO	46.10
MgO	3.03
Ignition loss	39.40
	97.97

Conasauga Clay

(Composite sample from 12 ft of drill hole)

Component	Per Cent
SiO_2	65.1
Al_2O_3	14.6

Component	Per Cent
Fe_2O_3	5.69
CaO	2.50
MgO	1.23
Na_2O	0.23
K_2O	3.50
Ignition loss	6.63
	99.48

The following compositions were made:

No.	Chickamauga −20 Mesh Limestone (g)	Hope Solution (ml)	Conasauga Clay (g)	Silica (Potter's Flint, 99+% SiO_2) (g)
1	60	250	50	
2	60	250	100	
3	60	250	50	50

In all cases the gels were formed in less than 1 hr. The calculated chemical analyses of these mixtures (ignited) are as follows:

No.	SiO_2 (%)	R_2O_3 (%)	CaO + MgO (%)	Alkalies (%)
1	36.7	30.6	30.9	1.8
2	47.1	27.9	22.5	2.5
3	57.6	20.5	20.7	1.2

The proportions of materials used for each gallon of Hope solution are given below:

No.	Chickamauga Limestone (lb)	Conasauga Clay (lb)	Silica (lb)
1	2	1.67	
2	2	3.33	
3	2	1.67	1.67

The mixtures were partially dehydrated in a dryer, but dehydration was not complete – gummy masses remained. These were placed on a hot plate, and copious fumes of NO_2 were evolved. They were then fired at 1700°F for about 3 hr, and additional NO_2 was given off. Pieces of the fired bodies were placed in water; the water surrounding No. 1 was highly basic, that surrounding No. 3 was moderately basic, and that surrounding No. 2 was only slightly basic. These basicities resulted because the lime had not completely reacted with the other materials present. The most complete reaction was obtained with No. 2. All the bodies will be fired at a series of higher temperatures.

It should be noted that the gels melted as soon as they were heated, which indicates that, if such gels are placed in a pit and they become warm, a liner may be needed.

After the conditions for making a satisfactory ceramic body from the gels with various additions have been determined, radioactive Hope solution will be used, and leaching tests will be carried out to determine whether the radioactive isotopes can be fixed in such a composition.

Retention of NO_3 Ion by Gels

With the knowledge that NO_3 ion has been found in the vicinity of some of the present pits, the following experiments have been carried out to determine whether the gels retain NO_3^-. Five-hundred-milliliter graduates, with openings at the bottom and at the 50-, 100-, and 150-ml graduations (Fig. 41), were used in these experiments.

Experiment 1. – Conasauga clay was packed in the bottom of the cylinder to just above the 150-ml graduation. A gel was made with 60 g of the −20 mesh Chickamauga limestone and 250 ml of the Hope solution, and the gel was poured into the cylinder. Water was admitted through the bottom opening to thoroughly saturate the clay.

At the end of five days the following qualitative results of tests for NO_3^- were obtained with the use of diphenylamine indicator:

Opening	Indication of NO_3^-
150 ml	Strong
100 ml	Moderate
50 ml	Weak
Bottom	Trace

These results indicate that there was little migration of NO_3^- under static conditions. The cork from the bottom opening was removed, and water was poured into the graduate. After nine days the following observations were made:

Opening	Indication of NO_3^-
150 ml	Strong
100 ml	Strong
50 ml	Weak
Bottom	Trace

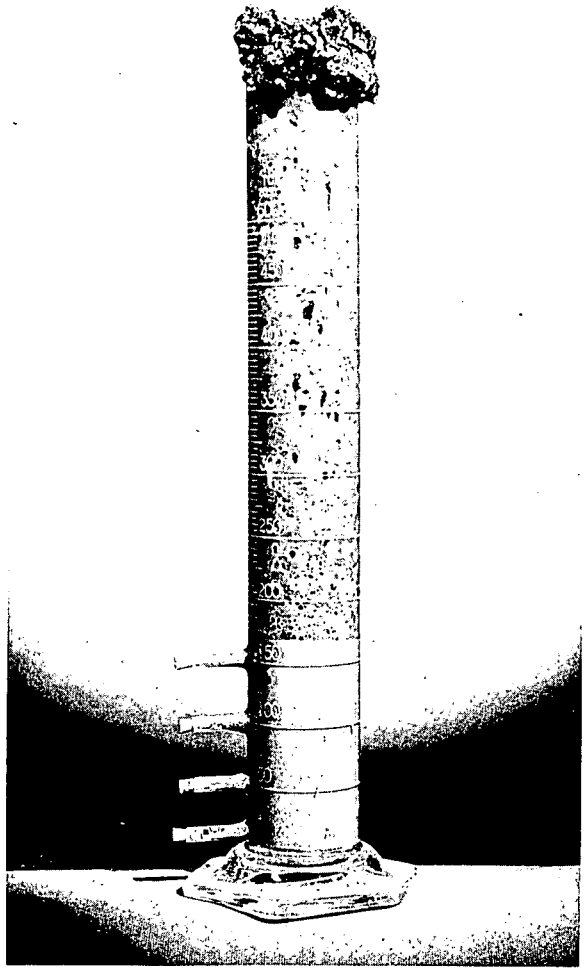

Fig. 41. Graduate (500 ml) Used in Testing Retention of NO_3 Ion by Gels.

Some migration of NO_3^- had occurred, but it was not marked.

Experiment 2. – Another graduate was used, and eight divisions of bentonite No. 90 were placed between the Conasauga clay and the gel. The bottom clay was saturated, as before, and after five days the following observations were made:

Opening	Indication of NO_3^-
150 ml	Trace
100 ml	Barren
50 ml	Barren
Bottom	Barren

Water was added to the graduate, as in experiment 1, and after nine days the following observations were made:

Opening	Indication of NO_3^-
150 ml	Moderate
100 ml	Weak
50 ml	Trace
Bottom	Barren

Conclusion. – A bentonite layer is fairly effective in reducing migration of NO_3^-.

Diffusion of Radioactive Strontium from Gels

Experiment 1. – Radioactive strontium was added to the Hope solution in sufficient quantity to give 15,000 counts/min/ml. This solution was used to make the gel, which contained 154 g of Chickamauga limestone to 500 ml of Hope solution. The graduate was packed to the top of the 150-ml opening with Conasauga clay; ½ in. of bentonite was placed on the clay and was, in turn, covered with a thin layer of the clay. The gel was poured into the graduate, and water was admitted through the bottom opening to saturate the clay. Small quantities of the clay were removed through the openings, and counts were made. This method is not precise because of the difference in the size of the samples. The results, however, are comparative.

Opening	Counts per Minute		
	After 9 Days	After 13 Days	After 18 Days
150 ml	42	319	1050
100 ml	27	55	624
50 ml	24	12	745
Bottom	8	12	270

The nine-day counting was done under static conditions. Water was poured on top of the gel at the end of nine days, and the bottom cork was removed. The gel had about 13,000 counts/min, and the water surrounding the gel 80 counts/min for a volume equal to that of the samples removed through the bottom openings. It is quite evident that fission products pass through the bentonite sandwich.

Experiment 2. – A graduate was packed in a manner similar to that used in experiment 1, except that the bentonite layer was omitted. The results

were as follows:

Opening	Counts per Minute	
	After 5 Days	After 9 Days
150 ml	647	1250
100 ml	41	1028
50 ml	20	552
Bottom	Background	76

The five-day counting was done under static conditions. Water was poured on top of the gel at the end of five days, and the bottom was left open.

The bentonite layer is of some assistance in retarding the passage of radioactive strontium.

Experiment 3. – A graduate similar to the two used previously was packed. After five days the bottom clay was damp but was not impregnated with water. Water was then allowed to flow into the bottom of the cylinder for one day, and the stoppers were replaced. The following results were obtained:

Opening	Counts per Minute		
	After 5 Days	After 6 Days	After 41 Days
150 ml	66	682	1446
100 ml	Background	Background	704
50 ml	Background	Background	313
Bottom	24	6	290

Results. – The results of these experiments show that the radioactive strontium will diffuse from the gel into wet clay underneath. This indicates that, if gel were placed in a pit below ground water, the radioactive isotopes would diffuse into the wet clay.

Investigation of Porous Ceramics as Isotope Sorbers

An investigation was carried out with porous fired-clay slugs which are capable of removing, through absorption and selective absorption, a considerable amount of radioactive particles and ions from waste liquors. A preliminary investigation suggests that the effect of cataphoresis in attracting radioactive ions into the clay slugs is somewhat erratic and does not change the order of removal from that accomplished by mere soaking, under the conditions investigated. Acid liquors do not give up the radioactivity to the slugs nearly so efficiently as do basic liquors. The removal of radioactive isotopes from basic waste liquors is selective in that the concentration of such radioisotopes in the enveloping liquid is materially reduced. The clay slugs are capable of being glazed and rendered virtually unleachable. Porosity of the slug is more important than the type of clay. Almost any type of clay is effective.

Diamond Drilling

Four cored holes have been drilled 200 ft deep in an area 400 × 400 ft lying between Haw Ridge and Copper Ridge; this area is under consideration as a test-pit site. From drill records, it appears that the weathered zone extends to 14 ft from the surface; below this zone is a fractured zone to 65 ft from the surface. At greater depth, the core strata appear to be relatively impervious.

HRP METALLURGY

E. C. Miller

PHYSICAL METALLURGY OF TITANIUM AND OF ZIRCONIUM ALLOYS

W. J. Fretague

Commercial Titanium

Impact tests have been completed on specimens machined from an unalloyed-titanium corrosion specimen holder (RC-70, heat 3102, REED item 11). Table 10 presents the loop history of the specimen holder.

In addition to the tabulated exposures, the holder was cathodically defilmed frequently in inhibited 5% sulfuric acid at room temperature.

Sufficient material of similar analysis (RC-70, heat 3102, REED item 11) in the as-received condition was available for 12 multiple-break impact specimens.

The impact data plotted in Fig. 42 indicate that the combination of loop exposure and cathodic defilming has drastically embrittled the material, raising the transition temperature from approximately 100 to above 200°C. This result is contrary to previous experience; attempts to embrittle unalloyed titanium both by cathodic treatment[1] in H_2SO_4 and by loop exposure to simulated HRP environments[2] have, in the past, been unsuccessful. The cathodic-defilming procedure may have introduced hydrogen into the metal and thus produced the observed embrittlement.

Additional impact tests have been performed on unalloyed titanium 75A, heat L782, REED item 24. These specimens were exposed to the loop environment described in Table 11, in the as-swaged-and-machined condition, in an effort to study the effect of cold-working on the rate of hydrogen adsorption

[1] W. J. Fretague, A. R. Olsen, R. G. Berggren, and J. J. Woodhouse, *Met. Semiann. Prog. Rep. Oct. 10, 1953*, ORNL-1625, p 9–10 and Fig. 5.

[2] W. J. Fretague, *Met. Quar. Prog. Rep. Oct. 31, 1952*, ORNL-1437, p 41.

TABLE 10. HISTORY OF UNALLOYED-TITANIUM CORROSION SPECIMEN HOLDER

HRP Loop Run No.	Solution: Uranium Concentration as UO_2SO_4 (g of U per liter)	Solution: Additions	Temperature (°C)	Time (hr)
I-3	40	0.042 M H_2SO_4 200-psi O_2	250	1036
F-20	300	200-psi O_2	250	117
D-1	300	50 ppm Tc 200-psi O_2	250	101
D-2	300	200-psi O_2	250	100
H-15*		1.0 M HCl 1.4 M H_2SO_4 0.2 M H_2O_2 Alkyl pyridine inhibitor 200-psi He	85	4
H-16	25	200-psi O_2	250	200
H-17	25	200-psi O_2	250	400
				1958

*Decontamination run.

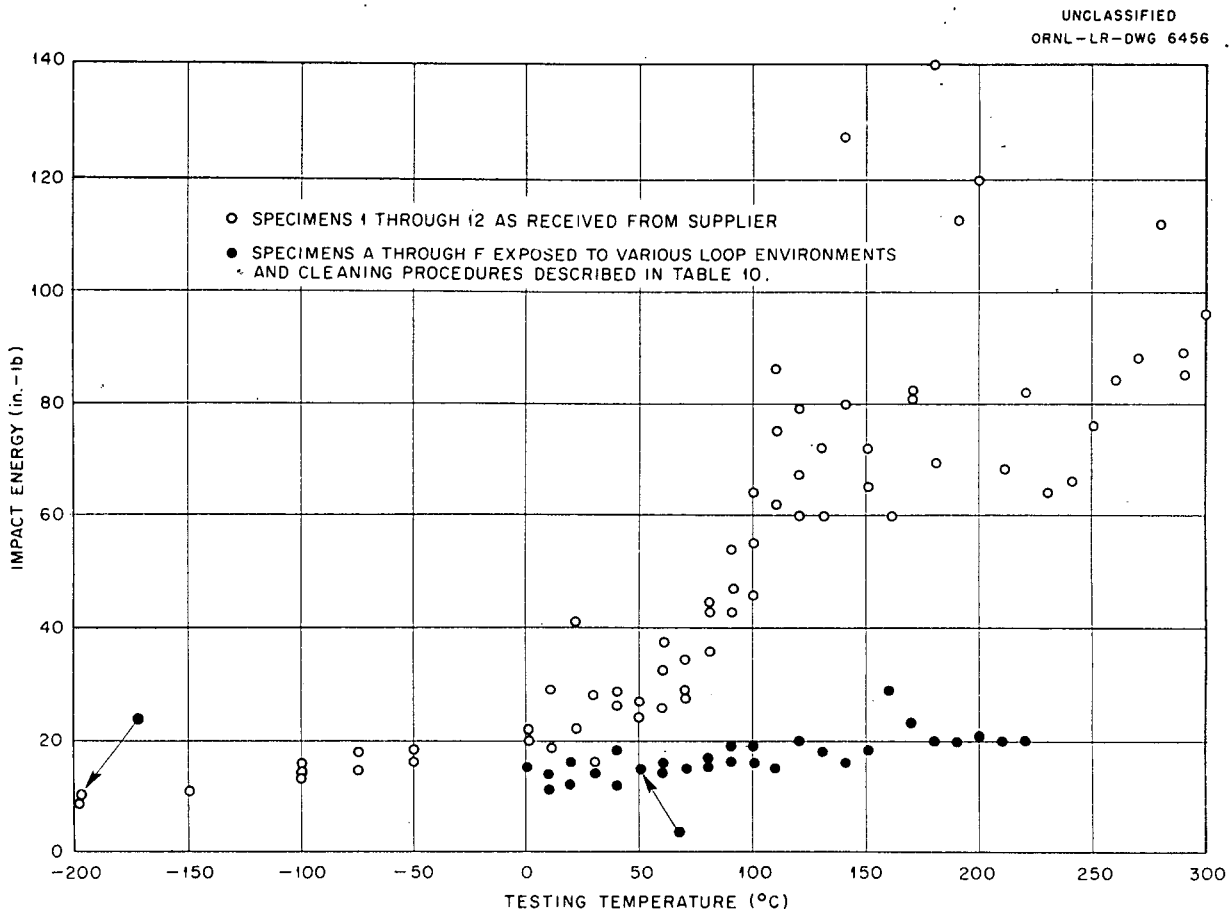

Fig. 42. Impact Energy vs Testing Temperature for Titanium (RC-70), Reed Item 11, Heat 3102.

by titanium, as measured by the impact behavior. The impact data obtained from these specimens are plotted in Fig. 43. A comparison of these results with those obtained for as-swaged[1] and for swaged-and-vacuum-annealed unalloyed titanium[3] does not reveal any effect on the impact properties that could be attributed to the treatment given to the specimens (prior to exposure) or to the corrosive environment in which they were exposed.

Four multiple-break impact specimens of unalloyed titanium (Ti-75A, heat L782, REED item 24) in the vacuum-annealed condition were impact-tested after exposure to the loop environment described in Table 12. The impact data obtained are plotted in Fig. 44. No significant difference in the impact behavior of these specimens as compared with that of similar specimens, exposed under similar conditions,[3] was observed.

Samples from the pressurizer section of an all-titanium loop that failed in service were analyzed for hydrogen by the vacuum-fusion method at Battelle Memorial Institute and at ORNL. The results are presented in Table 13, with a notation as to the location from which the sample was obtained.

Iodide-Titanium

Impact tests have been completed on a series of four iodide-titanium specimens that were exposed to simulated HRP environments in a dynamic-corrosion loop under the conditions outlined in Table 14. The impact data obtained are presented in Fig. 45, together with data previously obtained

[3] W. J. Fretague, A. R. Olsen, and R. G. Berggren, *Met. Semiann. Prog. Rep. April 10, 1953*, ORNL-1551, p 13–15 and Fig. 12.

TABLE 11. LOOP HISTORY OF AS-SWAGED-AND-MACHINED UNALLOYED-TITANIUM IMPACT SPECIMENS

HRP Loop Run No.	Solution		Temperature (°C)	Time (hr)
	Uranium Concentration as UO_2SO_4 (g of U per liter)	Additions		
A-67	15	0.006 M H_2SO_4	310–320	977

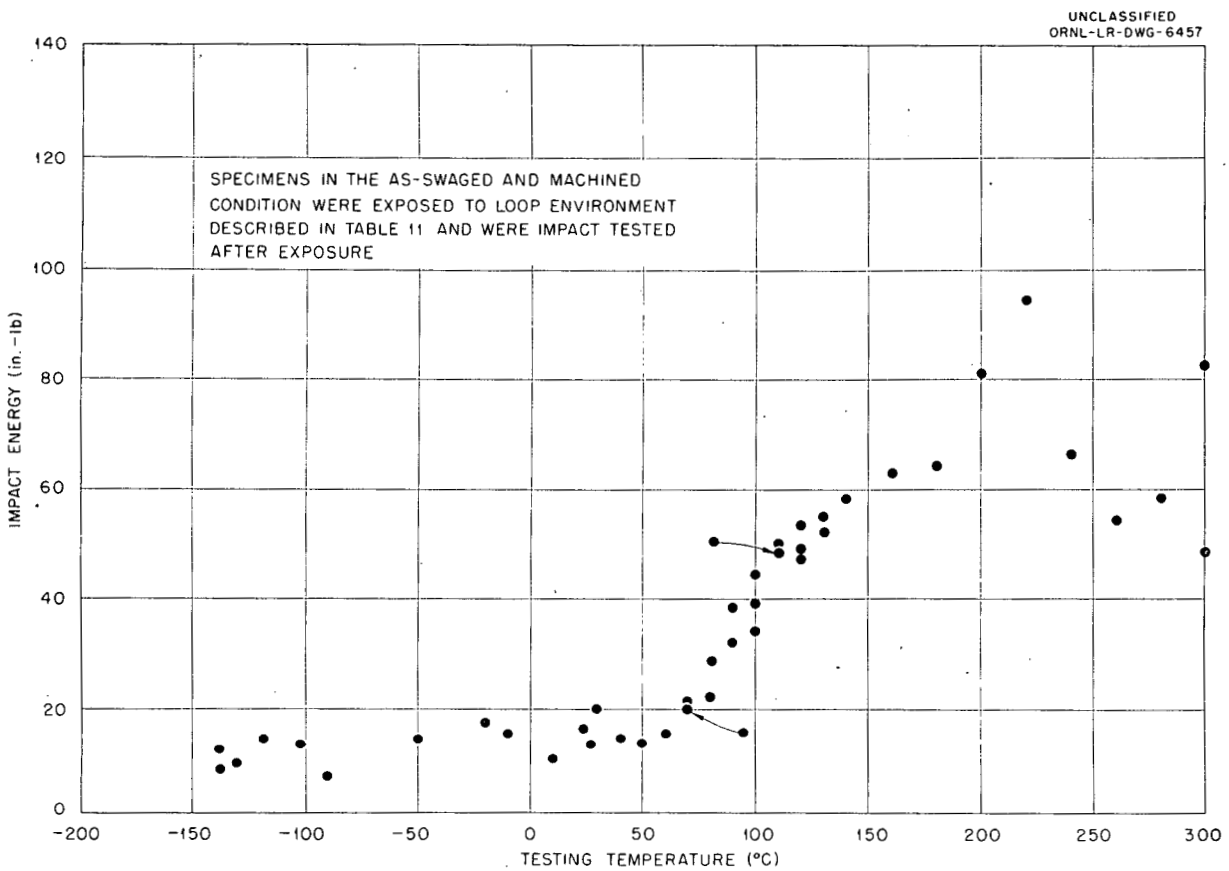

Fig. 43. Impact Energy vs Testing Temperature for Ti-75A, Reed Item 24, Heat L782.

for vacuum-annealed iodide-titanium. Exposure to the corrosive environment under the test conditions outlined had little or no effect on the impact behavior of the material tested.

Bureau of Mines Titanium

Impact specimens exposed to the HRP loop environment described in Table 15 were impact-tested. The resultant data are presented in Table 16. A comparison of these data with impact data on unexposed vacuum-annealed Bureau of Mines titanium[4] does not reveal any effect of the corrosive environment on the impact properties of the exposed samples under the test conditions.

Zirconium Alloys

Zircaloy-2 rod ($\frac{3}{8}$ in. in diameter) was cold-swaged to 0.217 in. in diameter, sandblasted,

[4]W. J. Fretague and J. O. Betterton, *HRP Quar. Prog. Rep. July 31, 1953*, ORNL-1605, p 121.

TABLE 12. LOOP HISTORY OF VACUUM-ANNEALED UNALLOYED-TITANIUM IMPACT SPECIMENS

HRP Loop Run No.	Solution		Temperature (°C)	Time (hr)
	Uranium Concentration as UO_2SO_4 (g of U per liter)	Additions		
G-11	300 (1.34 *M*)	0.3 *M* H_2SO_4 1000 ppm O_2	300	150

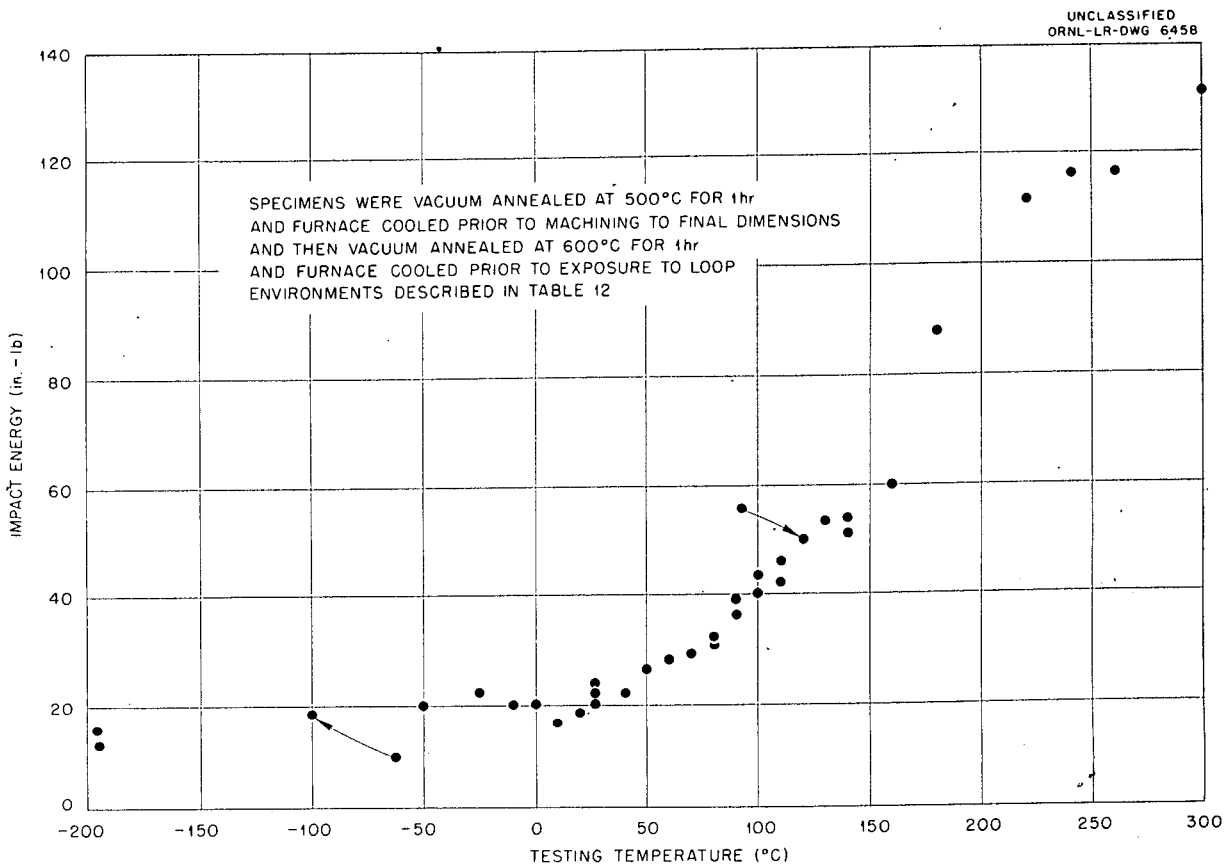

Fig. 44. Impact Energy vs Testing Temperature for Ti-75A, Reed Item 24, Heat L782.

pickled and vacuum-annealed at 750°C for 2 hr, and furnace-cooled. Impact specimens were machined from this annealed rod and tested over the temperature range from −197°C (liquid nitrogen) to +300°C. The impact data obtained are presented in Fig. 46. These data serve as a base line for comparison with similar specimens exposed to HRP loop environments prior to impact testing.

Tensile tests have been performed at room temperature and at 600°F on specimens cut from $\frac{5}{16}$-in.-thick welded Zircaloy-2 plate fabricated by Newport News Shipbuilding & Drydock Co. The results of these tests are listed in Table 17.

TABLE 13. HYDROGEN IN UNALLOYED TITANIUM FROM RUPTURED PRESSURIZER TUBE

Laboratory Performing Analysis					
Battelle Memorial Institute			Oak Ridge National Laboratory		
Sample code	Location	Hydrogen content (wt %)	Sample code	Location	Hydrogen content (wt %)
N 1633	As-received material	0.0109 0.0113	N 1640	As-received material	0.011
N 1635	Ruptured section of pipe	0.0083 0.0089	N 1639	Ruptured section of pipe	0.0086
N 1636	Section adjacent to fracture	0.0061 0.0061	N 1638	Section adjacent to fracture	0.0048*
			N 1641	Section away from fracture	0.0064

*This sample was smaller in size (0.7 g) than the other samples (1.2 to 1.9 g), and this probably accounts for the difference between results obtained by the two laboratories.

WELDING OF STAINLESS STEELS

W. J. Leonard

Evaluation of the Preplaced Consumable-Insert Heliarc Welding Technique for Root Pass

Weld penetration and soundness requirements stipulated by the HRE and HRP Welding Specifications, when the manual inert-gas-shielded nonconsumable-electrode welding process is used, require a great deal of operator training and qualification time. Even after having received such training, a qualified welder has difficulty in consistently meeting the quality requirements for the root pass. Therefore the process used by Electric Boat Div.[5] was evaluated for use in pipe welding. Type 347 stainless steel preplaced root wire, machined to the proper dimensions, was obtained. Type 347 stainless steel piping, sizes 3 to 8 in. in diameter and with wall thicknesses of schedules 20 and 40, was machined to proper weld-groove dimensions and assembled for welding.

The chemical compositions of the two heats of root wire were balanced so as to give 6 and 8% ferrite, respectively. The base metal was fully austenitic. Wall thicknesses varied from 0.200 to 0.322 in. Root passes made by this method were satisfactory and well within the HRP specification requirements. They required less operator skill than do existing welding methods, and there was no apparent difference in welding time. Improved weld quality resulted but was obtained at a somewhat higher cost because of the added expense of preplaced wire and initial machining.

A program is now under way to qualify this complete procedure and to set up an operator-qualification standard.

Welding Development on 1-in. Carbon-Steel Plates Clad with Type 347 Stainless Steel

The pressure vessel in the HRT design is to be a spherical outer container of 4-in. carbon-steel plate, clad with type 347 stainless steel on the interior, with an internal diameter of approximately 5 ft. The design is such that the final girth weld must be made from the outside only, rather than by the more common back-chipping method, which allows welding from both sides. Where the welding must be done from the carbon-steel side only, one suggested procedure is to fill the root and groove with stainless steel weld metal to a point above the interface between the carbon steel and stainless steel, follow this with an intermediate layer of a few passes of a material such as ingot iron, low-carbon steel, type 308L stainless steel, or

[5] T. A. Risch and A. E. Dohna, *Welding J. (NY)* 33, 670 (1954).

TABLE 14. LOOP HISTORY OF IODIDE-TITANIUM IMPACT SPECIMENS

HRP Loop Run No.	Solution		Temperature (°C)	Time (hr)
	Uranium Concentration as UO_2SO_4 (g of U per liter)	Additions		
A-67	15	0.006 M H_2SO_4	310–320	977

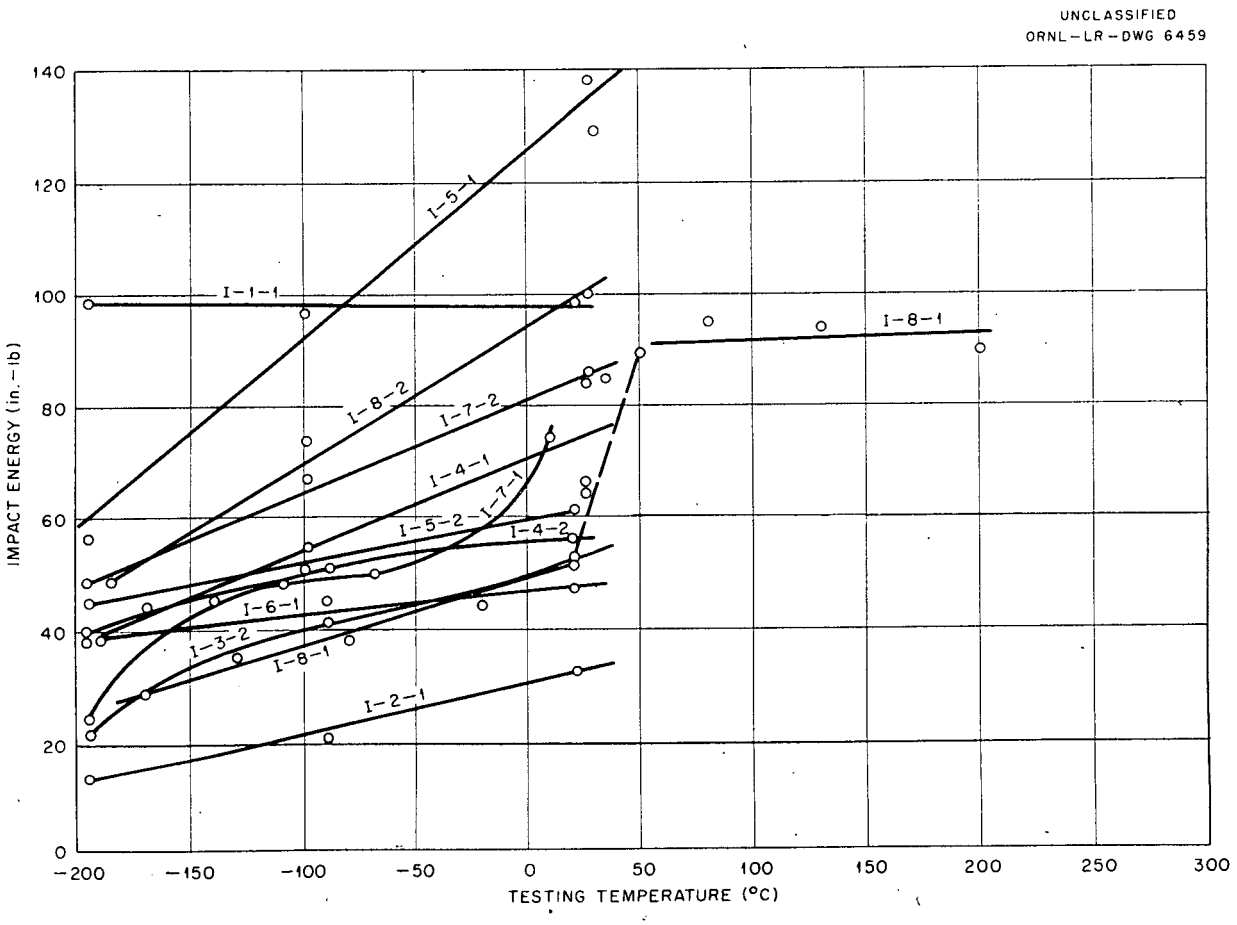

Fig. 45. Impact Energy vs Testing Temperature for Arc-Melted, Swaged and Vacuum-Annealed Iodide-Titanium. Specimens I-4-1, I-5-1, I-7-2, and I-8-2 were exposed, prior to impact testing, under the conditions listed in Table 14. All other specimens were tested in the vacuum-annealed and machined condition.

TABLE 15. LOOP HISTORY OF BUREAU OF MINES IMPACT SPECIMENS

HRP Loop Run No.	Solution		Temperature (°C)	Time (hr)
	Uranium Concentration as UO_2SO_4 (g of U per liter)	Additions		
G-9	300	50-psi O_2 at room temperature	300	427

TABLE 16. IMPACT ENERGY vs TESTING TEMPERATURE DATA FOR BUREAU OF MINES TITANIUM SPECIMENS EXPOSED IN HRP LOOP RUN G-9

(Scale used, 0–200 in.-lb)

Specimen No.	Break No.	Temperature (°C)	Impact Energy (in.-lb)	Remarks
B2-1	1	27	125	Threaded end*
	2	27	148	Did not break
	3	–197	182	50% fracture
B2-2	1	27	100	Threaded end*
	2	27	144	50% fracture
	3	–197	178	50% fracture
B3-1	1	27	100	Threaded end*
	2	27	133	60% fracture
	3	–197	142	75% fracture
B3-2	1	27		Broken by hand**
	2	27	128	60% fracture
	3	–197	156	60% fracture

*The ends of the specimens were threaded to enable them to be held in the specimen fixture in the loop; the threads extended below the point of impact of the striking hammer of the impact tester; and the deformation of the threads on impact gives rise to some error in the readings.

**Specimen was too short to be broken by the impact tester.

TABLE 17. RESULTS OF TENSILE TESTS ON ZIRCALOY-2 WELDED PLATE

Specimen No.	Testing Temperature	Yield Strength, 0.2% Offset (psi)	Tensile Strength (psi)	Elongation (%)	Reduction in Area (%)
ZW 33-1	Room temperature	55,000	55,000	0	0
ZW 33-2	600°F	28,000	37,000	20	63.4

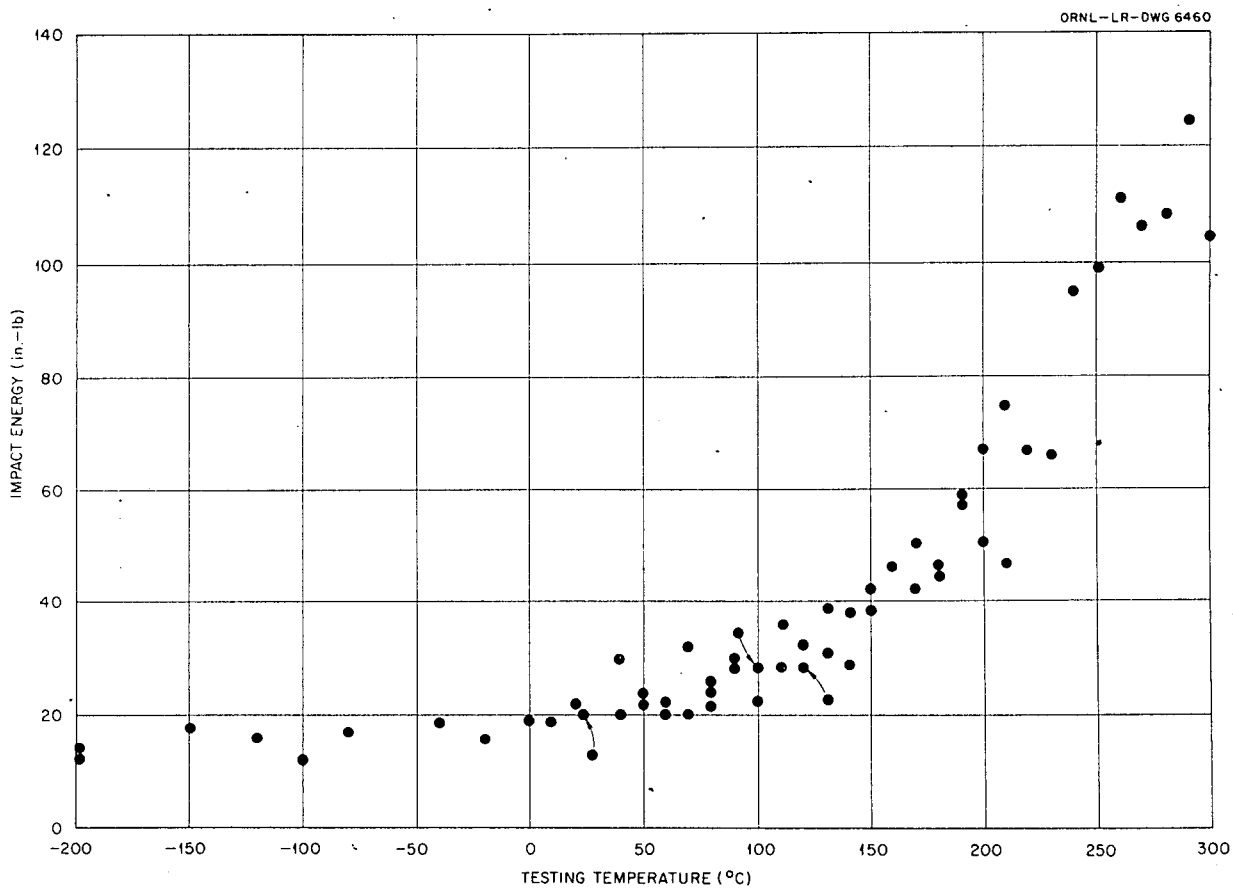

Fig. 46. Impact-Testing Behavior of Zircaloy-2 ($\frac{3}{8}$-in. Rod Swaged to 0.217-in.-dia Rod, Sand Blasted, Pickled, Vacuum Annealed at 750°C for 2 hr, and Furnace Cooled).

type 310 stainless steel, and complete the weld with low-hydrogen mineral-coated carbon-steel electrodes.

To evaluate several variations of this proposed welding sequence, a 1-in.-thick plate of ASTM A201 grade A carbon steel, with a 20% cladding of type 347 stainless steel, was obtained. The root face and groove were prepared by machining test specimens to accommodate the preplaced wire used in the Electric Boat Heliarc welding method. Previous work and qualification on this method of Heliarc welding indicated the desirability of using this method rather than manual Heliarc welding in conformance with HRP welding specifications, to obtain closer control of root penetration and weld soundness.

Six welds of this type were made in these specimens (Fig. 47), by using the Heliarc welding method described, with type 347 preplaced wire. Amperage was varied from 140 maximum to 90 minimum, for different weld metal passes; travel speed of the electrode was varied from 1 to 4½ in./min. These manipulations allowed control of the heat input per pass, thus regulating the resulting penetration and dilution. At each amperage level used, a heat input over a certain critical value resulted in cracking of the root pass. At a 140-amp welding current, a minimum welding speed of 4 in./min must be maintained to secure a sound root pass. At 90 amp a speed of 1 in./min or greater resulted in sound welds. At lower amperages, travel speed is less critical because of greater dissipation, percentagewise, of the total heat by the base plate. All passes that cracked were ground out and rewelded, so that eventually all plates had sound root passes.

These welds were completed up to the carbon-steel and stainless steel interface by filling with coated-electrode type 347 stainless steel. Some

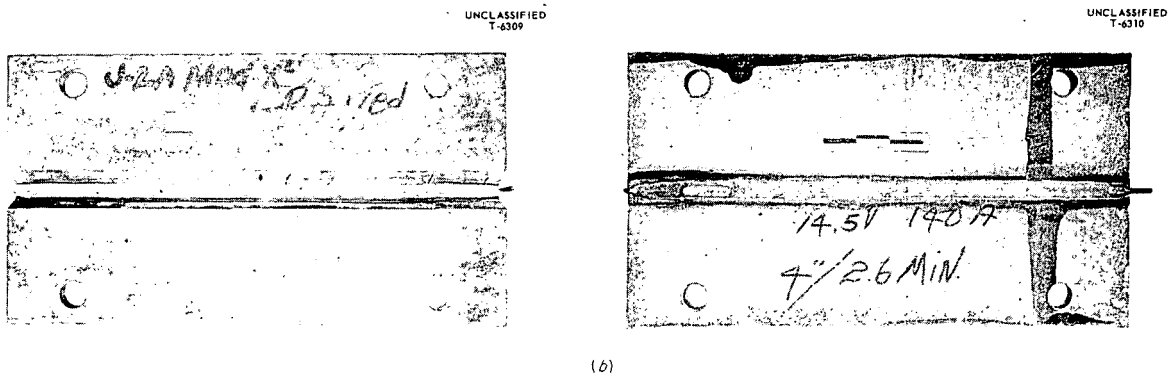

Fig. 47. Carbon Steel–Type 347 Stainless Steel Clad Plate with Heliarc Root Pass (Electric Boat Welding Technique). Cracking which occurred during welding shown from (*a*) face and (*b*) root side of weld.

were then given a cover pass or two of type 310 or 308L stainless steel coated electrode in accordance with the schedule set up for the program. One was finished by using carbon-steel electrodes of low-hydrogen mineral-coated types E6016 and E7016. The balance are to be completed by various special techniques.

The one completed weld indicates that this technique produces a sound weld, based on radiographic and liquid-penetrant inspections. However, until the specimens are sectioned for micrographic examination for microfissuring and are mechanically tested, no definite conclusions can be made as to the acceptability of this method of producing pressure-vessel welds.

Type 347 Stainless Steel Welds in Which Various Type 347 Stainless Steel Filler Metals Were Used

W. J. Leonard T. M. Kegley, Jr.

A grooved fillet weld was made to the inner wall of a type 347 stainless steel pipe ($\frac{1}{4}$-in. wall thickness) by using a $\frac{5}{8}$-in. plate (Fig. 48). A J-groove design was used, and the starting point of each successive pass was moved a short distance along the periphery so that sectioning of the weld would allow the weld cross section to be viewed at any stage of completion.

Figure 48 shows a section after the first pass, while Fig. 49 shows a section approximately half completed and a completed weld.

Figure 50 shows a cross section of this weld (*A*) and a similar weld (*B*). A further description of the passes, identified in Fig. 50, is given in Table 18.

Weldment *A* was made by using Heliarc welding for the first three passes. Cracks developed in the second and third passes. This area, which was almost fully austenitic, as a result of dilution of the base metal, is thought to be most susceptible to cracking under conditions of restraint. Figures 51 through 55 illustrate the microstructure at the indicated positions. It will be noted that cracking occurs in the filler metal of low ferrite content such as at positions *A*1 and *A*3.

Weldment *B* was made by Heliarc welding (inert-gas-shielded arc, tungsten electrode). The root

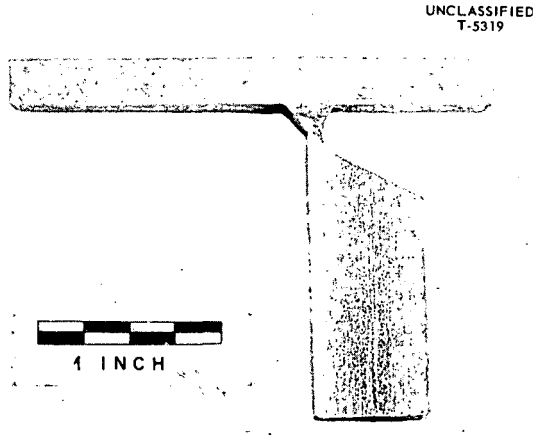

Fig. 48. Weld Cross Section with Root Pass, Illustrating Groove Design Used.

passes were made with low-ferrite filler metal and completed with high-ferrite filler wire. Some small cracks were observed in the root, where considerable dilution of the weld metal and base metal occurred. Figures 56 and 57 are photomicrographs of these areas. Cracking can be noted in the root of this weld (Fig. 50), whose microstructure is represented by Fig. 56.

[6]W. O. Harms and W. J. Leonard, *Met. Semiann. Prog. Rep. April 10, 1954*, ORNL-1727, p 19.

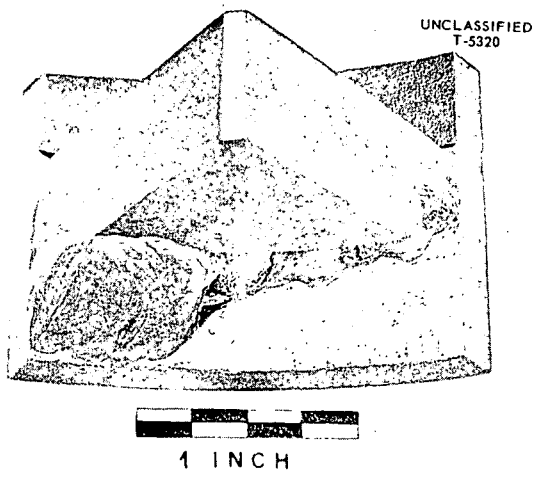

Fig. 49. Section of the Pipe Weld, Illustrating Welding Sequence.

Fig. 50. Weld Cross Section with All Welding Passes Completed. (*A*) Heliarc root pass with the balance coated electrode. (*B*) Heliarc weld.

METALLURGY OF CORROSION IN HOMOGENEOUS REACTOR ENVIRONMENTS

W. O. Harms W. J. Leonard

Stainless Steel Welds

The special flat-plate-type corrosion specimens described previously[6] were tested in oxygenated

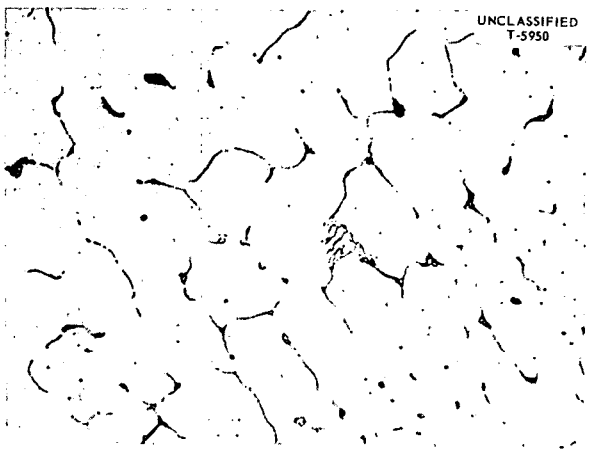

Fig. 51. Photomicrograph of Low-Ferrite Heliarc Root Pass at Position *A*1. Etchant: glyceria regia. 750X. Reduced 32%.

TABLE 18. DESCRIPTION OF WELDING PASSES SHOWN IN FIG. 50

Weld Position	Type	Welding Wire	Ferrite in Weld (%)
*A*1	Heliarc	Low ferrite	½
2	Metallic arc	Commercial coated electrode	5½, 6, 7
3	Metallic arc	Commercial coated electrode	1½
4	Metallic arc	Commercial coated electrode	6
5	Metallic arc	Commercial coated electrode used in 4; diluted 3 and base metal	
*B*6	Heliarc	Low ferrite	1
7	Heliarc	High ferrite	10

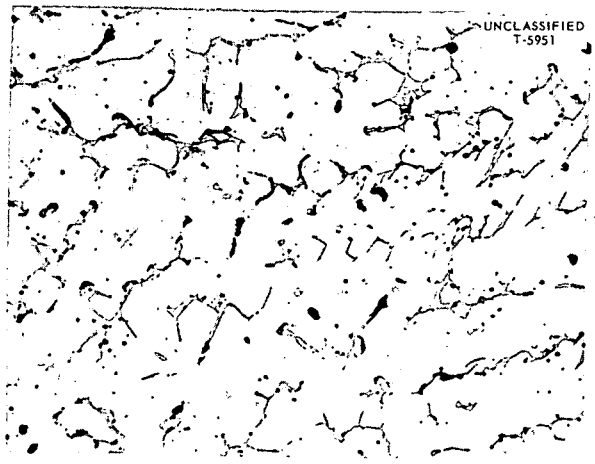

Fig. 52. Photomicrograph of Coated-Electrode Pass at Position *A*2, Having Ferrite and Carbides. Etchant: glyceria regia. 750X. Reduced 32%.

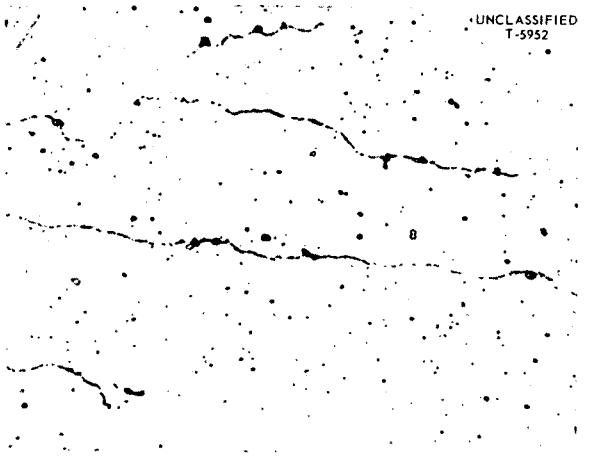

Fig. 53. Photomicrograph of Coated-Electrode Pass at Position *A*3, Having a Trace of Ferrite and Grain-Boundary Carbides. Etchant: glyceria regia. 750X. Reduced 31%.

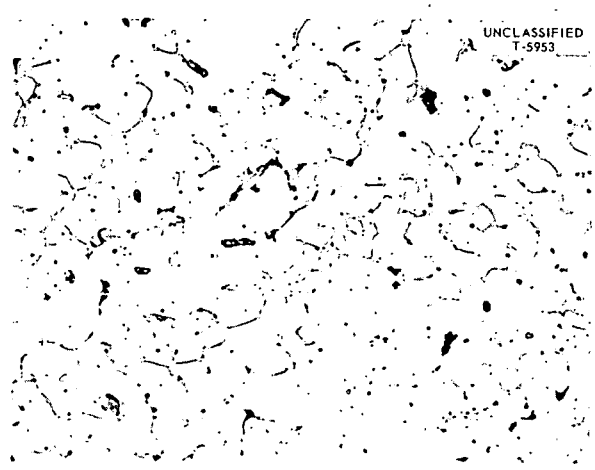

Fig. 54. Photomicrograph of Coated-Electrode Filler Pass at Position *A*4, Having Ferrite and Carbides. Etchant: aqua regia. 750X. Reduced 32.5%.

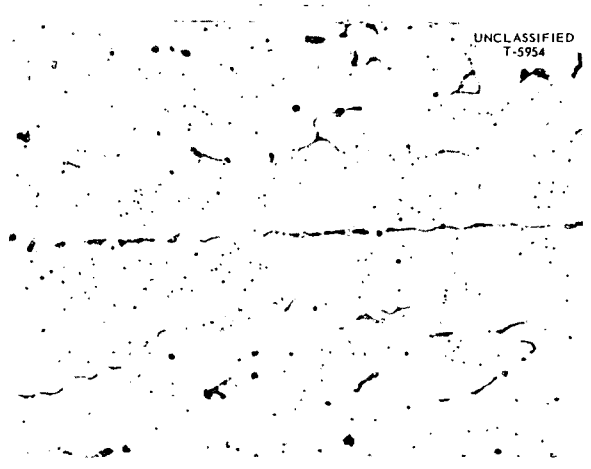

Fig. 55. Photomicrograph of Diluted Area at Position *A*5, Having Slightly Higher Ferrite Content Than Position *A*3. Etchant: glyceria regia. 750X. Reduced 32%.

0.17 *m* uranyl sulfate at 250°C and at a velocity of 20 fps for 400 hr. The results of this test, along with those of the previous 200-hr run made under otherwise similar conditions, are given in Table 19.

Specimens containing weld deposits of Composition H (experimental columbium-stabilized 18% Cr–13% Ni–5% Mn steel) exhibited superior corrosion resistance in holder B, but in holder A only small differences in weight losses were observed among the type 347, type 308L, and Composition H welds, and, in general, corrosion damage was substantially lower in holder A. This difference in behavior is difficult to understand, since the Reynolds modulus for flow through holder A was higher than for that through holder B, in which the specimens were 20% thicker.

Figure 58 shows the peculiar effect observed on Composition H welds in holder B. The zones near

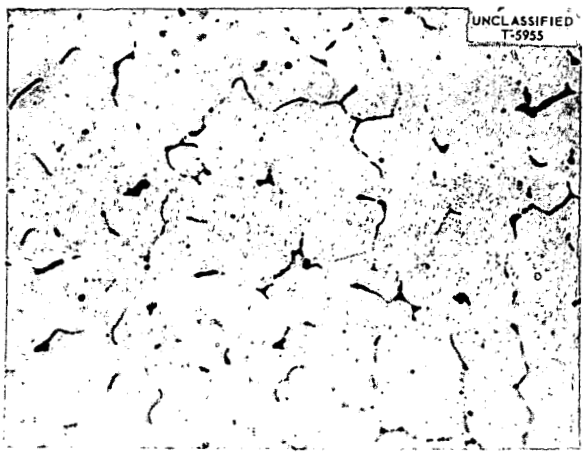

Fig. 56. Photomicrograph of a Low-Ferrite Heliarc Root Bead in Weld *B* (Position *B*6). Etchant: glyceria regia. 750X. Reduced 32%.

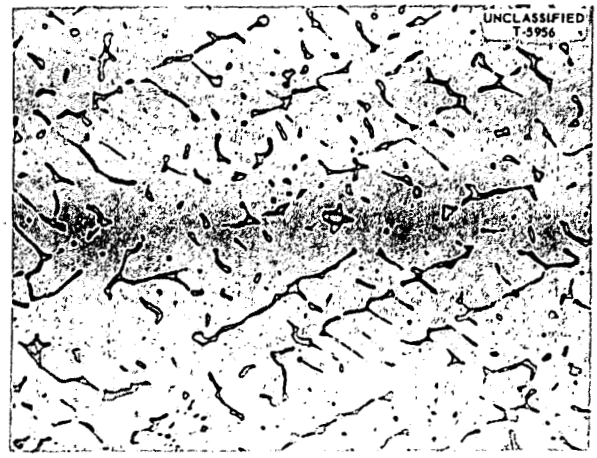

Fig. 57. Photomicrograph of a High-Ferrite Heliarc Filler Pass in Weld *B* (Position *B*7). Etchant: glyceria regia. 750X. Reduced 32%.

TABLE 19. RESULTS OF DYNAMIC-CORROSION TESTS ON SPECIAL FLAT-PLATE-TYPE WELDED AND BASE-METAL AUSTENITIC STAINLESS STEEL SPECIMENS*

	Base Metal	Weld Metal	Ferrite in Weld (%)	Defilmed Weight Loss (mg)	
				200 hr	400 hr
Holder A	347	None		83.0	115.4
	310	None		179.4	209.8
	347	347	8.0–8.5	73.9	111.7
	309SCb	None		81.9	196.1
	347	Composition H	0	96.1	186.7
	304L	None		53.6	114.1
	347	308L	9.0–11.0	98.0	174.9
	304	None		55.7	190.9
	347	Composition H	0	90.9	199.8
	347	None		84.9	199.3
Holder B	347	None		67.8	307.2
	347–304L	Composition H	0	51.8	396.6
	304L	Composition H	0	40.1	438.4
	304L	Composition H	0	**	473.4
	304L	None		39.2	504.5
	304L	308L	9.0–11.0	56.8	921.2
	304L–347	308L	9.0–11.0	68.3	893.1
	304L–347	347	8.0–8.5	78.2	560.0
	304L	347	8.0–8.5	57.6	712.3
	347	None		83.0	339.7

*Specimens were tested in 0.17 *m* uranyl sulfate, 250°C, 20 fps. Thicknesses of specimens in holder B were 20% greater than those in holder A. Welded specimens were tested in the as-welded condition, and wrought specimens were tested in the solution-annealed condition.

**Weighing error.

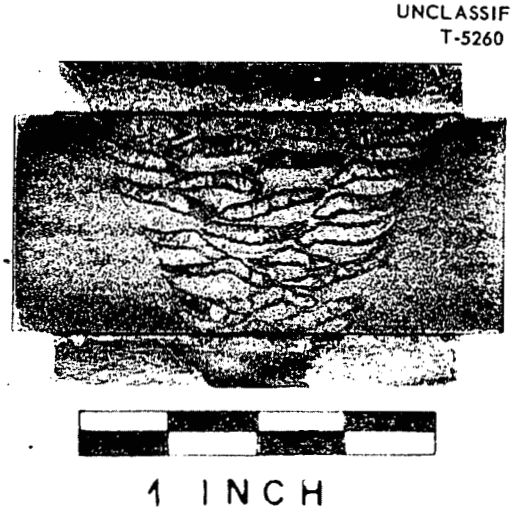

Fig. 58. Special Flat-Plate Welded Corrosion Specimen of Type 304L Stainless Steel Joined by Composition "H".

the top of each weld pass maintained protective oxide films, while bare-metal corrosion occurred on the remaining portions. A small amount of this type of behavior was observed on type 347 welds, but type 308L showed practically none. Metallographic examination revealed that the portions supporting stable films contained many randomly dispersed carbide particles, while the remainder exhibited the more typical quasi network due to interdendritic segregation. The thermal cycle corresponding to that undergone by the top portion of each pass has been calculated so that an all-weld-metal or a cast specimen can be heat-treated similarly and corrosion-tested at a later date.

Two additional sets of special flat-plate-type dynamic-corrosion specimens were machined from ¼-in. type 347 plates containing type 347 welds made by the Heliarc process with the use of a low-ferrite wire (2–4%) for one set and a high-ferrite wire (7–9%) for the other. Weld reinforcements were left on in the majority of cases so that the flow over coupons would approximate actual service conditions in butt-welded pipes. Differences in height of the face and the root reinforcements on these coupons caused variations in solution velocity, and the velocity effects were probably more severe than would normally be experienced at a butt-welded pipe joint. The specimens were tested in oxygenated 1.34 *m* uranyl sulfate solution at 250°C for 100 hr. The average velocity was 10 fps and the maximum was 16 fps. While averaged defilmed-weight-loss data hardly justified a distinction between the corrosion resistance of the high- and low-ferrite welds, it was observed that the films on samples containing 2 to 4% ferrite were somewhat more tenacious.

In order to get more information on the effect of ferrite content on the dynamic-corrosion resistance of austenitic stainless steel welds, all-weld-metal specimens ranging in ferrite content from 0 to 12% were tested in 0.17 *m* uranyl sulfate at 250°C under oxygen pressure and at velocities of 15 and 30 fps for 200 hr. These specimens were machined from the top half of ½-in.-thick weld pads deposited on type 347–buttered carbon-steel plate by using the argon-shielded tungsten-arc process under the following conditions: 200 to 220 amp, 12 to 16 v, and average travel speed of 4 in./min.

The results of runs M-23 and M-24 are shown in Table 20. Included in the main line in run M-23 was a chromized tube bundle consisting of seven tubes, ⅜-in. OD and 0.049-in. wall thickness, which underwent severe corrosion attack causing abnormally high concentration of hexavalent chromium ion in the solution. Since this is known to inhibit attack in uranyl sulfate, it was believed that the results of run M-23 required confirmation. Run M-24 was undertaken for this purpose, and it was observed that, although relative behavior was similar in both runs, differences were much more pronounced in the check run. These results indicate that, since alloy No. 4 (containing only a small amount of ferrite) showed by far the highest weight losses, the ferrite content per se is not so significant a factor in corrosion behavior as was suggested in previous runs. Previous data, however, indicate that ferrite has a deleterious effect on corrosion at higher uranium concentrations.

The several test results reported here indicate that factors other than ferrite content are operating to render these welds more or less corrosion resistant, at least at concentrations up to 0.17 *m* UO_2SO_4. To solve this problem will require considerable work in the identification of the various microconstituents and in the separation of these constituents so that independent chemical-composition and crystal-structure studies can be undertaken.

TABLE 20. DYNAMIC CORROSION OF AUSTENITIC STAINLESS STEEL WELD METAL CONTAINING VARYING AMOUNTS OF FERRITE

Alloy[a]	Ferrite in Weld[b] (%)	Weight Loss (mg/cm^2)			
		Run No. M-23[c]		Run No. M-24[c]	
		14.0 fps	28.4 fps	15.5 fps	30.5 fps
F	None	2.8	4.2	2.7	9.3
		1.5	1.6	3.6	8.0
H	None	2.5	13.8	3.5	51.5
		2.5	3.8	3.5	18.2
4	3.5–4.5	1.5	11.8	4.1	134.8
		1.2	11.6	4.2	154.9
P	6.0–6.5	1.7	3.1	2.3	10.2
		1.9	2.5	2.8	8.8
1	6.5–7.5	2.1	3.2	2.9	24.7
		1.2	2.9	2.4	15.2
3	7.5–8.5	1.1	2.4	1.3	6.2
		1.2	2.2	1.9	5.9
2	11.5–12.5	5.9	2.8	2.0	8.0
		5.9	2.7	2.0	6.7
Wrought-annealed type 347		1.3	12.7	5.7	4.6
		2.6	2.5	2.0	8.8
		1.4	11.8	5.8	5.8
		0.9	1.3	2.0	5.5
Wrought-annealed type 17-4 PH		0.7	1.3	1.4	8.2
		0.7	1.0	1.3	2.7

[a]Alloys 1, 2, 3, and 4 are type 347 stainless steel weld wires.
Alloy H is 19-13-5 Cr-Ni-Mn columbium-stabilized alloy.
Alloy F is 19-10-5 Cr-Ni-Mn not stablized.
Alloy P is 19-10-2.5 max Cr-Ni-Mn partially ferritic alloy.
Alloy 17-4 PH is 17-4-4 precipitation hardening Cr-Ni-Cu alloy in unhardened condition.

[b]Ferrite content determined by Magne-gage measurements.

[c]Conditions of runs M-23 and M-24: 0.17 *m* uranyl sulfate, 250°C, 200 hr. Rapid corrosion of a chromized tube bundle in the main line of run M-23 caused abnormally high concentration of Cr^{6+} in solution and correspondingly lower corrosion losses on specimens.

Commercial Titanium and Zircaloy-2 Welds

Welds were made in ¼-in. plates of Ti-75A and Zircaloy-2, with wire of the same compositions, in a dry box under a helium atmosphere. Special flat-plate-type corrosion specimens were machined from these plates without affecting the weld reinforcements. Four specimens of each type were tested in oxygenated 1.34 *m* uranyl sulfate at 250°C for 200 hr and at solution velocities ranging from 50 to 92 fps. Tenacious bulk scales of iron and chromium oxides were deposited on these specimens, but a thin light-green substrate film on the titanium and a thin gold-colored substrate film on the Zircaloy-2 protected the materials so that corrosion was negligible. The as-removed-and-scrubbed weight gains were comparable to those for samples of base material which were included in the run for comparison.

Intergranular Corrosion of Austenitic Stainless Steels

W. O. Harms

Tubing from H Loop Pressurizer Mixing Line. – Three failures occurred in the ¼-in. tubing of 0.035-in. wall thickness in the pressurizer mixing line of dynamic loop H during exposure to 1.34 *m* uranyl sulfate at 225°C and at an estimated velocity of 25 fps. A type 347 seamless tube failed after 492 hr, a type 316 welded tube after 22 hr, and a type 347 welded tube after 188 hr. The seamless-tube failure was not so clearly intergranular as were the failures in the welded tubes. Figure 59 illustrates the welded-tube failures.

Letdown Valve in HRE Mockup. – The components of a letdown valve in the HRE mockup, which was removed because of excessive leakage, consisted of type 347 stainless steel with a Stellite 6 overlay in the seat and on the guide stem and of a solid Stellite 6 plug. The weld deposit in both the seat and the stem exhibited porosity, and chemical analysis showed that cobalt and probably tungsten had been selectively leached from this alloy. Severe intergranular penetration in the type 347 material near the fusion zone was observed. This penetration was apparently due to the diffusion of carbon from the stellite, followed by precipitation of chromium carbides on slow cooling through the sensitizing temperature range.

Pin-Type Corrosion Specimens. – Metallographic examination of pin-type specimens of stainless steel types 316L, 316, 304L, 309SCb, 347, and 304 sensitized, which had been tested in oxygenated 1.34 *m* uranyl sulfate at 225°C and at flow rates of 17–18 and 65 fps, revealed the following:

1. Only the type 304L specimen escaped intergranular attack in high-velocity runs, in which types 316L, 316, and 309SCb showed poorest resistance to this type of attack.
2. At the low flow rates, types 316L, 304 sensitized, and 316 were intergranularly attacked. A typical microstructure of the type 304 specimen is shown in Fig. 60.

Huey Tests on Tubing and Plate Stock. – In cooperation with the HRP Static Corrosion Group, an investigation was initiated to determine whether HRP stainless steel stock passed laboratory-type corrosion tests. Seven samples of types 304L and 347 tubing and plate were subjected to the boiling 65% nitric acid test (Huey test) to determine their susceptibility to intergranular corrosion. This test, which consists of up to five 48-hr exposures to the boiling acid, requires that acceptable material show corrosion rates of less than 2.0 mils per month for each 48-hr period. Results of this study, the details of which have been reported elsewhere,[7] were as follows:

[7] J. L. English, *HRP Quar. Prog. Rep. April 30, 1954*, ORNL-1753, p 106.

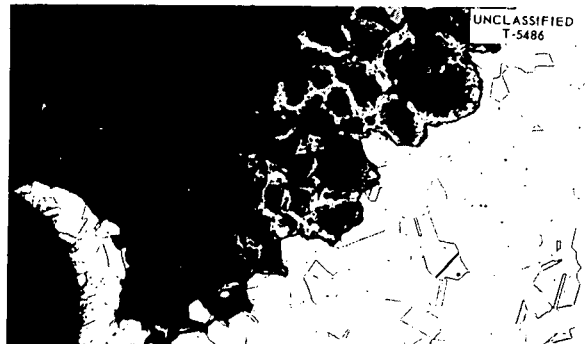

Fig. 59. Microstructure at Penetration in Type 316 Stainless Steel Welded Tubing from Pressurizer Mixing Line of H Loop. Etchant: aqua regia. 250X. Reduced 32%.

Fig. 60. Microstructure of Sensitized Type 304 Stainless Steel After Corrosion Testing in 1.34 *m* Uranyl Sulfate at 225°C. Etchant: aqua regia. 1000X. Reduced 32%.

1. Welded type "304L" tubing from one supplier showed corrosion rates as high as 58.5 mils per month after a sensitizing treatment. Chemical analysis later revealed that this material contained 0.075% carbon and was either a straight type 304 stainless steel or had picked up a substantial amount of carbon during processing.

2. Seamless type 347 stainless steel tubing from another supplier failed the Huey test after a sensitizing treatment. Chemical analysis then showed this material to be deficient in columbium, the Cb/C ratio being 0.3 instead of 10.

3. Even though catastrophic corrosion due to the dropping-out of grains did not occur within the five test periods, some type 304L and 347 materials maintained corrosion rates from 1 to 3 mils per month greater than the rates allowable in existing specifications.

Stress-Corrosion Cracking in Austenitic Stainless Steels

Tubing Failures in Dynamic Loop C. – Two transgranular failures on the inside of 90- and 180-deg bends of $\frac{3}{8}$- and $\frac{1}{2}$-in. schedule-40 type 347 stainless steel are believed to have occurred as the result of the combined effects of stress and corrosion. Details of an investigation of these failures and photomicrographs have been published elsewhere.[8] It was interesting to note that these parts, which had not been stress-relieved after bending, were in service for almost 7800 hr before failing. The failures occurred shortly after a 1000-hr run at 100°C, in which Oak Ridge tap water was sprayed on the pipe for temperature control. The scale that formed on the first failure was of the boiler type, containing large amounts of calcium and magnesium. The second failure had received considerable protection from the magnesia-base lagging material but still had been wet by the tap water. The presence of 7 to 10 ppm of chloride ion in the water may have figured in the transgranular stress corrosion observed. The boiling 42% magnesium chloride test showed that specimens from the bent portion of the tube were considerably more susceptible to transgranular cracking than was a specimen from a straight pipe section.

Failure of Type 347 Capillary Tubing in In-Pile Mockup Loop. – Leaks in the 0.060-in. capillary tubing of both the hydrogen and the oxygen lines of in-pile mockup loop BB-2 resulted when transgranular cracking occurred. The presence of caked uranyl sulfate in the oxygen line suggested that cracking was due to stress corrosion. Since the time of this failure, two of the small pressurizer assemblies have been given partial stress-relief heat treatments at 950°F for 6 hr in hydrogen.

Laboratory Tests. – Two simulated HRT tube-to-tube-sheet assemblies, in which $\frac{3}{8}$-in.-OD, 0.049-in.-wall, type 347 stainless steel tubes had been expanded in a rolling operation by 0.006 and 0.0015 in., were tested in boiling 42% magnesium chloride solutions. In addition, as-received tubes were tested for comparison. Cracks were observed after 5 hr in the expanded end of the 0.006-in.-rolled specimen, near the surface of the tube sheet. After 10 and 15 hr, tubes in this assembly showed many cracks in those areas where the rollers "machined into the tubing." On the other hand, the 0.0015-in.-rolled material showed only a few minor superficial cracks, even after 15 hr of exposure. No cracks were observed in the as-received tubing. This indicates that the use of the lighter expansion renders much less probable a stress-corrosion failure in the HRT heat exchanger.

The addition of new personnel has made possible a continuation of the research program outlined in the previous report.[9] One hundred and sixty constant-stress specimens have been formed in the special jig. These include two compositions of type 304L and one each of types 347, 309SCb, and 316L, covering a large range of martensite-forming susceptibilities.

[8] E. C. Miller, W. O. Harms, and T. W. Fulton, *HRP Quar. Prog. Rep. April 30, 1954*, ORNL-1753, p 117–119.

[9] W. O. Harms and E. C. Miller, *Met. Semiann. Prog. Rep. April 10, 1954*, ORNL-1727, p 20.

FABRICATION METALLURGY

J. E. Cunningham

EXPERIMENTAL FABRICATION OF ALUMINUM FUEL ELEMENT

Fabrication studies were conducted on the preparation of composite fuel plates with the thickness of aluminum cladding reduced to 10 and 5 mils. The purpose of the studies is to improve reactor performance of the resulting fuel component by further lowering the aluminum-to-water volume ratio.

Examination of the test plates revealed that thin-clad fuel plates can be successfully prepared by the present technique, with only one defect. The defect appeared as small "pockmarks" or pits randomly located on the surface of the plates immediately after the flux-annealing operation. In some instances, these surface pits extended to a depth of approximately 3 mils or one-half the depth of the cladding at this point in the fabrication schedule for the preparation of fuel plates with 5 mils of aluminum cladding.

Although these surface imperfections are essentially ironed out during the following cold-rolling step, additional work was performed in an effort to determine the exact cause of the objectionable surface pits and to eliminate them. In the flux-annealing operation, where the defect occurs, a slurry of commercial aluminum brazing flux (Eutector 190) and methyl alcohol is employed to facilitate removal of hydrogen to prevent blister formation.

Type 2S aluminum plates immersed in a large volume of molten Eutector 190 flux heated to both the flux-annealing and brazing temperature were completely corroded away in a relatively short time. Chemical analysis indicated that the resulting globule that formed in the bottom of the crucible was actually a Zn-Al alloy containing 5 to 30 wt % Zn. The source of the zinc was undoubtedly the brazing flux, which contains 8 to 14 wt % $ZnCl_2$.

Similar tests showed that the amount of alloying or pitting could be greatly reduced by lowering the $ZnCl_2$ content of the brazing flux. The substitution of $SnCl_2$ for the zinc compound arrested the alloying action completely. Brazed T-joints prepared with the modified low-zinc and stannous chloride–bearing fluxes showed a corrosion resistance superior to that of samples prepared with regular Eutector 190 flux when tested for 24 hr in boiling water. Initial attempts to braze full-sized dummy fuel elements with these modified fluxes, however, were not successful and indicate a need for further investigation. The low-zinc-content brazing flux is presently being employed in the flux-annealing operation during manufacture of enriched fuel components.

MANUFACTURE OF REACTOR COMPONENTS

J. H. Erwin

Replacement Fuel and Control-Rod Units for MTR

A total of 105 fuel units and two control rods were fabricated and forwarded for operation of the MTR and startup of the Reactivity Measuring Facility (RMF) during the period from March 1 through September 1, 1954. The fuel units were the 19-plate type prepared with braze-clad side-plate material, and each contained 200 g of U^{235}. Fuel units containing plates of heat Nos. D-292 through D-301 were flux-annealed with 1.5% zinc–bearing flux.

One of the control rods forwarded was of standard design, while the other was modified with a single-piece aluminum extrusion substituted for the four-piece lower bearing stainless steel section.

New Loading of BSF Fuel Elements

A new set of enriched fuel elements was prepared for service at higher power in the Bulk Shielding Facility. The loading consisted of 25 standard, full fuel sections for housing control rods and two dummy fuel components.

Borax Model II Fuel Units

A total of 68 enriched fuel elements and 22 unassembled fuel plates were supplied to Argonne National Laboratory for Borax Model II experiments. The standard unit consisted of a 10-plate element, and each unit was loaded with 93.3 g of U^{235} fuel.

Special Fuel Assembly for LITR

A special assembly consisting of nine enriched-fuel–bearing plates, spaced to provide a central

cavity for irradiation experiments in the LITR, was supplied to the Solid State Division.

Test Elements for Omega West Reactor

Six dummy fuel units were fabricated and forwarded to the Los Alamos Scientific Laboratory for preoperational checking before startup of the Omega West Reactor. The units have identical end box adapters on each end to permit inversion of the unit after part-time service.

Control Rods for Pennsylvania State College

A set of three safety control rods and one regulating rod was furnished for service in the proposed research reactor at Pennsylvania State College.

Film Boiling Experiment

A modified control rod and four enriched-fuel test sections with varying fuel contents of U^{235} are in process of fabrication for MTR film boiling experiments by Phillips Petroleum Co.

Alclad U-Al Alloy Test Plates for BNL

An order for 120 MTR-type fuel plates was completed for testing and component-assembly studies at Brookhaven National Laboratory. The order consisted of 30 depleted-uranium plates each of (1) 5 wt % U–Al alloy core with 20 mils aluminum cladding, (2) 5 wt % core alloy with 15 mils cladding, and (3) 14 wt % core alloy with 20 mils cladding and 14 wt % core alloy with 15 mils cladding.

Neutron-Production Slugs for Hanford and Savannah River

Cast, enriched U-Al alloy billets supplied by Y-12 were extruded and drawn into rod stock needed in the production of approximately 2000 slugs for Savannah River and 5000 slugs for Hanford.

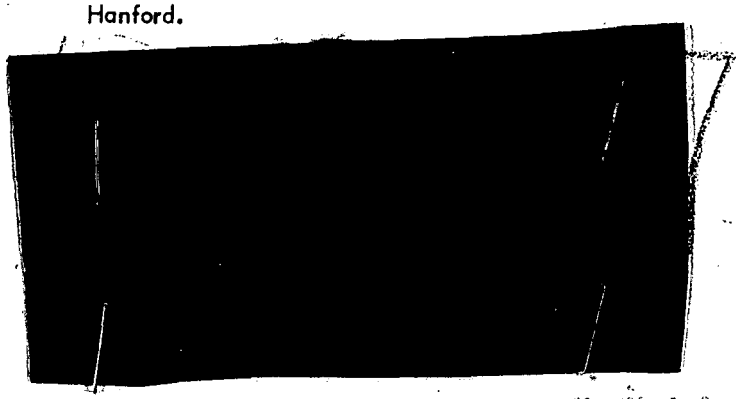

PREPARATION OF U-Al ALLOY PRODUCTS FOR CHEMICAL PROCESSING STUDIES

Normal-Uranium MTR Fuel Components for Phillips Petroleum Co.

Ten normal-uranium fuel elements of the design currently employed in operation of the MTR were prepared and shipped to the Idaho Chemical Plant for chemical processing studies.

Depleted U-Al Alloy Slugs for DuPont

Approximately 4000 extruded and 1000 cast, depleted U-Al alloy slugs of various specifications were prepared and delivered to Savannah River.

Miniature U-Al Alloy Slugs

The Chemical Technology Division was furnished approximately 30,000 extruded and 2000 cast subsized slugs of 5 wt % U–Al alloy for continuous-dissolving studies.

Cast and Extruded "J" Slugs for Phillips Petroleum Co.

Approximately 1000 cast and 2000 extruded "J" slugs of 7–5 wt % normal and depleted U–Al alloy were prepared and shipped to the Idaho Chemical Processing Plant.

Cast and Extruded "J" and "SRO" Slugs

Approximately 4000 extruded and 3000 cast slugs of both 5 and 7–5 wt % normal U–Al alloy were produced for processing studies by the Chemical Technology Division.

MISCELLANEOUS FABRICATION WORK

Iodine-Thorium Wire and Foil for North American Aviation, Inc.

Experimental samples of iodine-thorium wire and foil were prepared for North American Aviation, Inc. The foil samples measured 1 by 48 in. by 3, 5, 10, and 20 mils in thickness, while 100 ft of wire in each of the 3-, 10-, and 20-mil-dia size was supplied.

Highly Depleted Uranium Slugs for LITR Irradiation

Several highly depleted (0.035% U^{235}) uranium slugs were fabricated for canning and irradiation in the LITR. The slugs were prepared by extrusion of a 4-in.-dia cast billet to 1.5-in.-dia rod, which was machined into 1.8-cm-dia by 4-cm-long slugs.

Enriched U-Al Alloy Slabs for Savannah River

Two highly enriched U-Al alloy slabs were fabricated to assist DuPont in developing tubular fuel elements. The alloy composition of the slabs was 15 and 19.9 wt % U^{235} aluminum alloy, but both slabs measured 8.9 × 36 × 0.080 in. in thickness.

Zirconium Alloy Specific-Heat Specimens

Specimens of zirconium containing 1 and 4 at. % silver and 10, 20, and 30 at. % aluminum were prepared from solution-treated arc-cast melts and forwarded to Carnegie Institute of Technology for specific-heat measurements. An 8 at. % silver alloy was also prepared, but on metallographic examination an unidentified phase was revealed at the grain boundaries, which probably was the result of incomplete quenching. The specimen will be solution-treated again with a faster quench in an effort to eliminate the objectionable phase.

Enriched-Uranium Disk for Lid Tank Facility

A new enriched-metallic-uranium source plate is being fabricated for the Lid Tank Facility of the ORNL Graphite Reactor. The plate contains approximately 2 kg of U^{235} and measured 28 in. in diameter by approximately 0.040 in. in thickness.